

Department of Geography  
GEO 511: Master Thesis  
January 2016

# Master Thesis

## Investigation of Volcanic Sediments on the Nebrodi Mountains



Author:  
Dieter Halpern  
Schwandenholzstrasse 24,  
8052 Zurich  
dieter.halpern@uzh.ch  
S07726367

Supervisor and Faculty Member: Prof. Dr. Markus Egli  
Physical Geography Geochronology  
Department of Geography  
University of Zurich – Irchel  
Winterthurstrasse 190  
CH-8057 Zurich Switzerland

# Table of Content

ABSTRACT.....	1
Abbreviations.....	2
I. INTRODUCTION.....	3
Aim.....	5
II. MATERIALS AND METHODS.....	6
Basics.....	6
Lapilli.....	6
Dating Techniques.....	7
Area of Investigation.....	8
Geographic and Climatic Situation.....	8
Field Work.....	11
Site and Area Selection.....	11
Soil Samples.....	12
Ash Thickness.....	14
Experimental Setup.....	14
Systematic Sampling.....	15
Laboratory Analyses.....	16
Methodological Approach: Chemical and Physical Analyses.....	16
Chemical and Physical Analyses.....	17
Samples Preparation.....	17
Soil Reaction (pH).....	17
Bulk (Dry) Density ( $\rho_b$ ).....	18
C-H-N-Elemental Analysis (Combustion Method).....	18
Organic Matter.....	18
X-Ray Fluorescent Analyser (XRF).....	18
X-Ray Diffractometric (XRD).....	19
Atomic Absorption Spectroscopy (AAS).....	19
Soil Colour Description (Munsell Soil Chart).....	19

Loss on Ignition (LOI) .....	19
Grain Size Analysis –Wet Sieving and X-ray-Sedigraph .....	20
Stable Organic Material Method for <sup>14</sup> C (10 % H <sub>2</sub> O <sub>2</sub> ) .....	20
Diffuse Reflectance Infrared Fourier Transformation (DRIFT) .....	20
Organic Carbon Stocks Calculation (SOC) .....	21
Weathering Indices .....	21
<b>III. RESULTS .....</b>	<b>23</b>
Systematic Sampling.....	23
Soil Maps (Ash Thickness) SII .....	25
Soil Maps (Ash Thickness) SIII.....	26
Soil Profiles.....	27
Physical and Chemical Analyses .....	27
Soil Morphology and Characterization of the Soil Pits .....	32
Morphology of Soil Profile SI .....	32
Morphology of Soil Profile SII .....	33
Morphology of Soil Profile SIII.....	34
Morphology of Soil Profile Floresta .....	35
Morphology of Soil Profile Sila.....	36
General Characteristics of Soil Profiles .....	37
Soil Textural Triangle .....	39
Oxalate Extraction of the Elements Fe, Al and Mn (Sila) .....	40
Oxalate Extraction of the Elements Fe, Al and Mn (Nebrodi) .....	41
Measured Total Carbon Content (%).....	42
Measured (K+Ca) / Ti Ratio .....	43
Soil Reaction pH .....	44
Total Carbon Content (%).....	44
C/N Ratio .....	45
Carbon Stocks Analysis .....	46
XRD Analysis .....	47

DRIFT Analysis .....	48
Origin Determination .....	49
Total Alkali-Silica (TAS).....	49
TAS-Diagram: Magma Series.....	52
TAS-Diagram: Investigated Sites and Their Clusters.....	53
TAS-Diagram: Chemical Comparison of Lapilli.....	54
K <sub>2</sub> O/SiO <sub>2</sub> Diagram: Volcanic Materials and Their Clusters.....	55
K <sub>2</sub> O/SiO <sub>2</sub> Diagram: Nebrodi Soils Compared to Other Volcanic Materials .....	56
K <sub>2</sub> O/SiO <sub>2</sub> Diagram: Volcanic Material All Sites.....	57
K <sub>2</sub> O/SiO <sub>2</sub> Diagram: Average Parent Magmas and Their Development .....	58
Age Determination.....	60
Weathering Indices .....	60
Radiocarbon <sup>14</sup> C.....	64
IV. Discussion.....	65
General Soil Analyses.....	65
DRIFT and XRD.....	66
Soil Reaction pH.....	67
Soil Carbon .....	68
Origin Determination .....	69
Age Determination.....	73
Radio Carbon Analysis <sup>14</sup> C.....	73
Weathering Indices .....	74
Carbon Stocks .....	76
Chemical Composition of the Volcanic Material .....	76
V. CONCLUSION.....	78
VI. ACKNOWLEDGMENTS .....	80
VII. PERSONAL DECLARATION .....	81
VIII. REFERENCES.....	82
IX. APPENDIX.....	88

## List of Tables

Tab. 1 Soil pits description .....	13
Tab. 2 Samples and analyses conducted on soil profiles .....	16
Tab. 3 Systematic sampling for ash thickness at site II .....	23
Tab. 4 Systematic sampling for ash thickness at site III.....	24
Tab. 5 Total concentration of major element oxides, inorganic volatile compounds and organic matter content by horizons .....	37
Tab. 6 Average composition of parent material of Nebrodi .....	38
Tab. 7 Oxalate-extractable concentration, pH and bulk density of the sampled soils.....	38
Tab. 8 Wet sieving measurements of the fine earth material.....	39
Tab. 9 Minerals found within Sila and Floresta via XRD.....	47
Tab. 10 Minerals found within the analysed soil profiles via DRIFT .....	48
Tab. 11 Volcanic rock classification, according to the TAS-analysis .....	51
Tab. 12 Index-B results age determination .....	61
Tab. 13 WIP age determination .....	63
Tab. 14 Radiocarbon results.....	64

## List of Figures

Fig. 1 Pyroclastic rocks.....	7
Fig. 2 Principal dating methods used in paleo climatic research .....	7
Fig. 3 Geological structure of Sicily and research area .....	9
Fig. 4 Parent material .....	9
Fig. 5 Messina wheather station measurement .....	10
Fig. 6 Sampling areas.....	13
Fig. 7 Sampling site: SI.....	13
Fig. 8 Sampling site: SIII.....	13
Fig. 9 Sampling site: SII .....	13
Fig. 10 Pürkhauer.....	14
Fig. 11 Sample distribution at SII and SIII .....	15
Fig. 12 Morphology of soil profile SI.....	32
Fig. 13 Morphology of soil profile SII.....	33
Fig. 14 Morphology of soil profile SIII .....	34
Fig. 15 Morphology of soil profile Floresta.....	35
Fig. 16 Morphology of soil profile Sila .....	36

Fig. 17 Soil texture pyramid .....	39
Fig. 18 Oxalate extraction as a concentration-depth function .....	40
Fig. 19 Oxalate extraction as a concentration-depth function .....	41
Fig. 20 Total carbon content in percent (%) as function of depth .....	42
Fig. 21 (K + Ca) / Ti as a depth-function.....	43
Fig. 22 Total pH-values (CaCl <sub>2</sub> ) as a function of depth.....	44
Fig. 23 C/N ratio as function of depth .....	45
Fig. 24 Soil organic carbon content as depth function.....	46
Fig. 25 SOC stocks as an age function.....	46
Fig. 26 DRIFT .....	47
Fig. 27 TAS-Diagram: Magma series .....	52
Fig. 28 TAS Diagram: Clusters.....	53
Fig. 29 TAS Diagram: Lapilli comparison .....	54
Fig. 30 K <sub>2</sub> O/SiO <sub>2</sub> Diagram: Clusters of the investigated volcanic materials .....	55
Fig. 31 K <sub>2</sub> O/SiO <sub>2</sub> diagram for Nebrodi .....	56
Fig. 32 K <sub>2</sub> O/SiO <sub>2</sub> Diagram: Aeolian Islands, Etna and Sila .....	57
Fig. 33 Parent magmas and their development .....	58
Fig. 34 Index B, upper soils .....	60
Fig. 35 Index B, sub soils.....	60
Fig. 36 WIP upper soils.....	62
Fig. 37 WIP sub soils .....	62
Fig. 38 Radiocarbon dating.....	64
Fig. 39 XRD Sila, horizons 0-20 (top) and 40-60 (bottom).....	92
Fig. 40 XRD Sila, horizon 80-100 (top), Floresta, horizon 0-20 (bottom).....	93
Fig. 41 XRD Floresta, horizons 35-115 (top) and >200 (bottom) .....	94

## ABSTRACT

Recent studies have demonstrated that ando and ando-like soils are much more present in the Mediterranean regions than previously assumed (Scarciglia et al., 2008). These kinds of soils are not only important because of their “unique physical and chemical properties” which contribute to the functioning of ecosystems (Drouza et al., 2007; Vingiani et al., 2014), but within them also lies the key to the understanding of past, present and future hazards of volcanic events and they are thus of great importance to science and society (Zimmerer et al., 2016). Nevertheless, information regarding chronologies of quaternary volcanic events remains poorly understood (Giaccio et al., 2008; Zimmerer et al., 2016), especially in peri-volcanic areas where the origin of the soils is seldom known due to the abundance of different volcanoes in close proximity (Giaccio et al., 2008). This study follows the steps of previous studies in geochronological dating and origin determination of volcanic materials (Egli et al., 2008; Scarciglia et al., 2008; Maviris et al., 2010) by analysing volcanic soils from south Italy. For this task, several physical and chemical analyses were carried out in the field as well as in the laboratories at the University of Zurich. For the soil dating or soil age determination several geochronological methods, such as weathering indices and  $^{14}\text{C}$ , were used. According to the achieved results, the performed weathering-index analyses dated the soils as belonging to a volcanic activity span of about 100 ka BP. The  $^{14}\text{C}$  analyses on organic material found within specific soil layers of three soil profiles resulted in late Holocene ages, while the analyses of the chemical composition of the magma suggested a middle and late Pleistocene age. Based on the results, it was thus assumed that the collected and analysed soils are the result of thousands of years of offshore volcanism carried by wind and deposited at the near region of Nebrodi, Messina (ME). Lastly, thanks to the analysis of the chemical composition of the soils compared to pre-existing data, it was possible to identify the investigated soils of Nebrodi and Sila as distal volcanic materials. In other words, the analyses seem to suggest Lipari as the origin of the investigated soils.

## Abbreviations

Instruments and Methods		Locality	
XRF	X-ray Fluorescence	It	Italy
DRIFT	Diffuse Reflectance Infrared Fourier Transformation	RC	Region Calabria
		ME	Messina
BDD	Bulk Dry Density	CT	Catania
SSG	FAO Soil Survey Guidelines	UZH	University of Zurich
KA4	German Soil Sampling Guide		
TAS	Total Alkali Silica		
Org. M.	Organic Matter		
IVC	Inorganic Volatile Compounds		
LOI	Loss on Ignition		
XRD	X-ray Diffractometric		
SOC	Soil Organic Carbon		

Elements		Oxyanions		Units	
Zr	Zirconium	CaO	Calcium oxide	BP	Before present
O	Oxygen	CaCO <sub>3</sub>	Calcium Carbonate	Cal.	Calibrated age
C	Carbon	MgO	Magnesium Oxide	y	Year
Si	Silica	MgCO <sub>3</sub>	Magnesium Carbonate	a	Year
K	Potassium	Fe <sub>2</sub> O <sub>3</sub>	Iron Oxide	Ka	A thousand years
P	Phosphorus	Al <sub>2</sub> O <sub>3</sub>	Aluminium Oxide		
K	Potassium	MnO	Manganese Oxide		
Ca	Calcium	Na <sub>2</sub> O	Sodium Oxide		
Ti	Titanium	K <sub>2</sub> O	Potassium Oxide		
Mn	Manganese	SiO <sub>2</sub>	Silicon Oxide		
Fe	Iron	Ca(OH) <sub>2</sub>	Calcium Hydroxide		
Na	Sodium	Mg(OH) <sub>2</sub>	Magnesium Hydroxide		
Mg	Magnesium				
Al	Aluminium				

# I. INTRODUCTION

The basic rule of nature is that  
nothing remains the same over long periods of time (Eash et al., 2008).

Volcanic eruptions are spectacular natural events (Giaccio et al., 2008) that have captured man's curiosity since prehistoric times. On the one hand, they can be of great benefit to man but on the other, they can also cause great harm and thereby provide a major impetus for their study (Fisher & Schmincke, 1984). If we look at the Mediterranean area during the past late quaternary period, which encompasses the last two millions years, it can be described as a time marked by a great number of highly explosive volcanic events (Giaccio et al., 2008; Scarciglia et al., 2008). These have clearly left their marks on today's landscapes. In particular, fine volcanic material generally affects large areas around volcanic centres causing notable alterations to the ecosystem in close and distant regions (Giaccio et al., 2008). The evaluation of these fine grained materials can provide us with a powerful tool for Quaternary studies, allowing us to not only date them, but to also correlate them to a specific source sometimes located at a great distance (Giaccio et al., 2008). According to Zimmerer et al. (2016), information about timescales of magmatism and ages of eruptions is crucial in order to understand the history as well as the hazards of active and dormant volcanic areas. Zimmerer et al. (2016) also claim that knowledge of eruption ages can be further used to "calculate hazard parameters such as recurrence rates and repose periods, as well as to identify vent migration patterns that are crucial to eruption forecasting". In spite of their social and geological importance, chronologies for quaternary volcanic events remain poorly understood (Zimmerer et al., 2016). To this date, there have been several numerical methods used for the purpose of dating volcanic sediments, such as radio carbon ( $^{14}\text{C}$ ), potassium to argon decay ( $^{40}\text{K}/^{39}\text{Ar}$ ), fission-track geochronology, uranium to lead decay ( $^{235}\text{U}/^{207}\text{Pb}$ ) or cosmogenic nuclides ( $^{10}\text{Be}$ ). However, the necessary conditions for these numerical methods are often not guaranteed and hence many researchers also make use of relative dating techniques (Böhlert et al., 2011). As a consequence, it is thought that a multimethodological approach, i.e. a combination of the numbers retrieved from numerical analyses and relative dating methods, can possibly yield more accurate results (Giaccio et al., 2008). Such a multimethodological approach was also used in the following master thesis. Within the scope of our analyses, the origin and age of volcanic sediments located in Europe's most complex and volcanically active zone, namely the "Mediterranean Basin", were investigated (Pichler, 1984). In the case of Sicily, Italy, the large physical presence of volcanic materials scattered all about the region is a constant reminder of the once intense volcanic activity of the area. However, the origin of these volcanic materials is seldom known due to the abundance of different volcanoes in close proximity (Giaccio et al., 2008). In fact there are some areas in which volcanological as well as quaternary studies are, according to Giaccio et al. (2008), "still in their infancy". As a consequence, this master thesis aims to

investigate several Andosol-like profiles along a short slope sequence (1000 to 1300 m.a.s.l.) located within the area of Nebrodi, Messina in south Italy. This area has been a silent witness to the volcanic events that have covered the area with ashes and related volcanic material, which eventually evolved into the soils on which we stand today. The study of these volcanic sediments is of a general interest within the field of volcanology and quaternary sciences since they may enhance the knowledge of the eruptive history and “the dynamics of sediment accumulation in volcanic areas” (Di Vito et al., 2008). As a consequence to this, the results of this master thesis will provide further insight into the volcanic history of south Italy and thus contribute to our understanding of this region’s soil development.

## Aim

This master thesis deals with the study and analysis of volcanic material that today constitutes the soils located in north-east Sicily in the mountainous terrain known as Nebrodi, Province of Messina (ME). The main objective of this study is to determine the origin and age of the aforementioned volcanic material. In order to do this, soil volcanic material was sampled and brought to the laboratories of the geography department at the University of Zurich, Switzerland (UZH). Once there, the collected material was submitted to a large number of chemical and mineralogical analyses aimed at investigating and understanding the physical and chemical composition. Within the scope of this master thesis, it is crucial to understand these physical and chemical properties in order to achieve the proposed main objectives since they provide the key for dating and origin determination (Fisher & Schmincke, 1984).

The following master thesis operates under the hypothesis that at least one great volcanic eruption happened in the past which covered the entire area of Nebrodi with volcanic debris. This hypothesis is based on the large amount of ash and other volcanic material found about the area of interest. Within this framework, the following master thesis aimed to find the volcano(es) that could be determined as the source of the collected material as well as the period of time during which the volcano(es) erupted.

As a result, the following questions were raised:

- Is it possible to determine the origin volcano of the collected soil samples by analysing their chemical components? And if yes,
- Is it possible to estimate the period of time during which the source erupted as the age of these soils layers are investigated and dated by means of relative and numerical dating techniques?

## II. MATERIALS AND METHODS

### Basics

As stated before, the search for the origin of the collected material is one of the main objectives of this master thesis. Some published works, such as the one by Fisher and Schmincke (1984), have stated that it is indeed possible to determine the origin through the study of the chemical and mineralogical composition of igneous material. However, one basic concept must first be acknowledged, namely that soils are essentially made of rocks as they are comprised of fragmented and chemically weathered rocks including sand, clay and silt (Eash et al., 2008). Consequently, inorganic soil material aside from its current physical texture and size (rocky or powdery) is or was at one point a rock and as such, inorganic soil material is largely made of silicate minerals (Eash et al., 2008). In other words, around 90 percent of these silicate rocks consist of the following oxides: Si, Ti, Al, Fe, Mg, Ca, Na, and K (La Tour, 1989). These oxides can be seen and used as an identity document (ID) that directly connects the sampled materials to the source. Therefore, within this master thesis it is attempted to classify the volcanic rocks (that once formed the sampled soils) by means of chemical determination of the magma and differentiation processes (Fisher & Schmincke, 1984).

For this study, we used the total alkali silica diagram (TAS) to locate and compare our samples to pre-existing data on volcanic material. The TAS diagram is a widely recognized diagram based on purely chemical parameters for the classification of volcanic material, which is, according to Le Maitre (1984), to a certain degree comparable to the well-known QAPF diagram of Streckeisen (1978). We opted for this chemical method of classification because the sampled material is too fine-grained and this makes it almost – if not entirely – impossible to determine the mineralogical composition even for a microscopic study.

### Lapilli

Special interest was given to small pyroclastic material hidden within the soil horizons, the so-called lapilli (Lat. little stone) (USGS, 2009). The discovery of these specific rocks was thought to yield a first sign of the source since the site of research is located at around 15 kilometres from the next volcanic vent and because volcanic bombs normally cannot reach remote locations from its origin (Fisher & Schmincke, 1984).

As stated by Thorarinsson (1954), lapilli are a subdivision of tephra, which is the general term used to describe volcanic material (rock and lava) that has been blasted into the air by an eruption or carried upwards by a cloud of hot gas and often used as a synonym for pyroclastic material (Fisher & Schmincke,

1984). Lapilli by definition are small (tephra) materials ranging from 2 to 64 mm (Schmid, 1981; Fisher & Schmincke, 1984; USGS, 2009). The classification of pyroclastic rocks resembles the classification principles of clastic sedimentary rocks as shown in *fig. 1*. Ash can be seen as the equivalent to sand, lapilli are analogous to gravel and blocks and bombs correspond to boulders.

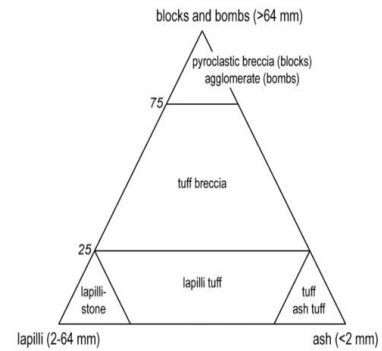


*Fig. 1* Pyroclastic rocks according to the classification principles defined by the IUG. (Le Maitre, 2005).

## Dating Techniques

By dating techniques (or methods) we understand the processes by which the age of physical material can be estimated within a chronology or a calendar system. Accurate dating is of tremendous importance to scientific disciplines as for example geochronology. Without reliable estimates of the age of past events it is impossible to first, investigate whether they happened simultaneously or not (i.e. whether one event took place after another) and second, to correctly assess the rate at which past environmental changes happened (Bradley, 2015).

According to Bradley (2015), a dating method is a so-called umbrella term that can be divided into four categories: (a) Radioisotopic methods, (b) paleomagnetic methods, (c) chemical methods and (d) biological methods. This master thesis only makes use of radioisotopic methods, which are those that work under the principle of atomic decay rates, and chemical dating methods, which are based on time-dependent chemical changes in the sample or chemical characteristics of the sample. Moreover, each of these dating methods can further be classified as either relative or absolute.

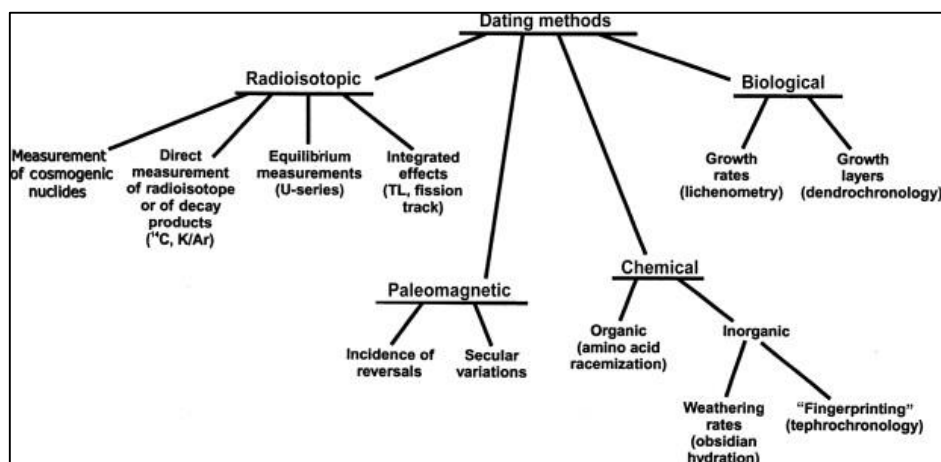


*Fig. 2* Principal dating methods used in paleo climatic research according to Bradley (2015).

It is well known that not all dating techniques are able to provide reliable numerical age but rather so-called relative age (Bradley, 2015). The methods used for the latter are known as relative dating techniques. Relative dating techniques compare the age of one sample with another in order to determine the relative order of past events (Wagner, 1995). In other words, relative dating techniques do not provide the absolute (numerical) age of a sample. However, it is possible to calibrate the relative age using a numerical dating technique so that one can retrieve the absolute age of a sample (Egli et al., 2012). Absolute<sup>a</sup> dating methods are those that determine the age of a sample on a specified time scale by providing a numerical age. Absolute dating methods work based on the principle that unstable atoms undergo radioactive decay through the loss of nuclear particles. This process will cause an element to transform into a new element or daughter product. The decay rate at which an element transmutes is constant and occurs at a known interval of time. It is the internal clock of matter. Therefore, by measuring the concentration of an isotope, one is able to indicate the amount of time that has passed since the sample was emplaced (Bradley, 2015).

For this master thesis we used several techniques in order to date the collected materials all based on the principle that soil evolution can only occur as time passes. Therefore, the study was focused on the analysis of time-dependent processes, such as weathering rates, for assessing the age of the samples (Bohn et al., 1985). For this task, several indices have been employed to characterise chemical weathering in the sampled soils (e.g. Nesbitt & Young, 1989). According to Dahms et al. (2012), most indices used to characterise chemical weathering in soils function under a similar principle based on the ratio between mobile and immobile elements. For this study, the index-B of Kronberg and Nesbitt (1981), the molar ratio of (K+Ca) / Ti (Harrington & Whitney, 1987) and the weathering index of Parker (WIP) (Parker, 1970) were used. In addition to this and as recommended by Böhlert et al. (2011), the results were combined with a relative or numerical dating method since on the one hand, soil development may have been perturbed by external factors and on the other, it is well known that soils do not develop linearly. Lastly, we opted for the radio carbon dating method as our age control approach.

## Area of Investigation

### Geographic and Climatic Situation

The main study area lies within the Nebrodi mountain region surrounded by most of the present active volcanoes. Strictly speaking, the study area is located in the north-eastern region of Sicily, Italy. The Nebrodi mountains together with the Madoni and the Peloritani range form a mountain chain known as the

---

<sup>a</sup> For this thesis, the terms absolute and numerical dating methods are used interchangeably although some authors claim this to be incorrect since the term 'absolute' implies an unwarranted certainty and precision (Colman et al., 1987).

Sicilian Apennines (Pichler, 1984). In turn, the Sicilian Apennines are restricted largely within the province of Messina (ME). Geographically, the study area is encompassed only within the Nebrodi mountains and it is characterised by a mountainous terrain with the highest elevation at 1846 m.s.l.m. However, in terms of geology, the island of Sicily can be divided into several geological domains and thus the study area is found in the crystalline region belonging to the Peloritani mountains (Monti Peloritani) (Pichler, 1984). As shown in *fig. 3*, the study area rests north-west of Mount Etna and between the Peloritani mountains and the Madonie region. In addition to the volcanic material in this particular area, the majority of the rocks forming the parental material (C-horizon) are comprised of large flysch sequences (turbidity flysch), which are massive quartz-arenite (sandstone) made up merely of detrital quartz (Pichler 1984).

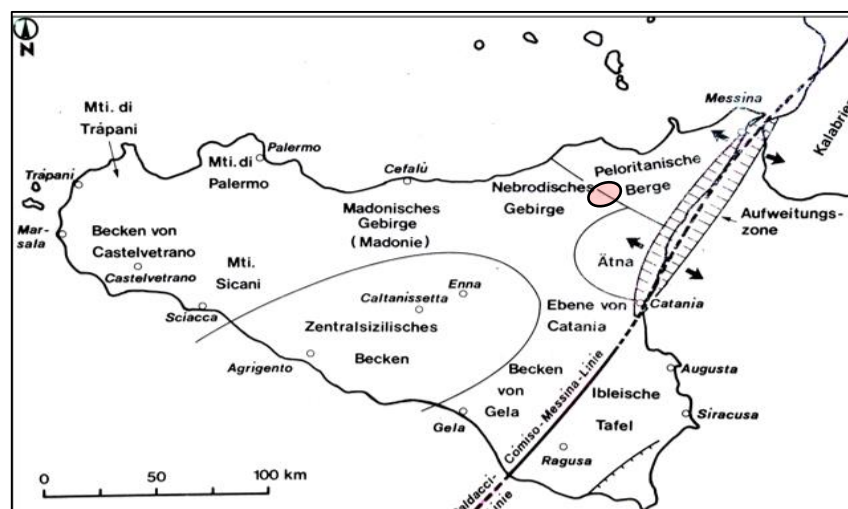


*Fig. 3 Geological structure of Sicily and research area; modified from Pichler (1984).*



*Fig. 4 Parent material quartz-arenite*

Concerning plant diversity, all sites (SI, SII and SIII) presented the same kind of vegetation but with a different percent of soil coverage. Generally speaking, the main vegetation covering the areas can be summarised as follows: Fern with circa 60 percent or more is the most abundant plant at all three sites, followed by approximately 30 percent of grass areas without higher vegetation. The remaining ten percent or less of the investigated areas were covered with low Maquis (shrubs shorter than 1 metre), being the least abundant plant cover in the investigated areas.

According to the weather station “Messina” (located at 54 m.a.s.l.), the local climatic conditions for the region of Messina are the following: Hot Mediterranean climate with a dry summer in a subtropical climate with some moderate seasonal changes. Summers are generally hot and dry thanks to the subtropical high pressure systems that dominate the area, while winters are characterised by rainy weather due to polar fronts. The mean annual temperature of the region of Messina is about 18° C, while the mean annual precipitation is about 831.5 mm (Climatemps.com, 2015). Regional environmental conditions within a large time span (125 to 15,000 years) are considered steady according to Egli et al.’s study (2008) for the near area of Mount Etna. Thus, according to the “Holdridge Life Zone System”, the region of Messina can be classified as a warm temperate dry forest biome (FAO, 2013).

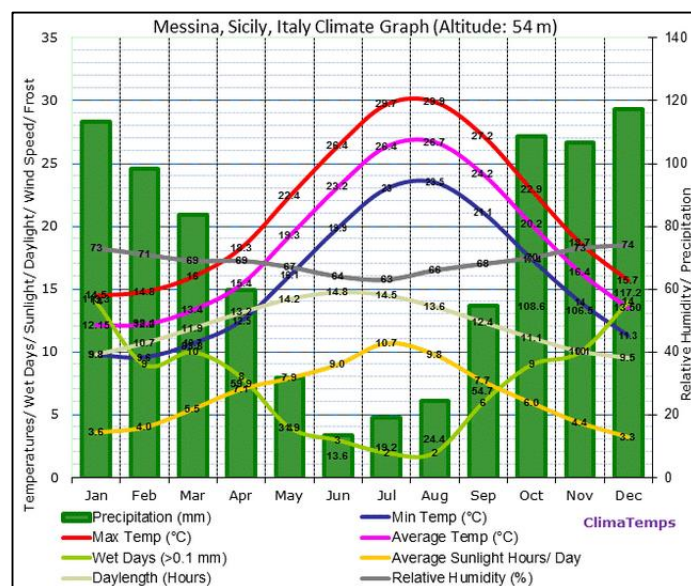


Fig. 5 Messina weather station measurement (<http://www.sicily.climatemps.com/>).

## Field Work

### Site and Area Selection

Within the scope of this study, only a limited area of the entire Nebrodi mountain region can be studied. Consequently, an important tool used to select the area to be sampled were bio-indicators. According to Siddig et al. (2015), bio-indicators are plant communities selected based on their sensitivity towards a specific environmental attribute and thus they act as a measure of environmental settings. They provide us with information regarding the conditions of the substrate on which they grow. For this study, fern was used as an indicator plant since – in contrast to other plants growing on the island of Sicily – the habitat preference and hence distribution reflects “abiotic features such as substrate, rather than an intricate combination of climatic and co-evolutionary features” (Troia et al., 2012). The investigated area on which fern was primarily found had an acidic substrate (pH-values ranging from 4 to 6), which is a typical feature of volcanic soil as it is provided by the geochemical composition of the rocks within the area (Siddig et al., 2015). Furthermore, the sampling areas were chosen based on the following arguments:

- The sampling areas are located within the area of interest, namely the Nebrodi mountains.
- The sampling areas were selected when a large part of the surface was covered by fern.
- Material sampling at the selected areas was accepted by local authorities and landowners.
- Thus, access to the sampling area was guaranteed.
- Weather conditions allowed the sampling work to be conducted.
- The terrain did not hinder the access to the sampling area.

Additionally, in order to conduct an extended search and quantification of the amount of ash inside the sampling areas, sites were selected when:

- Enough space was available, meaning open landscapes with no physical object that might hinder the conduct of a systematic sampling.

## Soil Samples

According to Walworth (2006), the first and most important step in soil analysis lies in the collection of the soil samples since soil analyses and their outcomes are only as good as the samples sent to the respective laboratory. Therefore, the sampling process was conducted under the supervision of Prof. Dr. Markus Egli and performed in accordance with the recommendation stipulated in the German Soil Sampling Guide (1994) (henceforth KA4) and the FAO soil survey guidelines (henceforth SSG) (2015).

The sampling process was conducted during the last week of March 2015. During this time, three sites were selected. Soil pits were dug up to the C-horizons when possible. All sites received a numerical name based on the order in which they were examined. Hence, the sites are called “site one”, “site two” and “site three” (i.e. SI, SII and SIII). Site one is located on a flat terrain at the top of a hill with an exposition and slope equalling zero degrees. Its geographic position can be located at 37°59’15.5’’ N and 14°58’41.1’’ E at an elevation of 1269 m.a.s.l. Site two is located on a tilted surface. Its slope and exposition are 11 degrees and 345 degrees north. The geographic position of SII can be located at 37°59’01.6’’ N 014°57’51.6’’ E at an elevation of 1279 m.a.s.l. Lastly, site three is located on an uneven terrain. Its slope and exposition are 80 degrees and 90 degrees north. SIII’s geographic position can be located at 37°59’05.9’’ N 014°59’16.8’’ E at an elevation of 1243 m.a.s.l.

Upon excavation, all soil pits were cleaned and photographed. Soil horizons were identified and their colours were determined using a Munsell soil colour chart as recommended by KA4 (1994). At each soil pit, soil samples were taken as carefully as possible in order to adequately represent what the soils’ natural states were before sampling (SSG, 2015). Earth samples of all soil horizons were sampled from bottom to top and rapidly put into labelled plastic bags in order to avoid contamination. To ensure the correct execution of chemical and physical analyses at least one kilogram per soil horizon was collected (Hitz et al., 2002), minding not to collect any large rocks. Also, a total of 70 soil core cylinders (two per soil horizon) were used for inspecting the soil bulk density of the soil profiles. Site features such as exposition, slope, roots and rock quantification were registered directly at the soil pits. The only chemical analysis conducted on the field was the measure of pH using pH-test-strips.

In addition to the soil material collected in March 2015 from the above mentioned areas, two “external” soil profiles “floresta” and “sila” – named after their region of origin – were incorporated into this study based on the need for having a reference and outer point of comparison. Geographically speaking, the soil samples of “floresta” were extracted from the area of interest (Nebrodi) in the region of Floresta at around 4 kilometres from sites I, II and III. On the other hand, the sampled material of site “sila” were extracted from the region of Sila, Italy, on the mainland at a distance of approximately 200 kilometres from the main area of interest. In sum, the following master thesis encompasses the analysis of a total of six soil pits (SI, SII, SIII, Floresta, Sila and Sila-DH) of five different study sites.

Site	Region	Depth of Soil Pit	Horizon No.	Land Use	Elevation m.a.s.l.
SI	Nebrodi	160 cm	6	Pasture	1,269
SII	Nebrodi	170 cm	6	Pasture	1,279
SIII	Nebrodi	170 cm	6	Pasture	1,243
Floresta	Nebrodi	> 200 cm	7	Pasture	1,264
Sila	Calabria	100 cm	5	-	1,572
Sila DH	Calabria	100 cm	5	-	1,572

Tab. 1 Soil pits description.

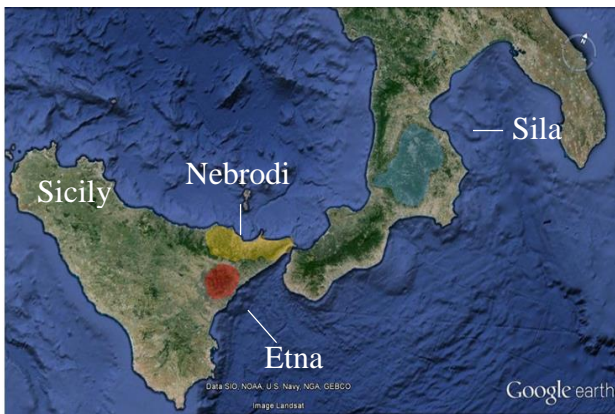


Fig. 6 Sampling areas. Areas from which the volcanic material was extracted (Nebrodi and Sila).



Fig. 7 Sampling site: SI.



Fig. 8 Sampling site: SIII.



Fig. 9 Sampling site: SII.

## Ash Thickness

### Experimental Setup

High ash concentration within the soil is a sign of an active volcanic history. However, the thickness of these ash layers in turn reflects the magnitude of past eruption events. The investigated area presents massive ash-layers which lead us to assume that at least one great volcanic eruption must have taken place in the past, since the area lies circa 14 kilometres from the next volcano. In order to quantify the extent and thickness of ash layers in the area of interest, a small systematic sampling was conducted. The site known as SI as well as its surroundings could not be sampled because of the unfavourable weather conditions. Consequently, only the surrounding areas of the sites SII and SIII were investigated. The area surrounding SII is located within the locality of Monte Polverello (ME) (N: 37°59'01.6", E: 014°57'51.6"). The elevation at this area ranges from 1257 to 1322 m.a.s.l. with a mean elevation of 1281 m.a.s.l. and is situated approximately 11 kilometres north from the centre of the town of Randazzo, Catania. The area surrounding SIII is located at Favoscuro, Messina (N: 37°59'05.9", E: 014°59'16.8"). The elevation at this area ranges from 1238 to 1282 m.a.s.l. having a mean elevation of 1256 m.a.s.l. and is situated around 5 kilometres from the town of Floresta, Messina.

As mentioned before, both sites present almost the same type of vegetation. The typical vegetation at both sites consists of fern, grass and small bushes (smaller than 1 metre), as shown in *fig. 8* and *9*. Both sites are located on private property and have thus been exposed to human impact. At both sites the land is used mainly for cattle and horse ranching. Sampling was conducted using a one-metre long Pürkhauer and a Garmin GPSmap® 60CSX device. The sampled area around site II has an extension of circa 284 metres width and 272 metres height encompassing a total area of approximately 77,248 square metres. The extension of the sampled area surrounding site III has an approximate width of 287 metres and a height of 77 metres. It encompasses a total area of 25,994 square metres. Graphic representations were created using the open source geographic information system (GIS) Quantum-GIS (QGIS).



*Fig. 10 One metre long Pürkhauer used for the systematic search of ash depositis at site II and III.*

## Systematic Sampling

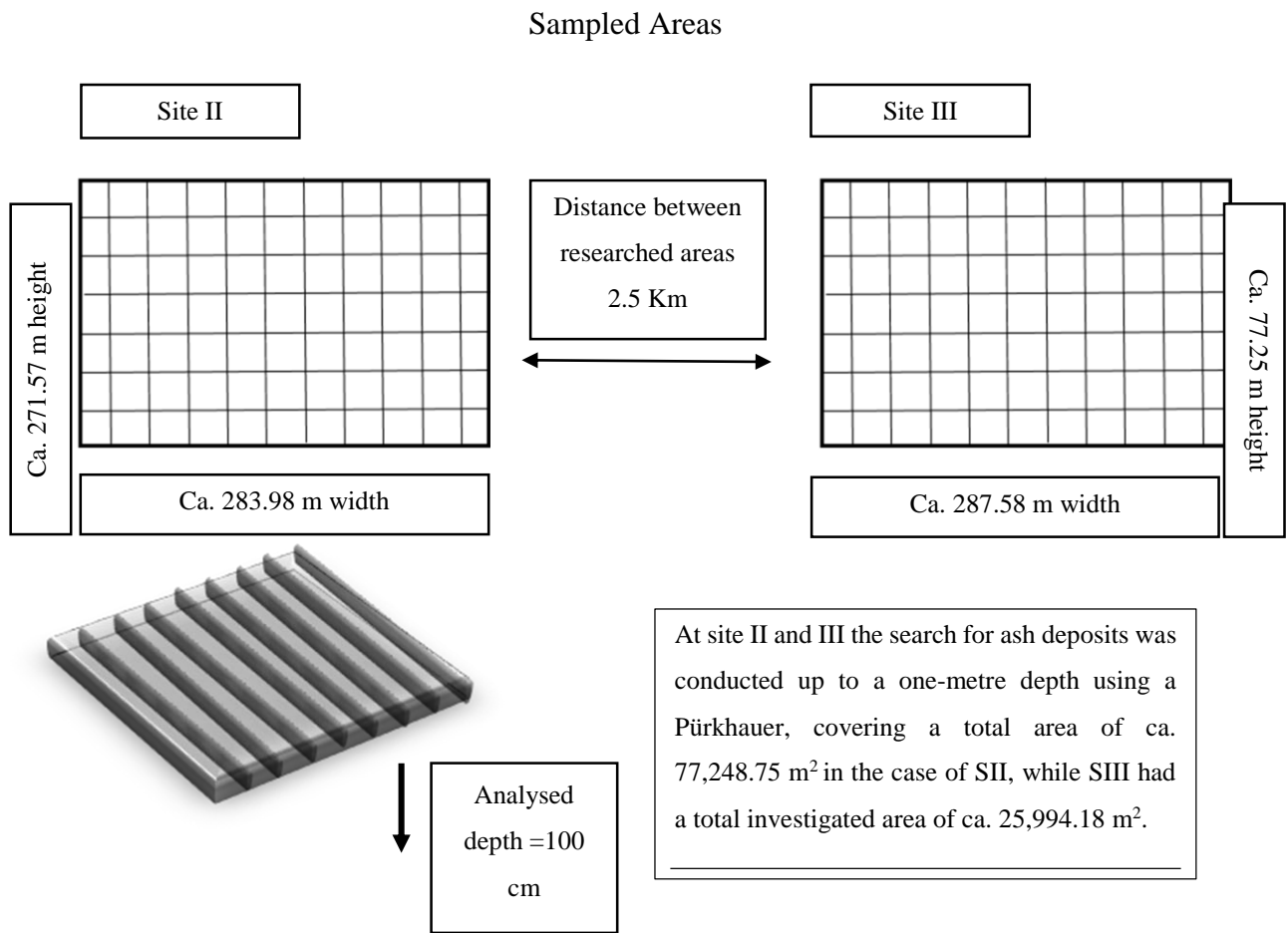


Fig. 11 Sample distribution at SII and SIII using Google maps tool.

## Laboratory Analysis

### Methodological Approach: Chemical and Physical Analyses

Analyses	Sample	Floresta	Sila	Site 1	Site 2	Site 3	Sila_DH
Sieving		✓	✓	✓	✓	✓	✓
Colour				✓	✓	✓	✓
Density		✓	✓	✓	✓	✓	✓
Loss on Ignition				✓	✓	✓	✓
XRF		✓	✓	✓	✓	✓	✓
AAS		✓	✓	✓	✓	✓	✓
Grain Size Analysis		✓ a)	✓ a)				
DRIFT		✓	✓	✓	✓	✓	✓
pH		✓	✓	✓	✓	✓	✓
<sup>14</sup> C		✓ a)	✓ a)	✓ a)		✓ a)	✓ a)
XRD		✓ a)	✓ a)				
C/N		✓	✓	✓	✓	✓	✓

a) Partial experiment not conducted for the entire soil profile.

Tab. 2 Samples and analyses conducted at the soil profiles.

## Chemical and Physical Analyses

The following chapter is ordered chronologically and describes the chemical and physical procedures conducted on the soil samples from the field.

### Samples Preparation

Upon extraction, all soil samples were sealed within plastic bags and transported to the laboratory of the University of Zurich (UZH), Irchel campus. Once in the laboratory, the samples were unsealed and placed into porcelain plates where litter remains were carefully removed. Afterwards, all samples were dried in the oven at 60°C for two days. The weight of all soil samples was measured and registered at all times in order to obtain the soil moisture and the total dry weight of the material. All samples were sieved manually and separated into two fractions using a 2 mm mesh sieve. Fraction one, also called coarse earth fraction, comprises the material larger than 2 mm. Contrary to that, fraction two or fine earth fraction includes all the material smaller than 2 mm (Stahr et al., 2012). The coarse earth fraction (> 2 mm) was weighed again in order to obtain the skeleton mass. Due to its importance for the soil system, physical and chemical parameters were determined for this last fraction (< 2 mm) (Eash et al., 2008). According to formal requirements, some quantities of fine earth fraction were further ground using a planetary ball milling machine or centrifugal mill machine. Upon sieving, the volcanic material found within the soil profiles and termed as lapilli (Lat. little stones) was removed from the sample and ground manually using a porcelain mortar and pestle for further chemical analyses. Soil material contained within soil cores was carefully extracted and set to dry for 48 hours at a temperature of 60° C for further analyses.

### Soil Reaction (pH)

For the determination of the pH-value or soil reaction, the first step consisted of calibrating the pH-metre. The calibration of the pH-metre was set up by using two liquid standards with the pH-value of four and seven. The calibration processes were finished after 5 to 10 minutes. Afterwards, 10 g of fine earth (fraction < 2 mm) of every single layer were carefully added to 35 Beaker glasses (35 horizons in six soil profiles), which had been filled with 25 ml solution of 0.01 mol/g CaCl<sub>2</sub> (solution ratio 1:2.5). Subsequently, the solution in the Beaker glasses was mixed using a magnetic stirrer (Sigma-Aldrich ® Heidolph MR 3001K) at a velocity of 500 rotations per minute. The mixing process was performed in the following way: The solution was first mixed during 5 minutes and then rested for another 5 minutes. This cycle was conducted three times for a total of 30 minutes. At the end, the pH was measured using a glass electrode metre for a period of 10 minutes.

## Bulk (Dry) Density ( $\rho_b$ )

The bulk (dry) density ( $\rho_b$ ) was determined by dividing the weight of the dry sample ( $M_s$ ) by the volume of the metal soil cores ( $V_c$ ) as it is shown in the formula below. Results of this operation are expressed in the metrical form of  $\text{g/cm}^3$ .

$$BDD = \frac{M_s}{V_c}$$

## C-H-N-Elemental Analysis (Combustion Method)

The total organic carbon (C) and nitrogen (N) values were gathered using a Leco® C-H-N elemental analyser (CHNS-932, USA). For this task, two different quantities of oven-dried finely ground earth were required. On the one hand, 2 mg (0.002 g) of the topsoil and, on the other hand, 3 mg (0.003 g) of the subsoil were needed. Upon weighing, the material was inserted into tin-capsules which were later combusted in the CHN-analyser through oxygen-rich environment. As a result, a series of gases ( $\text{CO}_2$ ,  $\text{H}_2\text{O}$ ,  $\text{N}_2$  and  $\text{SO}_2$ ) with exception of  $\text{N}_2$  were transported and removed from the system by a so-called carrier gas<sup>b</sup>. Finally,  $\text{N}_2$  was measured by thermal conductivity and the result was displayed as weight percent for the elements carbon and nitrogen. In our case, the total C corresponds to organic carbon as carbonates were not present within the soils (Egli et al., 2008).

## Organic Matter

Organic matter was determined by using the total C (achieved via CHN-analyser) multiplied by the constant 1.72 (Mirabella et al., 2005).

## X-Ray Fluorescent Analyser (XRF)

The analysis of major and trace elements in geological fine materials (Na, Mg, Al, Si, P, K, Ca, Ti, Mn and Fe) were determined through the non-destructive chemical analyser, better known as XRF (Fitton, 1997). For this task, 5 g capsules of finely ground soil powder belonging to each soil horizon were irradiated with high incident x-ray energy. As a result, atom instability was reached forcing the electrons to reallocate themselves. As this happened, a new x-ray echo was transmitted revealing the identity of elements encompassed in the soil horizons.

---

<sup>b</sup> The carrier gas employed was helium.

## X-Ray Diffractometric (XRD)

The method known as X-ray diffractometric (XRD) was conducted only to some selected samples. The XRD analysis is used to determine the structure of crystal substances and their relative content within a fine milled soil sample. The principle behind this method is that each mineral is able to reflect X-rays in a different incidence angle due to its particular crystal structure. Consequently, each mineral has its characteristic reflection peak which can be seen as a signature of the analysed element (Beckhoff et al., 2006). Thanks to a detector device it is possible to read the intensity as well as the angle in which the energy was reflected. In our case, this information was amended and presented as a diffractogram in which the diffracted intensity was shown as a function of a scattering angle. Further, by using the maximum measured values and comparing them to a large databank the program known as “DIFFRACplus EVA” was able to determine the kind of element and the amount encompassed within the analysed sample. For this task, soil material smaller than 32  $\mu\text{m}$  belonging to the site profiles Floresta and Sila was smoothed and compacted manually using razor blades in order to have a plain surface that could be measured by the machine Bruker-AXS (D8 Advance).

## Atomic Absorption Spectroscopy (AAS)

The quantitative concentration of the chemical elements manganese (Mn), aluminium (Al) and iron (Fe) was determined in solution with the AAS. The elements Al, Mn and Fe were extracted by using a  $\text{NH}_4$  Oxalate solution buffered at pH 3 ( $\text{Mn}_o$ ,  $\text{Al}_o$ ,  $\text{Fe}_o$ ) (Schwertmann, 1964; McKeague et al., 1971).

## Soil Colour Description (Munsell Soil Chart)

Colour description is one of the standard processes of any soil analysis. The soil colour determination along the soil profile was conducted on the field as well as in the laboratory in order to reduce uncertainty and guarantee reliability. The soil colour identification was performed using a Munsell Soil Chart that enables one to not only establish the colour (hue), but also the grade of darkness and lightness (value) and the colour intensity (chroma) (Pendleton & Nickerson, 1951). For this, small wet soil samples were held beside a Munsell soil chart and compared with one another under different light conditions.

## Loss on Ignition (LOI)

The method known as loss on ignition was conducted in order to burn the inorganic volatile compounds as described by Mirabella et al. (2005). For this task, LOI was determined in 2 g of oven-dried (60°C for two

days) soil material ignited at 1000° C over a period of two hours. For the cooling process, the material was carefully removed from the oven and set to rest in a glass desiccator for 24 hours. The material was weighed before and after the drying period in the oven.

### Grain Size Analysis: Wet Sieving and X-Ray Sedigraph

As stated by Egli et al. (2008), the fine earth fraction (< 2 mm) of some selected soil samples was pre-treated with H<sub>2</sub>O<sub>2</sub> (3%) before the the grain size distribution of the soils was assessed. For this task, soil samples were filtered through a series of progressively smaller sieves ranging from 2 mm to 0.032 mm. A total of eight sieves were stocked forming a tower on a shaker machine. As the shaker machine started to vibrate, tap water mixed with the soil sample ran through until discharged water came out clean. The material trapped by the sieves was oven dried for 2 days at 60° C and weighed. All discharged water was collected and let to settle for two days within a synthetic container. After two days, the now settled material within the containers was heated for a couple of minutes while a sample was taken and treated with hydrogen peroxide (H<sub>2</sub>O<sub>2</sub>) at a 1:1 ratio. To prevent the sample from resettling, ultrasound waves were employed for 5 minutes before the sedimentometre (SediGraph 5100) started working.

### Stable Organic Material Method for 14C (10 % H<sub>2</sub>O<sub>2</sub>)

The samples were prepared as follows: First, the soil samples were tested for carbonate existence with hydrogen chloride (HCL). Then, 2 g of fine (pre-dried) soil fraction (<2 mm) belonging to the first soil horizon of every soil profile were carefully weighed. Afterwards, the fine earth was wet with distilled water and rested for 10 minutes. As the ten minutes were finished, 180 ml of 10 % hydrogen peroxide (H<sub>2</sub>O<sub>2</sub>) were added to the samples. Further, the samples were heated and kept at a temperature of 45° C for a period of 7 days (168 hours). After the 7 days, the solution was poured out manually leaving only the remaining soil sample, which was then washed with distilled water while the pH was constantly controlled. The samples were oven dried once more at 50° C for two days and then transported to the ETH where the final <sup>14</sup>C measurements were performed.

### Diffuse Reflectance Infrared Fourier Transformation (DRIFT)

In order to investigate the mineral composition of the soil samples, an infrared spectroscopy technique known as DRIFT was employed. All samples were prepared in accordance with the so-called “powder method”. First, soil samples were heated for 2 hours at 105° C. Then, 30 mg of finely ground soil sample together with 270 mg of potassium bromide (KBr) were introduced to 5.0 ml Appendorf type microtubes

(Appendorf Safe Lock Tube <sup>TM</sup>, Germany) and set to shake for 45 seconds at a frequency of 10.0 Hz. Subsequently, the samples were heated for two hours at 60° C and analysed using a DRIFT-device at the UZH. Furthermore, since the classification was done manually, the identification of mineral peaks was in some cases unclear. Thus, a further analysis via R-statistics was conducted. For this task, we used a code provided by Dr. Samuel Abiven. The code basically looks for a specific segment (also called wavelength) in the data and compares it to the neighbouring segments. If the analysed segment turns out to be a local maximum the existence of a peak can be determined. The employed code is presented in the appendix.

## Organic Carbon Stocks Calculation (SOC)

According to Marvris et al. (2010), soil profiles tend to increase their carbon content over time. Therefore, we intended to correlate these carbon stocks with the calculated age of the soil profiles. C-stocks were measured as shown by several authors (Marvris et al., 2010; Dahms et al., 2012) using the following equation:

$$C_{stocks} = \sum_{a=1}^n C_{con} \cdot \Delta z \cdot p(1 - rm)$$

Where C-stocks represent the element abundance in kg/m<sup>2</sup>, C<sub>con</sub> the element concentration (kg/t), Δz stands for layer thickness (m), p for soil density (t/m<sup>3</sup>) and RM for the mass proportion of rock fragments.

## Weathering Indices

### *Index B*

In order to quantify the chemical weathering that the soil has undergone we used the B-index of Kronberg and Nesbitt (1981). The B-index performs based on the ratio of the base cations (mobile elements) to Al and/or Si (non-mobile elements). According to Munroe et al. (2007), weathering and leaching generate a loss of mobile elements over time, which in turn generates an enrichment of non-mobile elements. Consequently, the lower the index the higher the loss of mobile elements and the older the sample. The element molecular weights needed for the B-index, were first divided by their percentage weight (%) before the index could be employed. Element weights in percentage were obtained from the XRF measurements. The Index B is defined by the molar ratio of:

$$B = \frac{CaO + K_2O + Na_2O}{Al_2O_3 + CaO + K_2O + Na_2O}$$

*Molar Ratio of (K+Ca) / Ti*

As stated by Dahms et al. (2012), the molar ratio of (K+Ca) / Ti has been used to date rocks and can also be used as a weathering index ( $W_{\text{inx}}$ ) based on the fact that K and Ca are mobile elements, while Ti is considered to be an immobile element (Egli & Fitze, 2000; Stiles et al., 2003). This index functions according to the same principle as the Index B. The lower the ratio the higher the amount of weathering (Egli et al., 2008) and thus the older the sample. For this study, we used the molar ratio defined as follows:  $W_{\text{inx}}$  is the weathering that a soil has undergone. The number “1” is the element in g/kg divided by “2”, which is the molecular weight of the same element. Element weight in percentage was obtained from the XRF measurements. The (K+Ca) / Ti index is defined by the molar ratio of:

$$W_{\text{inx}} = \left( \frac{K_1}{K_2} + \frac{Ca_1}{Ca_2} \right) / \frac{Ti_1}{Ti_2}$$

*Weathering Index of Parker (WIP)*

Another weathering index employed was the index known as WIP. The WIP, created by Andrew Parker (1970), is an index designed specifically to study silicate rocks (Dahms et al., 2012). However, in its concept similar to the other weathering indices since it also works based on the ratio between mobile and immobile elements. Nevertheless, this index distinguishes itself from others by being resistant to local deviations (Dahms et al., 2012) and by only taking into account alkali and alkaline earth metals such as beryllium (Be), magnesium (Mg), calcium (Ca), strontium (Sr), barium (Ba) and radium (Ra) without excluding aluminium oxide ( $Al_2O_3$ ) (Price & Velbel, 2003). The weathering index WIP is defined by the molar ratio of:

$$100 * \left[ \left( \frac{2Na_2O}{0.35} \right) + \left( \frac{MgO}{0.9} \right) + \left( \frac{2K_2O}{0.25} \right) + \left( \frac{CaO}{0.7} \right) \right]$$

(Parker, 1970)

### III. RESULTS

#### Systematic Sampling

The following two tables show the location of the samples in the field and their respective elevation above sea level as well as the thickness of the ash layers located within a one-metre solum.

Profile: Site No. II						
<u>Point</u>	<u>Northings</u>	<u>Eastings</u>	<u>Elevation</u>	<u>Ash Thickness</u>	<u>Sand</u>	<u>Feature</u>
Nr.	N°	E°	(m)	(cm)	(cm)	
p0	37°58'56.3"	014°57'47.4"	1322	20	80	
p1	37°58'56.9"	014°57'45.9"	1312	30	70	
p2	37°58'57.4"	014°57'44.4"	1286	> 100	0	
p3	37°58'58.2"	014°57'42.3"	1288	20	80	
p4	37°58'59.2"	014°57'41.1"	1296	0	100	
p5	37°59'00.1"	014°57'39.7"	1316	80	20	
p6	37°59'01.4"	014°57'38.3"	1314	50	50	
p7	37°59'02.6"	014°57'39.6"	1318	15	85	
p8	37°59'01.5"	014°57'40.8"	1307	0	100	
p9	37°59'00.5"	014°57'42.2"	1306	20	80	
p10	37°58'59.5"	014°57'43.5"	1293	75	35	
p11	37°58'58.4"	014°57'44.6"	1289	>100	0	
p12	37°58'57.6"	014°57'45.7"	1304	10	90	
p13	37°58'57.0"	014°57'47.7"	1296	30	70	
p14	37°58'57.7"	014°57'49.2"	1285	>100	0	
p15	37°58'58.5"	014°57'47.9"	1285	90	10	
p16	37°58'59.3"	014°57'47.8"	1278	5	100	
p17	37°59'00.6"	014°57'46.1"	1287	5	95	
p18	37°59'01.4"	014°57'44.5"	1287	55	45	TM
p19	37°59'02.3"	014°57'43.4"	1297	15	85	
p20	37°59'03.3"	014°57'42.4"	1297	50	50	
p21	37°59'04.2"	014°47'43.1"	1277	55	45	
p22	37°59'03.3"	014°57'44.6"	1257	50	50	
p23	37°59'02.5"	014°57'46.2"	1271	0	100	TM
p24	37°59'01.7"	014°57'47.7"	1268	100	0	
p25	37°59'00.7"	014°57'49.0"	1261	>100	0	
p26	37°59'00.6"	014°57'49.9"	1270	>100	0	
p27	37°59'00.9"	014°57'51.3"	1277	100	0	
p28	37°59'00.0"	014°57'52.7"	1273	80	20	
p29	37°59'00.8"	014°57'51.4"	1272	75	25	
p30	37°59'01.7"	014°57'50.0"	1265	100	0	
p31	37°59'02.8"	014°57'48.7"	1267	40	60	
p32	37°59'03.3"	014°57'47.2"	1270	30	70	
p33	37°59'04.1"	014°57'45.6"	1271	65	35	
p34	37°59'05.2"	014°57'44.0"	1273	80	20	
p35	37°59'05.9"	014°57'45.0"	1263	>100	0	
p36	37°59'05.0"	014°57'46.7"	1263	50	50	L
p37	37°59'04.2"	014°57'48.1"	1260	0	100	
p38	37°59'03.2"	014°57'49.5"	1261	35	75	
p39	37°59'02.1"	014°57'50.9"	1266	95	5	
p40	37°59'01.3"	014°57'52.1"	1279	55	45	
p41	37°59'00.4"	014°57'53.7"	1283	40	60	
p42	37°59'01.7"	014°57'53.7"	1288	20	80	
p43	37°59'03.4"	014°57'51.9"	1263	>100	0	
p44	37°57'04.5"	014°57'50.8"	1261	100	0	
p45	37°57'05.5"	014°57'48.5"	1258	>100	0	
p46	37°57'06.2"	014°57'47.1"	1259	>100	0	

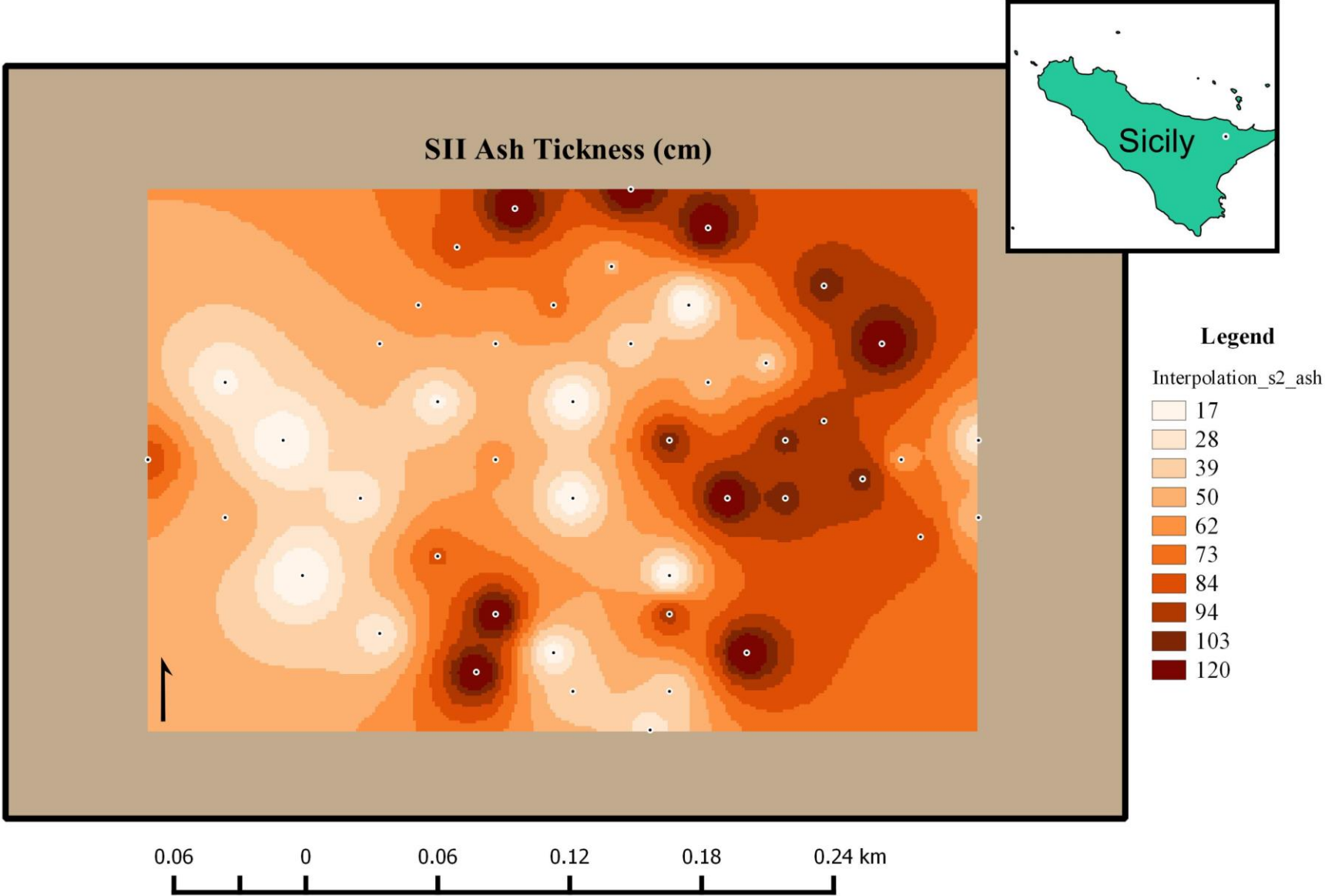
Tab. 3 Systematic Sampling for ash thickness at Site two

Profile: Site No. III						
Point -Nr.	Northings N°	Eastings E°	Elevation (m)	Ash Thickness (cm)	Sand (cm)	Feature
s0	37°59'07.9"	014°59'12.9"	1282	>100	0	
s1	37°59'06.7"	014°59'12.7"	1275	2	98	BC
s2	37°59'05.8"	014°59'11.4"	1273	45	60	
s3	37°59'04.3"	014°59'10.4"	1271	40	60	
s4	37°59'03.0"	014°59'09.5"	1272	0	100	
s5	37°59'01.6"	014°59'08.3"	1271	0	100	
s6	37°59'00.4"	014°59'07.5"	1274	15	85	
s7	37°59'00.1"	014°59'07.2"	1273	1	99	
s8	37°59'00.7"	014°59'08.1"	1265	75	25	
s9	37°59'00.9"	014°59'09.1"	1259	100	0	
s10	37°59'01.3"	014°59'09.7"	1257	65	35	WS
s11	37°59'02.7"	014°59'10.6"	1254	0	100	
s12	37°59'05.5"	014°59'14.7"	1250	2	98	
s13	37°59'04.8"	014°59'13.1"	1247	85	15	
s14	37°59'05.5"	014°59'14.7"	1250	0	100	
s15	37°59'06.3"	014°59'15.7"	1253	2	98	
s16	37°59'07.7"	014°59'16.2"	1252	25	75	TM
s17	37°59'13.3"	014°59'21.2"	1240	10	90	
s18	37°59'06.6"	014°59'17.4"	1238	5	95	
s19	37°59'05.4"	014°59'16.3"	1244	>100	0	
s20	37°59'04.7"	014°59'15.0"	1243	5	95	
s21	37°59'03.7"	014°59'13.8"	1239	>100	0	
s22	37°59'02.7"	014°59'12.6"	1242	30	70	
s23	37°59'01.8"	014°59'11.5"	1245	>100	0	
s24	37°59'00.2"	014°59'10.5"	1249	70	30	
s25	37°59'00.0"	014°59'09.8"	1253	70	30	

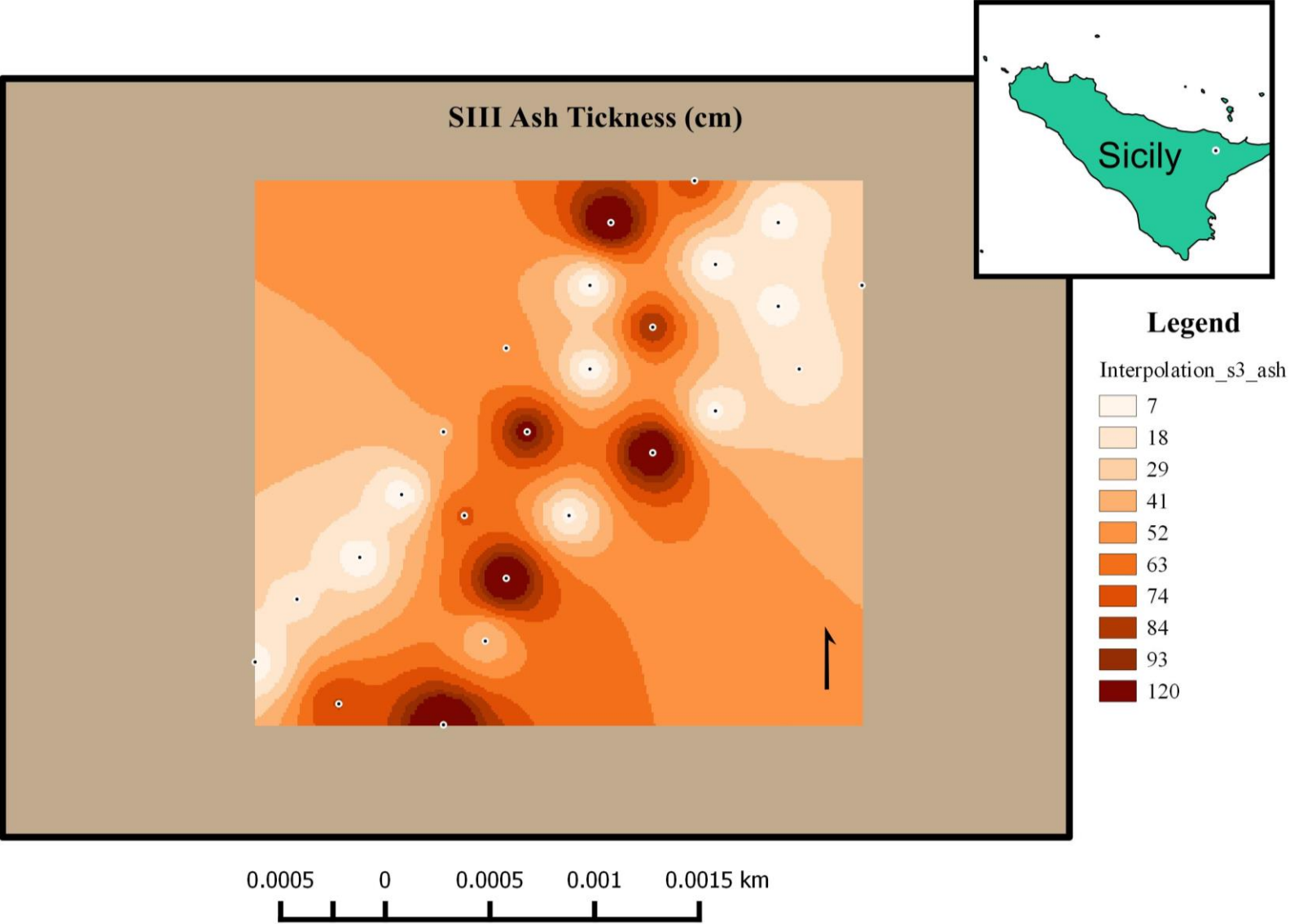
Tab. 4 Systematic Sampling for Ash thickness at Site Tree.

Totally Mixed = TM, Water Saturated = WS, Lapilli = L.

Soil Maps (Ash Thickness) SII



Soil Maps (Ash Thickness) SIII



## Soil Profiles

### Physical and Chemical Analyses

#### *Soil Profile I*

Soil profile SI is located at 37°59'15.5'' N and 14°58'41.1'' E at an elevation of 1,269 m.a.s.l. and it is illustrative of a soil evolved from pyroclastic deposits. Geographically speaking, the exposition and slope both equal zero. Overall, soil I shows a relatively high sand content with an approximated percentage of 53.36, followed by 26.73 percent silt and 19.9 percent clay (*tab. 8*). Accordingly, the soil texture at SI corresponds to a sandy clay loam (*fig. 17*). The profile is mainly made of volcanic ash and it has three visible horizons (A, AB, B) (*fig. 12*). One massive umbric (10 YR 1.7 / 1) first "A" horizon that stretches from the top down to 130 cm, followed by two more – comparatively small – horizons. The total depth of the soil profile is 160 cm. The average bulk dry density (BDD) is 1.12 g cm<sup>-3</sup> for the entire profile. The BDD ranges from 0.83 g cm<sup>-3</sup> at the top to 1.58 g cm<sup>-3</sup> at the bottom (*fig. 12*). On average, the first 130 cm belonging to the "A" Horizon have a BDD smaller than 1, while the rest of the profile shows a BDD above 1 (*tab. 7*). According to the USDA (1993), the soil profile can be described as "very strong acidic" due to its mean pH-value of 4.78. Also, because of the low pH-value, it is assumed that there are no carbonates located within the soil profile. As visible in *fig. 12*, the pH-value decreases with depth (from 4.9 to 4.6). Regarding the C/N-ratio, SI has a mean value of 14.8. The C/N-ratio increases with depth. It has its minimum value in the top soil (11.32) and its maximum at the bottom (24.4). Consequently, the nitrogen availability declines with the depth (*fig. 12*). As expected, organic matter decreases with depth as well (*tab. 5*). The total C (%) measured by the CHN-analyser decreases with the depth from its global maximum of 11.0 at the top to its global minimum of 0.39 at the bottom of the soil profile (*fig. 20*). The total C-stocks (kg/m<sup>2</sup>) increase with the depth for the first 100 cm reaching a global maximum of 28.9 kg/m<sup>2</sup>. Afterwards, the values decrease to a global minimum of 1.23 kg/m<sup>2</sup> as the next horizon begins. The concentrations of oxalate extractable Al, Fe and Mn behave similar to the C-stocks. First, they increase with the depth and after 100 cm the values decrease as the next horizon begins (*fig. 19* and *tab. 7*). Site I (SI) exhibits the highest value for the total average organic carbon per site with 102.50 kg/m<sup>2</sup> according to our results.

#### *Soil Profile II*

The soil profile SII is located at 37°59'01.6'' N and 014°57'51.6'' E at an elevation of 1,279 m.a.s.l. The geographical exposition of the site is 345° N with a slope of 11°. The profile has six visible horizons (A1, A2, IIBA, IIBw, IIIBc, IVBc) (*fig. 13*). The first two umbric (7.5 YR 3/1 and 7.5 YR 7/1) "A" horizons make up the majority of ash material and extend from the top to a depth of 50 cm. The total depth of the

soil profile is 170 cm. Overall, soil II shows a relatively high sand content with an approximated percentage of 48.66, followed by 27.86 percent silt and 23.48 percent clay (*tab. 8*). Accordingly, the soil texture at SII corresponds to a sandy clay loam (*fig. 17*). The average bulk dry density (BDD) is  $1.07 \text{ g cm}^{-3}$  for the entire profile. Initially, the BDD decreases with the depth for the first 90 cm (from 1.00 to  $0.74 \text{ g cm}^{-3}$ ) and then it starts to rise as deeper horizons are reached. On average, the first 90 cm have a BDD smaller than 1. As for the rest of the profile, the average BDD is higher than 1 (*tab. 7 and fig. 13*). According to the USDA (1993), the soil profile is “very strong acidic” with a mean pH-value of 4.9. Due to the low pH-value it is assumed that there are no carbonates located within this soil profile. The pH-value decreases with the depth (5.7 to 4.0) (*fig. 13*). Regarding the C/N-ratio, site 1 has a mean value of 23.1. The C/N-ratio increases with the depth with the exception of the horizon IIIBc (90-130), for which the equipment did not measure any nitrogen concentrations. The C/N-ratio has its minimum value (12.5) in the top soil and its maximum at the bottom (80.9). Consequently, the nitrogen availability increases with depth (*fig. 13*). The amounts of organic matter decrease with depth (*tab 5*). The total C (%) measured by the CHN-analyser increases with the depth for the first 50 cm and then decreases as the next two horizons begin, followed by a slight increase at the bottom of the soil profile (*fig. 20*). The total C (%) decreases from a local maximum of 4.81 at the top to its global minimum of 0.30 at the bottom of the soil profile. The total C-stocks ( $\text{kg/m}^2$ ) decrease from their local maximum of  $71 \text{ kg/m}^2$  at the top to their global minimum of  $1.07 \text{ kg/m}^2$  at the bottom of the soil profile. The concentrations of oxalate extractable Al and Fe increase with depth up to approximately 90 cm and then decrease abruptly as the next horizon begins. In contrast to this, the Mn concentration decreases continuously with the depth (*fig. 20 and tab. 7*). The total average organic carbon content at SII is  $36.72 \text{ kg/m}^2$ .

### *Soil Profile III*

Soil profile SIII is located at  $37^{\circ}59'05.9'' \text{ N}$  and  $014^{\circ}59'16.8'' \text{ E}$  at an elevation of 1,243 m.a.s.l. The exposition is  $90^{\circ}$  North and the slope  $80^{\circ}$ . The profile has six visible horizons (A1, A2, IIBw, IIIBCg, IIIBC, IVBc) (*fig. 14*). Similar to SII, SIII has two dark (umbric) (10 YR 3/2 and 10 YR 1.7/1) “A” horizons comprising the majority of ash material. They extend from the top to a depth of 75 cm. The total depth of the soil profile is 170 cm. Overall, soil III shows a relatively high sand content with an approximated percentage of 66.83, followed by 18.5 percent silt and 14.56 percent clay (*tab. 8*). Accordingly, the soil texture at SIII corresponds to a sandy loam (*fig. 17*). The average bulk dry density (BDD) is  $1.35 \text{ g cm}^{-3}$  for the entire profile. Initially, the BDD decreases with the depth for the first 75 cm (from 1.31 to  $0.97 \text{ g cm}^{-3}$ ) and then starts to rise as we reach the third and fourth horizon (depth 75 to 135 cm). However, the BDD decreases again in the last two horizons. Only the soil horizon lying between 50 and 75 cm shows a BDD below 1. As for the rest of the profile, the average BDD is always higher than 1 (*tab. 7 and fig. 14*).

According to the USDA (1993), the soil profile is “extreme acidic” with a mean pH-value of 4.4. It is assumed that there are no carbonates present in the soil profile due to the low pH-values. The pH-value decreases with the depth (4.9 to 3.9) (*fig. 14*). Regarding the C/N-ratio the equipment did not measure any concentrations for the horizons 110-135 and 155-170. However, general observations can still be made. SIII has a mean C/N-value of 13.9. The C/N-ratio increases with depth up to 110 cm. The C/N-ratio has its minimum value (14.4) in the top soil and its maximum at a depth of 75 cm (28.7) (*fig. 14*). Thus, there is more nitrogen available at the top than at the bottom. In general, the amount of organic matter decreases with depth (*tab. 5*). The total C (%) measured by the CHN-analyser revealed a clearly decreasing trend with the depth. The total C (%) decreases from 1.91 at the top to 0.26 at the bottom of the soil profile (*fig. 20*). The total C-stocks (kg/m<sup>2</sup>) also decrease with the depth from 12.4 kg/m<sup>2</sup> at the top to 0.4 kg/m<sup>2</sup> at the bottom. The concentrations of oxalate extractable Al, Fe and Mn behave in the same way as in SII (*fig. 20* and *tab. 7*). The total average organic carbon content at SIII is 27.54 kg/m<sup>2</sup>.

### *Soil Profile Floresta*

Soil profile Floresta is located at 37° 59'02,13" N and 14°57'51,37" E at an elevation of 1,264 m.a.s.l. The exposition is zero and the slope is 4°. The profile has six visible horizons (A1, A2, Btm, 2C, 3Co, 4Cb and 5C) (*fig. 15*). The soil profile is generally of a lighter colour. The first two “A” horizons have the same colour in wet conditions (10 YR 2/1) and can only be differentiated in dry conditions. They extend from the top down to a depth of 35 cm. The total depth of the soil profile is > 200 cm. Overall, Floresta shows a relatively low sand content with an approximated percentage of 34.7, followed by 28.16 percent silt and 36.8 percent clay (*tab 8*). Accordingly, the soil texture at Floresta corresponds to a clay loam (*fig. 17*). The average bulk dry density (BDD) is 0.99 g/cm<sup>3</sup> for the entire soil profile. The BDD increases with depth (from 0.80 to 1.30 g cm<sup>-3</sup>). The soil horizons lying between 0 and 135 cm have a BDD below 1, as for the rest of the profile, the average BDD is higher than 1 (*tab. 7 and fig. 15*). According to the USDA (1993), the soil profile can be described as a “strong acidic” with a mean pH-value of 5.0. It is assumed that there are no carbonates within the soil profile due to the low pH-value measured. In general, the pH-value decreases with depth (5.0 to 4.5) apart from the exception of the horizons 2C, 3Co and 4Cb (115-200 cm) (*fig. 15*). Regarding the C/N-ratio, Floresta has a mean value of 8.1. Overall, the C/N-ratio decreases with depth and slightly rises towards the bottom. The C/N-ratio has its minimum value (2.7) at a depth of 180 cm (Horizon 4Cb) and its maximum at the top 0-20 cm (11.3) (*fig. 15*). In general, the percentage of organic matter decreases with depth (4.8 to 0.6 %). However, there is a sharp increase between 35 and 115 cm (*tab. 5*). The total C (%) measured by the CHN-analyser revealed a clear decreasing trend. The total C (%) decreases from 3.21 at the top to 0.34 at the bottom of the soil profile (*fig. 20*). The total C-stocks (kg/m<sup>2</sup>) also decrease with the depth, from 4.87 kg/m<sup>2</sup> at the top to 0.34 kg/m<sup>2</sup> at the bottom. The concentrations of

oxalate extractable Al, Fe and Mn do not show any clear trends as they fluctuate along the soil profile (*fig. 19* and *tab. 7*). The total average organic carbon content at Floresta is 16.27 kg/m<sup>2</sup>.

### *Soil Profile Sila*

Soil profile Sila is located at 039°16'50'' N and 016°32'19'' E at an elevation of 1,572 m.a.s.l. The exposition is 195° North and the slope 7°. The profile has five visible horizons (A1, A2, Bw, B and C) (*fig. 16*). In contrast to all other sites, soil profile Sila has no dark horizons. The soil profile displays a variety of brown colours (10 YR 3/4, 10 YR 4/6, 10 YR 6/4, 10 YR 6/3). Compared to the other soil profiles, this is the shallowest soil profile. The total depth of the profile is 100 cm. Overall, Sila shows a relatively large sand content with an approximated percentage of 56.23, followed by 31.26 percent silt and 12.5 percent clay (*tab. 8*). Accordingly, the soil texture at Sila corresponds to a sandy loam (*fig. 17*). The average bulk dry density (BDD) is 1.14 g cm<sup>-3</sup> for the entire profile. The BDD increases with the depth (from 0.87 to 1.37 g cm<sup>-3</sup>). Only for the first 40 cm is the BDD lower than 1. For the soil horizons between 40 and 100 cm, the BDD is higher than 1 (*tab. 7*). According to the USDA (1993), the soil profile is “strong acidic” with a mean pH-value of 5.0. Due to the low pH at this soil profile it is assumed that there are no carbonates present. The pH-value increases with depth for the first 80 cm and then decreases slightly (*fig. 16*). Regarding the C/N-ratio, the site has a mean value of 11.4. The C/N-ratio decreases with depth (from 13.2 to 8.9). Overall, the amounts of organic matter decrease with the depth (from 10.8 to 0.71). The total C (%) measured with the help of the CHN-analyser revealed a clear decreasing trend. The total C (%) decreases from 5.86 at the top to 0.42 at the bottom of the soil profile (*fig. 20*). The total C-stocks (kg/m<sup>2</sup>) decrease with the depth from 9.99 kg/m<sup>2</sup> at the top to 1.02 kg/m<sup>2</sup> at the bottom. The total organic carbon content at Sila is 23.34 kg/m<sup>2</sup>. The concentration of oxalate extractable Mn is almost zero for the entire soil profile, while the concentration of Fe decreases with the depth from 4,213 to 230 mg/kg. In contrast to this, the amount of oxalate extractable Al presented an increase with the depth for the first 100 cm before decreasing to its local minimum of 10,493 mg/kg at the bottom of the soil profile (*fig. 19* and *tab. 7*).

### *Soil Profile Sila-DH*

Soil profile Sila-DH is a duplicate of the soil profile Sila and it is thus located at the same geographical coordinates. The profile has a total of five horizons (A1, A2, Bw, B, C) (*tab. 7*). The total depth of the soil profile is 100 cm. The average bulk dry density (BDD) is 1.09 g cm<sup>-3</sup> for the entire profile. The BDD increases with the depth from 0.83 to 1.43 g cm<sup>-3</sup>. Similar to Sila, Sila-DH has a BDD lower than 1 g/cm<sup>-3</sup> for the first 40 cm. Consequently, the BDD is higher than 1 gm/cm<sup>-3</sup> for the soil horizons between 40 and 100 cm (*tab. 7*). According to the USDA (1993), the soil profile is “strong acidic” with a mean pH-value

of 5.13. Due to the low pH at this soil profile it is assumed that there are no carbonates present in it. The pH-value decreases for the first 30 cm and then behaves like the soil profile Sila. In other words, it increases with depth for the first 80 cm and then decreases slightly (*tab. 7*). Regarding the C/N-ratio, the site has a mean value of 30.9. The C/N-ratio increases with depth. Overall, the amounts of organic matter decrease with the depth (from 7.73 to 0.93). Unfortunately, the equipment was not able to measure any value for the deepest 20 cm. The total C (%) measured by the CHN-analyser revealed a clearly decreasing trend with the depth. The total amount of C (%) decreases from 5.26 at the top to 0.54 at the bottom of the soil profile (*fig. 20*). The total C-stocks ( $\text{kg/m}^2$ ) decrease with the depth from  $8.43 \text{ kg/m}^2$  at the top to  $1.01 \text{ kg/m}^2$  at the bottom. The total average organic carbon content at Sila-DH is  $19.24 \text{ kg/m}^2$ . The concentration of oxalate extractable Mn is almost zero for the entire soil profile. Contrary to this, the oxalate extractable Fe increases in the first 30 cm where it also reaches its maximum ( $11,720 \text{ mg/kg}$ ). Afterwards, the value drops to zero. The amount of oxalate extractable Al shows no visible trend with depth (*fig. 19* and *tab. 7*).

# Soil Morphology and Characterization of the Soil Pits

## Morphology of Soil Profile SI

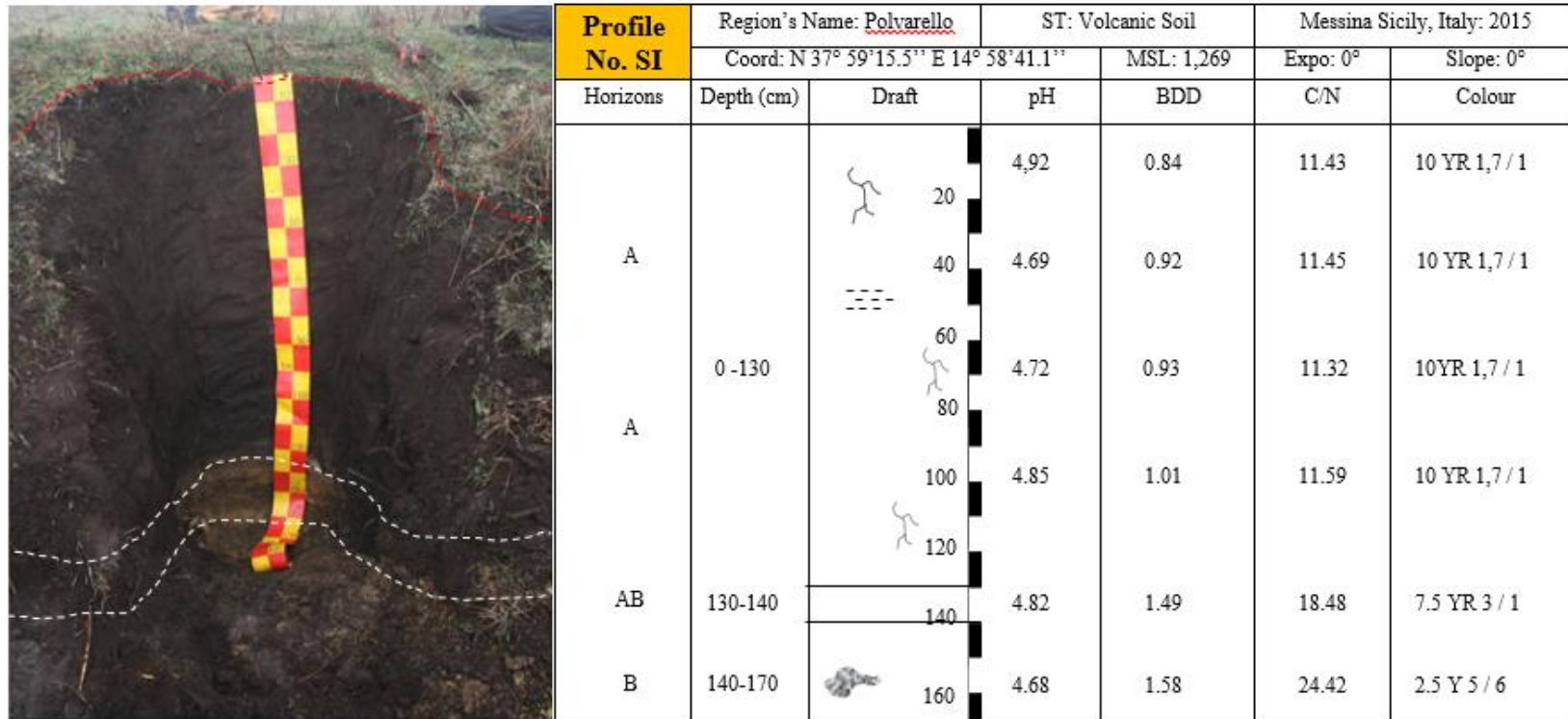
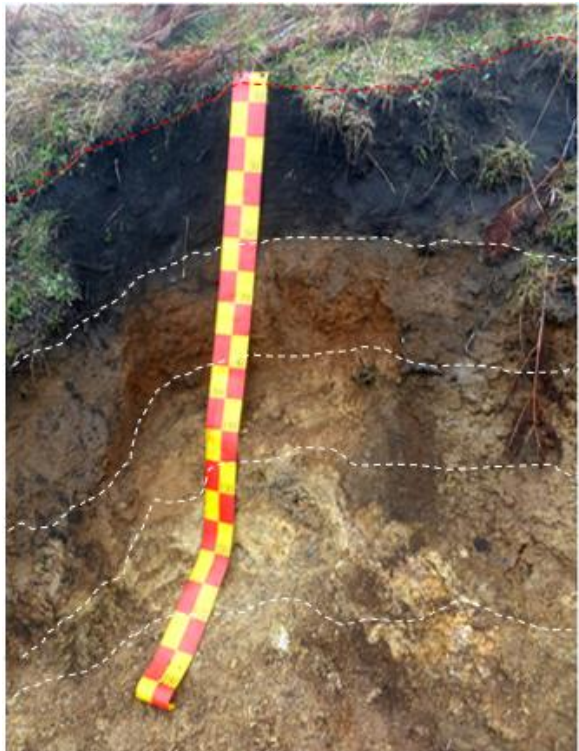


Fig. 12 Morphology of soil profile SI.

## Morphology of Soil Profile SII

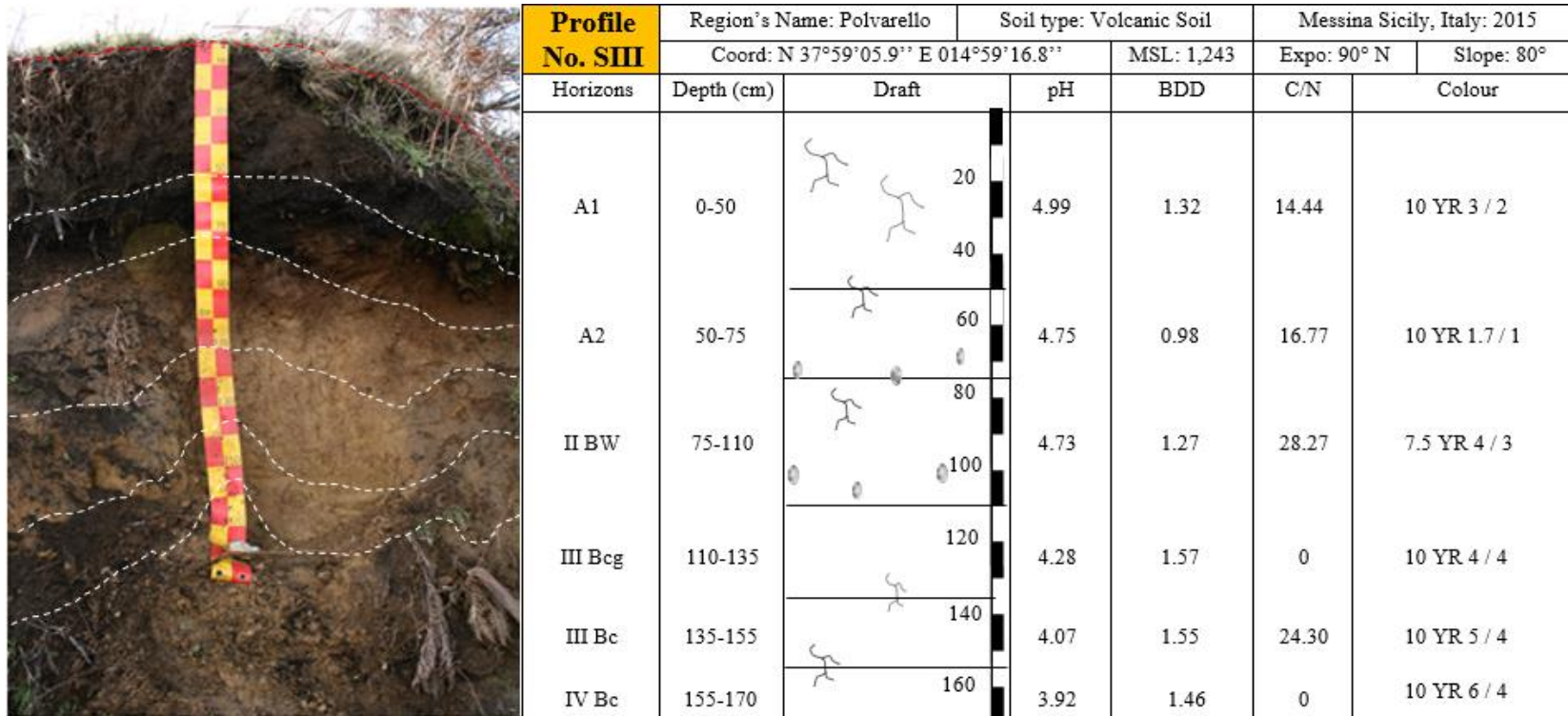


Profile No. SII	Region's Name: Polvarello		Soil type: Volcanic Soil		Messina Sicily, Italy: 2015	
	Coord: N 37°59'01.6" E 14°57'51.6"		MSL: 1,279		Expo: 345° N	Slope: 11°
Horizons	Depth (cm)	Draft	pH	BDD	C/N	Colour
A1	0-15		5.76	1.0	12.5	7.5 YR 3 / 1
A2	15-50		5.62	0.86	14.6	7.5 YR 1.7 / 1
II Ba	50-65		4.95	0.89	16.6	7.5 YR 4 / 4
II Bw	65-90		4.92	0.74	13.9	7.5 YR 4 / 4
III Bc	90-130		4.42	1.53	0	10 YR 5 / 4
IV Bc	130-170		4.02	1.38	80.9	10 YR 5 / 4

C/N measurements could not be made for the soil horizon 90 - 130.

Fig. 13 Morphology of soil profile SII.

## Morphology of Soil Profile SIII



*C/N measurements could not be made for the soil horizons 110-155 and 155-170.*

*Fig. 14 Morphology of soil profile SIII.*

## Morphology of Soil Profile Floresta



Profile Floresta	Region's Name: Floresta		Soil type: Volcanic Soil		Messina Sicily, Italy: 2015	
	Coord: N 37° 59' 02,13'' E 14°57' 51,37''		MSL: 1,264		Expo: 0° N	Slope: 4°
Horizons	Depth (cm)	Draft	pH	BDD	C/N	Colour
A1	0-20		5.00	0.80	11.30	10 YR 2 / 1
A2	20-35		5.00	0.80	9.91	10 YR 2/1
Btm	35-115	40	4.75	0.90	10.74	10 YR 3 / 6
		80				
2C	115-135		5.10	1.10	8.17	10 YR 3 / 4
3Co	135-180		5.30	1.10	7.64	7.5 YR 4 / 4
4Cb	180-200		5.75	1.25	2.68	2.5 Y 4 / 4
5C	>200		4.50	1.30	6.39	2.5 Y 4 / 0

Fig. 15 Morphology of soil profile Floresta.

### Morphology of Soil Profile Sila

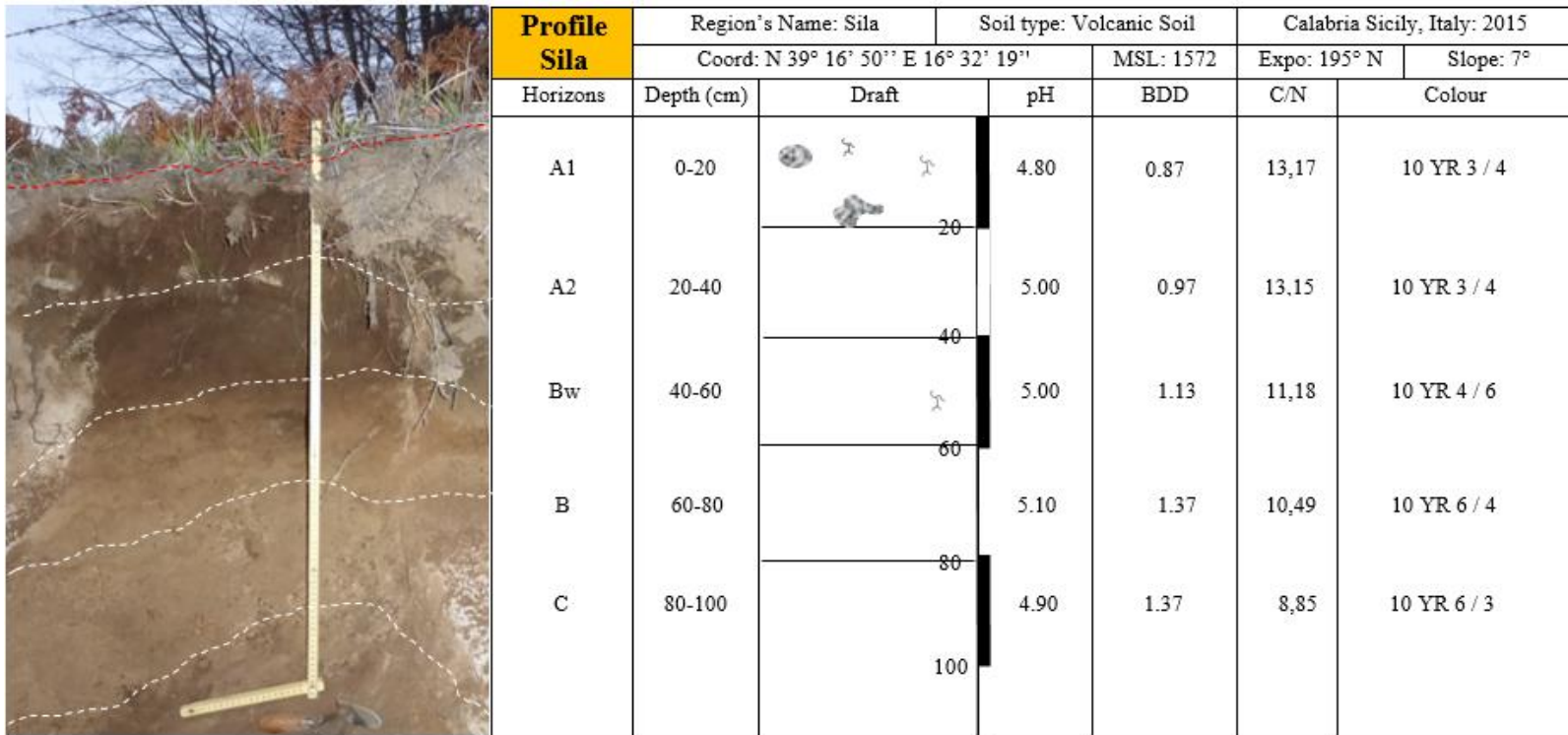


Fig. 16 Morphology of soil profile Sila.

## General Characteristics of the Soil Profiles

The composition of igneous rocks and their range reflects the average bulk composition of the crust. Principal elements are silicon (Si) and oxygen (O) and the most common oxide is silica (SiO<sub>2</sub>) with a percentage of 40 to 70. Further, important oxides are: alumina (Al<sub>2</sub>O<sub>3</sub>), magnesia (MgO), lime (CaO), soda (Na<sub>2</sub>O) and potassium (K<sub>2</sub>O). According to Dahms et al. (2012), high SiO<sub>2</sub>, Al<sub>2</sub>O<sub>3</sub>, Fe<sub>2</sub>O<sub>3</sub> and low base cation contents are a confirmation of the granitic characteristic of all sites. *Tab. 5* presents the total concentration of element oxides in weight percent for the investigated soil profiles obtained by means of XRF spectroscopy.

*Tab. 5 Total concentration of major element oxides, inorganic volatile compounds and organic matter content by horizons.*

Site	Depth (cm)	Horizon	Na <sub>2</sub> O %	MgO %	Al <sub>2</sub> O <sub>3</sub> %	SiO <sub>2</sub> %	P <sub>2</sub> O <sub>5</sub> %	K <sub>2</sub> O %	CaO %	TiO <sub>2</sub> %	MnO <sub>2</sub> %	Fe <sub>2</sub> O <sub>3</sub> %	LOI %	Org.M.	IVC
Sila	0-20	A1	1.94	0.47	19.34	50.00	0.26	2.48	2.13	0.74	0.09	5.12	17.43	10.24	7.19
	20-40	A2	1.86	0.48	20.18	52.04	0.24	2.65	2.28	0.74	0.08	5.24	14.21	6.87	7.34
	40-60	Bw	2.39	0.38	23.30	52.69	0.23	2.85	3.04	0.63	0.04	4.65	9.81	2.27	7.54
	60-80	B	2.47	0.37	23.61	53.68	0.26	2.89	3.33	0.68	0.03	5.07	7.60	1.39	6.21
	80-100	C	2.68	0.54	22.05	56.76	0.20	3.11	3.62	0.58	0.03	4.44	5.98	0.71	5.27
Floresta	0-20	A1	1.96	0.48	14.10	61.59	0.21	2.41	1.24	0.73	0.12	4.67	12.47	6.29	6.18
	20-35	A2	1.39	0.51	16.99	59.34	0.12	1.87	0.99	0.98	0.13	6.20	11.49	2.08	9.41
	35-115	Btm	1.77	0.56	22.33	45.06	0.45	1.12	2.00	1.56	0.14	8.30	16.72	1.84	14.88
	115-135	2C	2.75	0.62	24.02	43.91	0.72	0.94	3.67	1.63	0.21	8.63	12.89	1.01	11.87
	135-180	3Co	1.68	0.33	22.39	47.93	0.48	0.50	2.02	1.58	0.29	7.69	15.12	0.69	14.44
	180-200	4Cb	1.46	0.45	12.51	70.54	0.01	2.09	0.82	0.66	0.19	4.63	6.64	0.27	6.38
	>200	5C	0.46	0.40	8.75	72.64	0.01	1.23	0.43	0.51	0.01	6.95	8.60	0.55	8.05
SI	0-20	A	2.03	0.58	17.09	48.19	0.69	2.00	1.80	1.06	0.18	6.03	20.36	18.78	1.58
	20-50	A	1.99	0.58	18.61	51.52	0.67	2.11	1.55	1.12	0.19	6.29	15.37	15.37	0.00
	50-90	A	1.90	0.58	18.60	51.89	0.67	2.07	1.57	1.11	0.19	6.19	15.23	11.86	3.37
	90-130	A	2.17	0.61	19.35	51.68	0.71	2.09	1.71	1.15	0.19	6.29	14.07	13.00	1.07
	130-140	AB	1.90	0.82	19.95	64.72	0.22	2.87	1.33	0.70	0.09	3.93	3.48	1.62	1.85
	140-160	B	1.72	0.87	17.95	65.68	0.07	2.98	1.36	0.66	0.05	3.85	4.81	0.65	4.16
SII	0-15	A1	1.56	0.67	17.08	56.04	0.38	2.11	2.11	0.95	0.19	5.92	12.98	7.67	5.31
	15-50	A2	1.57	0.55	19.29	48.35	0.61	1.81	1.92	1.12	0.21	6.92	17.65	10.82	6.83
	50-65	IIBa	1.94	0.57	25.03	41.78	0.86	1.08	1.45	1.69	0.16	8.80	16.63	4.88	11.75
	65-90	IIBw	1.98	0.49	26.74	37.30	1.03	0.80	1.62	1.66	0.23	8.35	19.80	6.52	13.29
	90-130	IIIBc	0.92	0.44	10.20	76.07	0.05	1.45	0.49	0.49	0.16	4.41	5.33	0.44	4.89
	130-170	IV Bc	0.57	0.51	9.86	74.08	0.01	1.07	0.50	0.54	0.00	4.93	7.92	0.41	7.51
SIII	0-50	A1	2.12	0.70	16.73	67.05	0.15	2.93	0.97	0.57	0.07	3.29	5.42	2.97	2.45
	50-75	A2	1.96	0.64	21.48	53.64	0.52	2.28	1.00	1.06	0.13	5.81	11.50	6.63	4.87
	75-110	IIBw	1.95	0.69	23.76	56.75	0.49	2.33	1.15	1.03	0.09	5.28	6.48	1.51	4.97
	110-135	IIIBCg	2.09	0.66	16.87	68.94	0.05	3.14	0.72	0.52	0.07	3.36	3.58	0.37	3.21
	135-155	IIIBC	1.78	0.75	16.98	69.09	0.05	3.21	0.78	0.49	0.06	3.16	3.66	0.43	3.24
	155-170	IV Bc	1.44	0.83	17.23	65.36	0.04	2.92	0.79	0.66	0.07	4.30	6.36	0.40	5.96
Sila-DH	0-20	A1	1.96	0.56	22.98	51.24	0.22	2.47	2.13	0.87	0.11	5.91	11.54	7.73	3.81
	20-40	A2	2.13	0.40	24.91	47.90	0.33	2.56	2.96	0.79	0.05	5.84	12.13	5.46	6.67
	40-60	Bw	2.82	0.38	24.20	52.14	0.29	2.62	3.80	0.64	0.03	4.76	8.33	2.78	5.55
	60-80	B	3.57	0.41	25.74	53.55	0.31	2.58	3.98	0.62	0.03	4.67	4.53	0.74	3.80
	80-100	C	2.84	0.37	25.02	53.35	0.32	2.66	4.05	0.64	0.04	4.62	6.07	0.93	5.14

*Organic matter = total organic C x 1.72; total organic C was determined via a CHN-analyser. IVC = inorganic volatile compounds, estimated by LOI (loss on ignition). All analyses were conducted using only the fine earth fraction.*

The total concentrations of the major element oxides in weight percent for the quartz arenite found in the Nebrodi area are presented in *tab. 6*. The values were obtained via XRF spectroscopy.

*Tab. 6 Average composition of Nebrodi's parent material.*

Nebrodi n =2	Na <sub>2</sub> O (%)	MgO (%)	Al <sub>2</sub> O <sub>3</sub> (%)	SiO <sub>2</sub> (%)	P <sub>2</sub> O <sub>5</sub> (%)	K <sub>2</sub> O (%)	CaO (%)	TiO <sub>2</sub> (%)	MnO <sub>2</sub> (%)	Fe <sub>2</sub> O <sub>3</sub> (%)
Average Single Values	0.61	1.26	4.35	15.56	0.07	1.23	13.69	0.21	0.03	1.61
A	0.67	1.21	4.14	14.76	0.07	1.18	13.48	0.22	0.03	1.73
B	0.55	1.32	4.55	16.35	0.07	1.29	13.90	0.20	0.03	1.49

Further, the oxalate extractable concentration of the elements Al, Fe, Mn, together with the pH and dry bulk density is given in *tab. 7*.

*Tab. 7 Oxalate-extractable concentration, pH and bulk density of the sampled soils.*

Soil	Horizon	Depth (cm)	Al (mg/kg)	Mg (mg/kg)	Fe (mg/kg)	Bulk Density (g/cm <sup>3</sup> )	pH (CaCl <sub>2</sub> )
Sila	A1	0-20	5732.00	326.30	4213.00	0.87	4.80
	A2	20-40	6772.00	306.00	4003.00	0.97	5.00
	Bw	40-60	8825.00	58.50	1230.00	1.13	5.00
	B	60-80	9950.00	12.80	420.00	1.37	5.10
	C	80-100	9213.00	32.25	230.00	1.37	4.90
Floresta	A1	0-20	10493.00	453.25	5310.00	0.80	5.00
	A2	20-35	22955.00	424.60	7150.00	0.80	5.00
	Btm	35-115	1345.00	361.40	13010.00	0.90	4.75
	2C	115-135	10643.00	536.50	11090.00	1.10	5.10
	3Co	135-180	6808.00	1445.90	16450.00	1.10	5.30
	4Cb	180-200	304.00	101.20	2760.00	1.25	5.75
	5C	>200	0.00	23.10	2130.00	1.30	4.50
SI	A	0-20	7861.25	496.75	5950.00	0.84	4.92
	A	20-50	10683.13	523.75	6027.50	0.92	4.69
	A	50-90	11740.63	581.38	6817.50	0.93	4.72
	A	90-130	9663.75	458.88	6048.75	1.01	4.85
	AB	130-140	1028.13	201.50	2147.63	1.49	4.82
	B	140-160	363.88	169.00	728.38	1.58	4.68
SII	A1	0-15	4942.13	750.38	6947.50	1.00	5.76
	A2	15-50	14571.06	856.38	7410.00	0.86	5.62
	IIBA	50-65	38405.00	603.63	23262.50	0.89	4.95
	IIBw	65-90	63322.50	716.25	23212.50	0.74	4.92
	IIIBc	90-130	1219.50	1004.63	3713.75	1.54	4.42
	IV Bc	130-170	859.13	2.75	2825.00	1.39	4.02
SIII	A1	0-50	1447.25	180.00	1904.63	1.32	4.99
	A2	50-75	11284.38	355.88	7495.00	0.98	4.75
	IIBw	75-110	10860.42	214.17	6667.50	1.27	4.73
	IIIBCg	110-135	930.92	233.00	2193.25	1.57	4.28
	IIIBC	135-155	859.75	197.00	1677.38	1.55	4.07
	IVBc	155-170	1222.00	253.75	2042.50	1.46	3.92
Sila-DH	A1	0-20	7278.75	339.63	3955.00	0.90	5.13
	A2	20-40	7424.38	384.75	11720.00	0.83	5.01
	Bw	40-60	10795.00	50.13	2135.38	1.11	5.08
	B	60-80	6151.25	25.13	421.38	1.43	5.23
	C	80-100	9080.00	10.50	75.00	1.19	5.24

The soil texture per layer and the relative proportions achieved via wet sieving analysis are presented in *tab. 8*.

Site	Horizon	Depth (cm)	Sand %	Silt %	Clay %
Sila	A1	0-20	37.1	38.0	24.9
Sila	Bw	40-60	60.7	33.4	5.90
Sila	C	80-100	70.9	22.4	6.70
Floresta	A1	0-20	36.6	33.5	29.9
Floresta	Btm	35-115	54.0	31.0	15.0
Floresta	5C	>200	13.5	20.0	66.4
SI	A	0-20	34.8	44.7	20.5
SI	AB	130-140	68.3	16.6	15.1
SI	B	140-160	57.0	18.9	24.1
SII	A1	0-15	41.7	27.7	30.6
SII	A2	15-50	46.2	33.5	20.3
SII	IIBA	50-65	55.0	30.4	14.6
SII	IIBw	65-90	59.0	29.6	11.4
SII	IIBc	90-130	41.4	18.1	40.5
SIII	A1	0-50	63.6	18.3	18.1
SIII	IIBw	75-110	69.5	20.6	9.90
SIII	IVBc	155-170	67.7	16.6	15.70

*Tab. 8* Wet sieving measurements of the fine earth material.

## Soil Textural Triangle

Investigated Soil Profiles:

Red: Site I

Blue: Site II

Green: Site III

Black: Floresta

Yellow: Sila

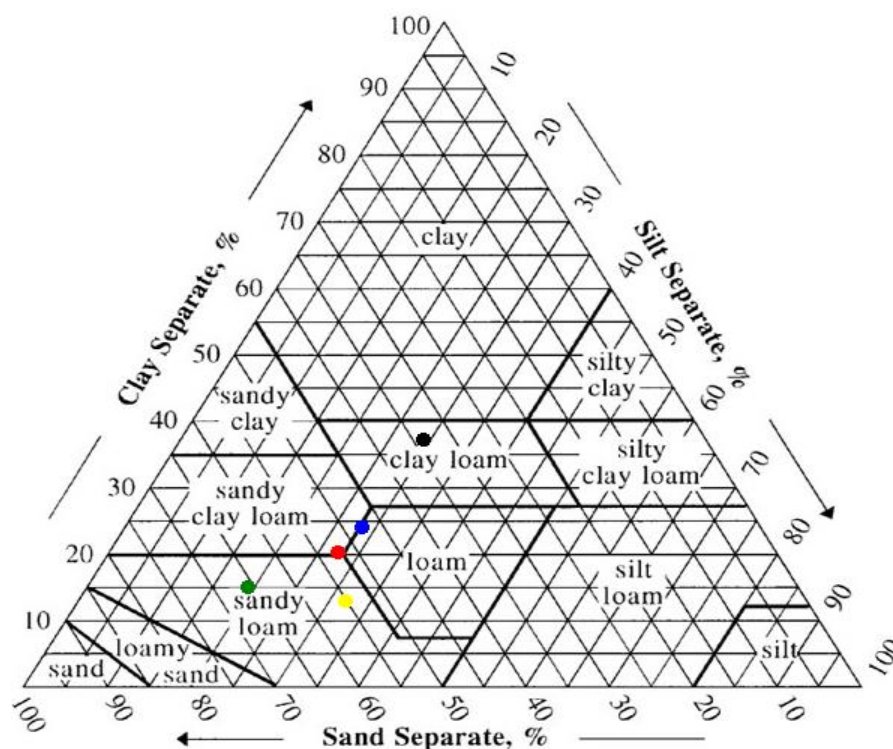


*Fig. 17* Soil texture pyramid according to the USDA (2014).

Oxalate Extraction of the Elements Fe, Al and Mn

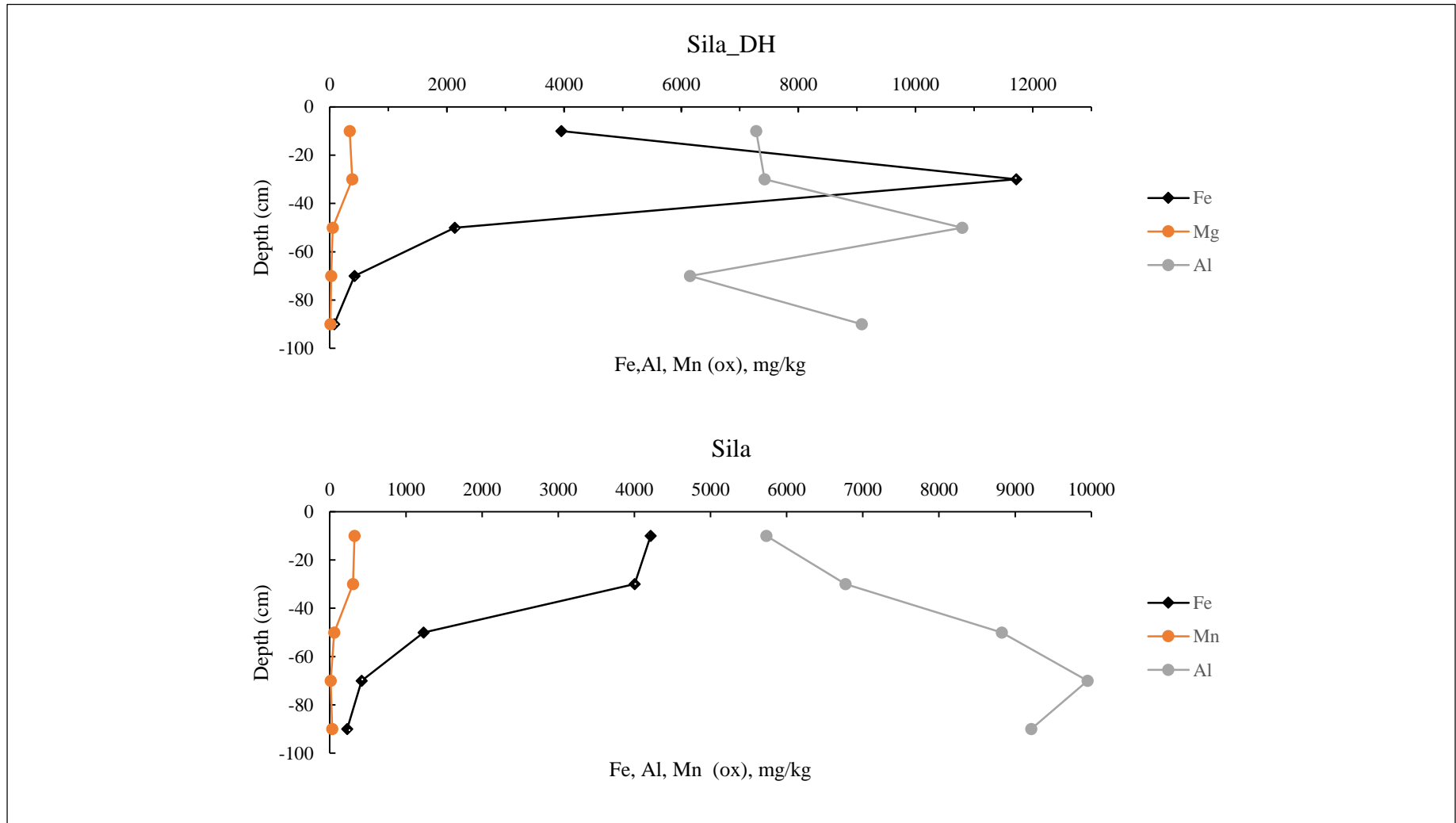


Fig. 18 Oxalate extraction as a concentration-depth function.

Oxalate Extraction of the Elements Fe, Al and Mn

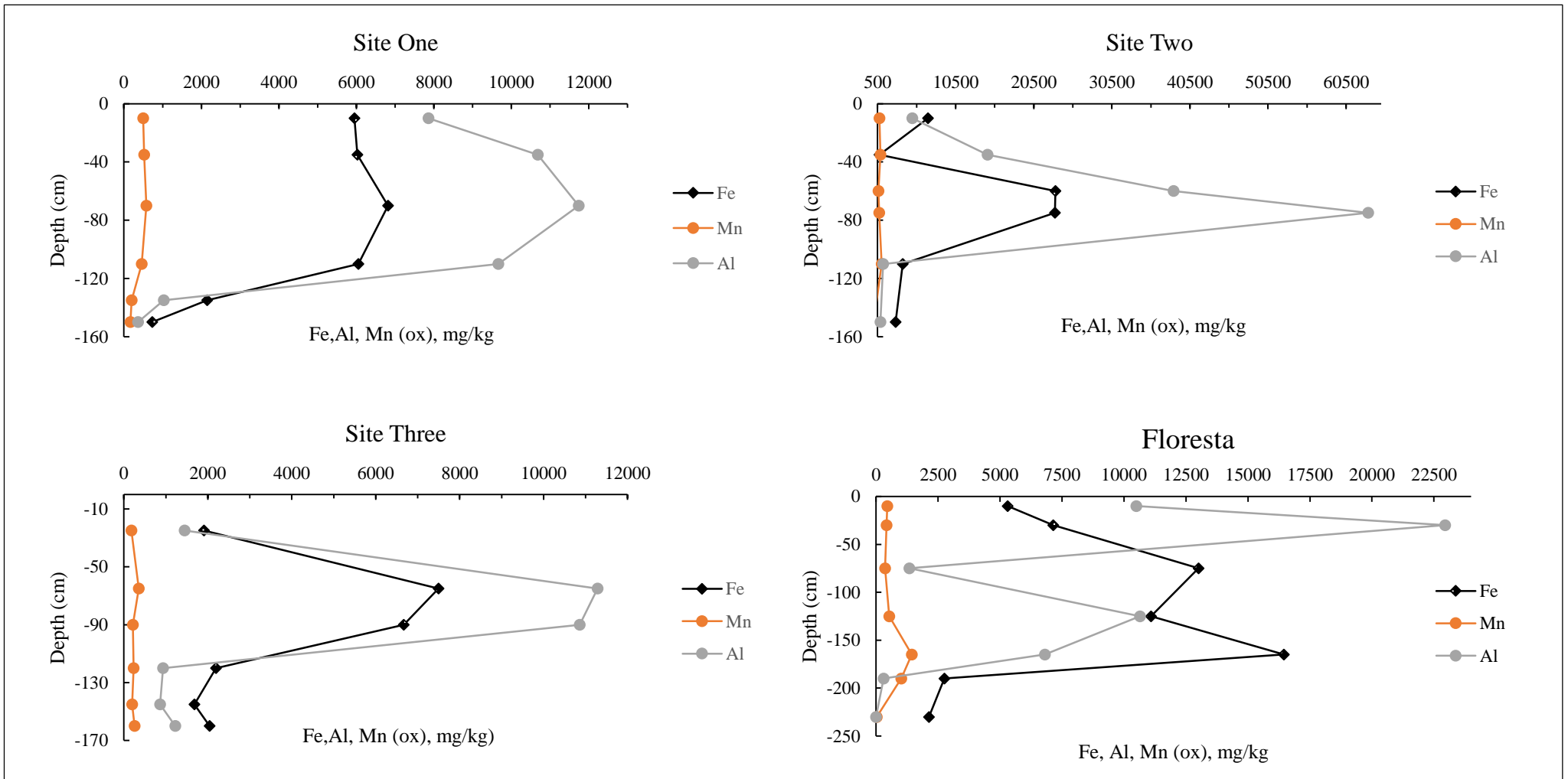


Fig. 19 Oxalate extraction as a concentration-depth function.

Measured Total Carbon Content (%)

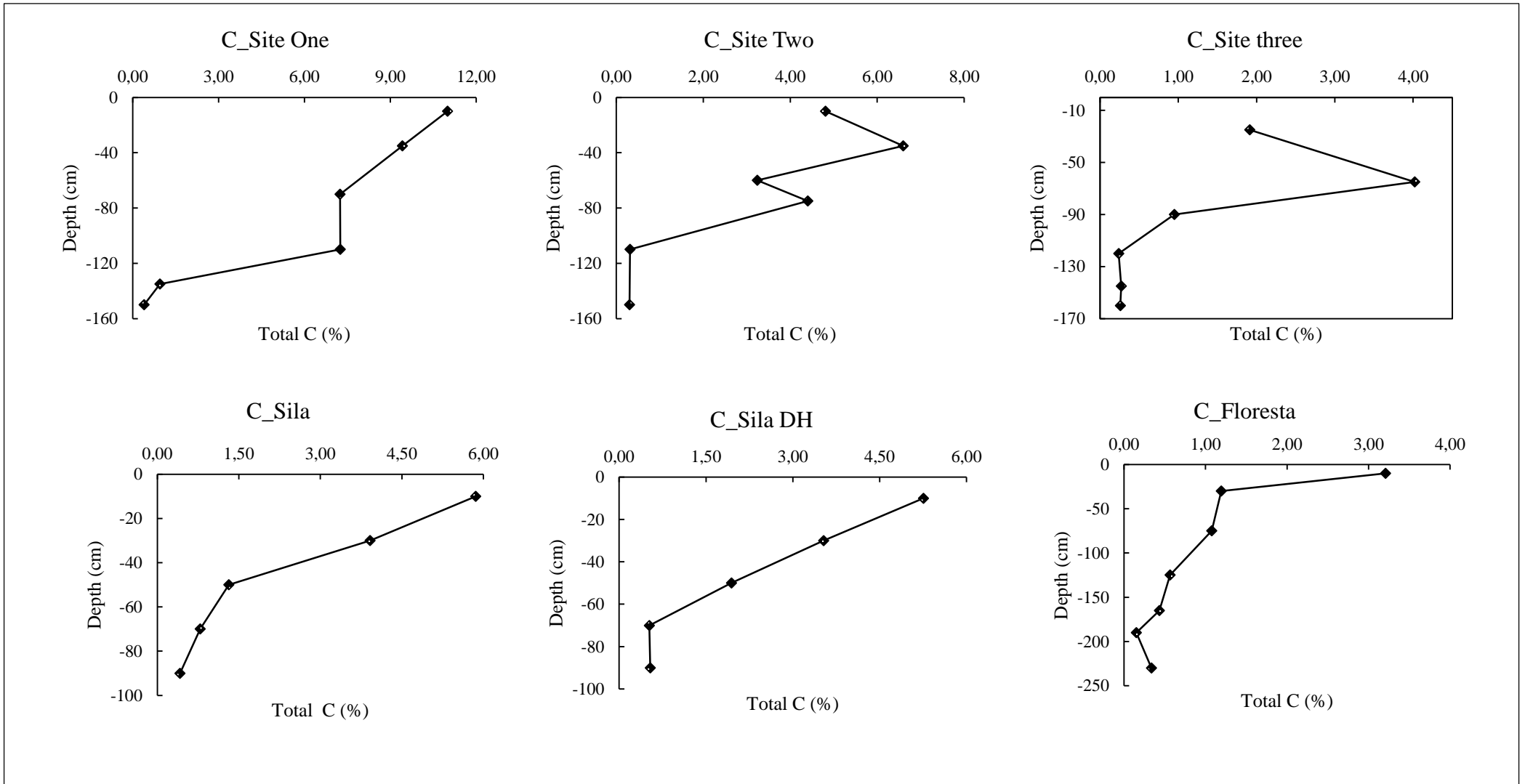


Fig. 20 Total carbon content in percent (%) as function of depth.

Measured (K+Ca) / Ti Ratio

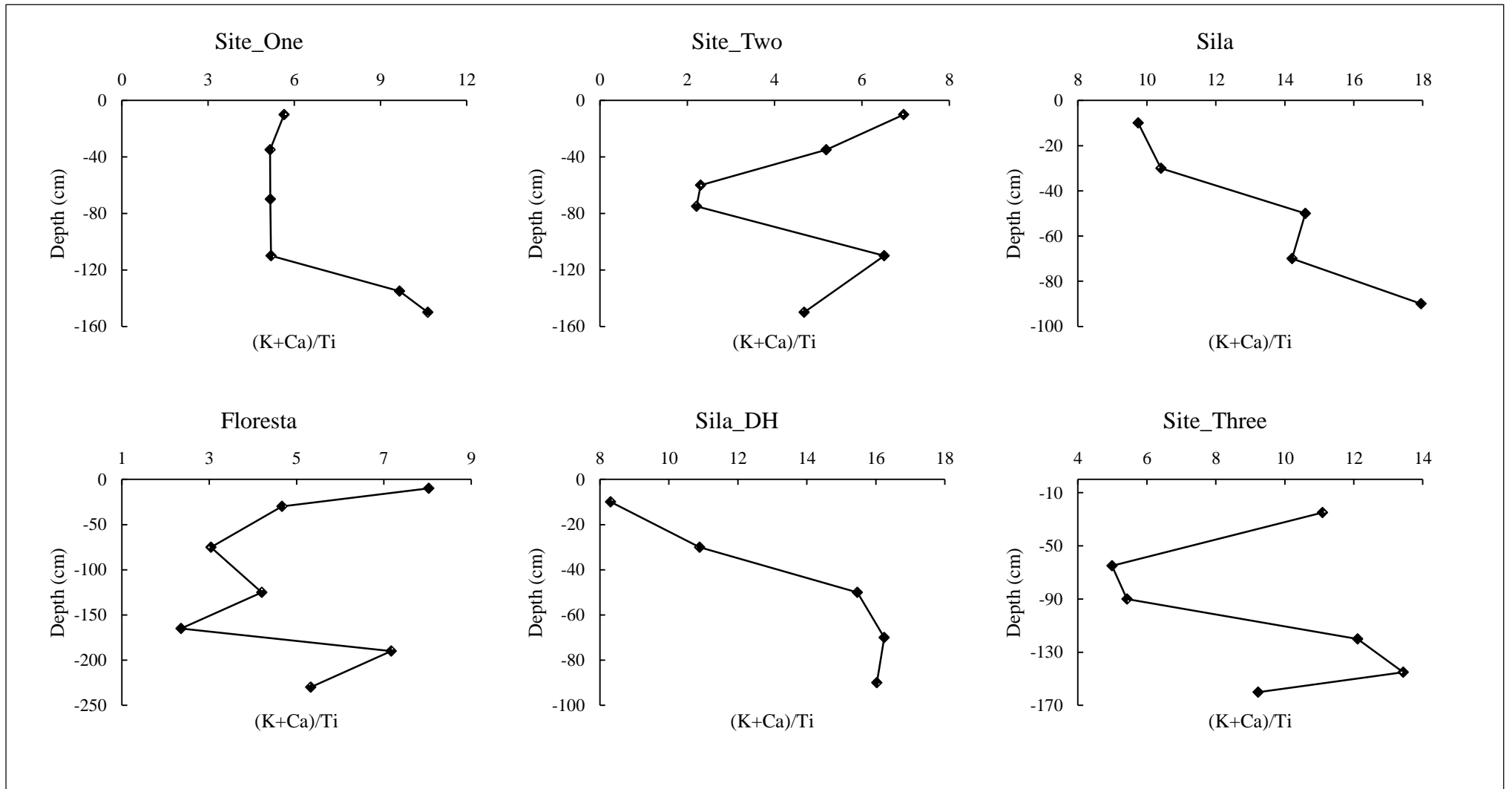
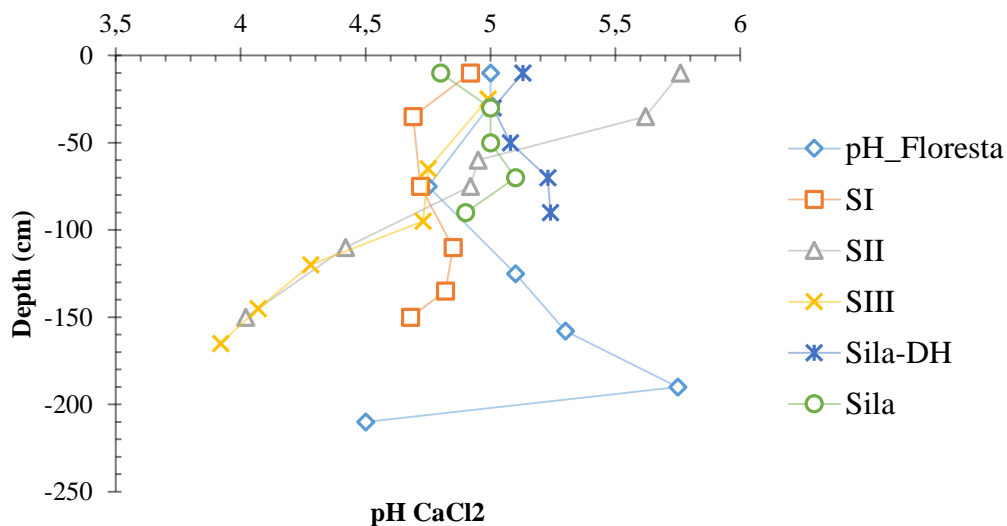


Fig. 21 (K + Ca) / Ti as a depth-function.

## Soil Reaction pH

As visible in *fig. 22*, the majority of the soil profiles have a pH-value close to 5 for the first 20 cm (top soil). Afterwards, all soil profiles have a pH-value ranging from 4.5 to 5.5 for the first 100 cm. Profile SII and SIII are the most acidic. Both reach values below 4.5 at a depth of 150 cm. At the same time, the highest pH-value measured and thus the lowest acidic milieu was found at profile SII with a value of 5.8, but only within the top soil. Not a single soil profile has a neutral pH-value. Two trends are detected: Overall, the soil profiles seem to maintain an acidic pH-value for the first metre. Additionally, the soil profiles tend to become strongly acidic with depth. Meaning, all sites show a decrease in pH towards their deepest soil horizons. In general, the investigated soil profiles can be denominated as “very strong acidic” or “strong acidic” according to the soil pH classification of the USDA (1993).



*Fig. 22 Total pH-values (CaCl<sub>2</sub>) as a function of depth.*

## Total Carbon Content (%)

As visible in *fig. 20*, the total carbon percentage measured by the CHN-analyser shows a clear negative trend. Overall, the percentage of carbon decreases with depth. The highest values were measured at site I, where the percentage of carbon reaches a value of 11. In general, the carbon content is higher within the first 10 cm of the soil profile. The only exceptions to this were sites SII and SIII. Both soil profiles showed an initial increase at a depth of 40 and 50 cm respectively.

## C/N Ratio

Nitrogen is the most abundant gas in the atmosphere, comprising 79%. In our soil, the main sources of nitrogen are so-called organic compounds. According to Sumner (1999), in soils with a significant amount of clay minerals (like illite capable of fixing  $\text{NH}_4^+$ ), around 90% of the soil nitrogen is contained within organic structures, followed by mineral nitrogen in the form of ammonium and nitrate ( $\text{NO}_3^-$ ). We use the C/N analysis in order to determine the amounts of nitrogen encompassed within the organic compounds. The C/N-ratio measured by the CHN-analyser is presented in *fig. 23*. A decrease in the ratio mean an increase in nitrogen availability. On the other hand, ratio increases or high values represent an increase in carbon availability (Stahr et al., 2012). According to the results, the ratio between carbon and nitrogen varied from 6 to 24. However, there is no overall visible trend exhibited by the sites. Yet, the sites can be separated into two groups: On the one hand, those in which the C/N-ratio increases with the depth and, on the other hand, those in which the ratio decreases with the depth. An increase towards the end of the soil pit was measured at the sites SI, SII and Sila-DH. In contrast to this, SIII, Floresta and Sila show an overall negative tendency. SIII, however, initially increases only slightly and then decreases again. Floresta and Sila show an entirely negative tendency towards the deeper layers. As shown in *fig. 23*, only two extreme values higher than 80 were measured (SII and Sila-DH).

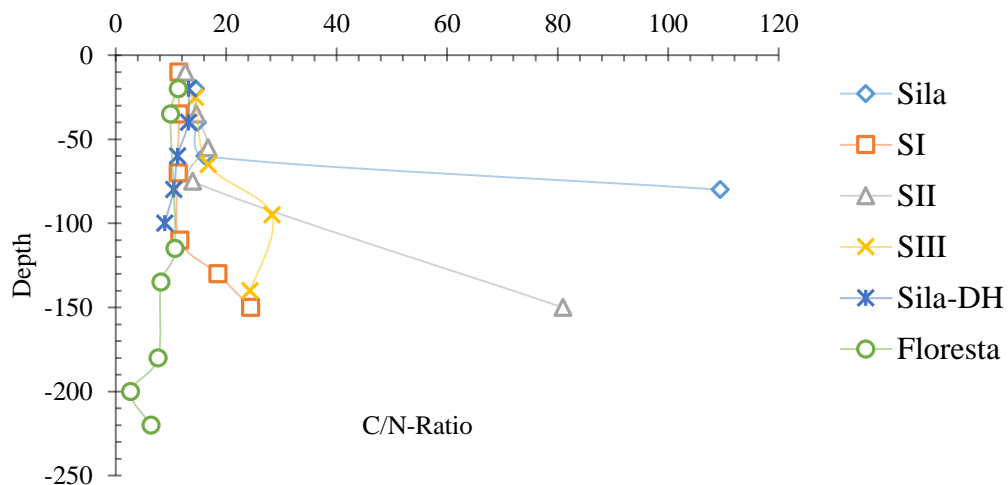


*Fig. 23 C/N ratio as function of depth.*

## Carbon Stocks Analysis

According to the analysis, the stocks of organic carbon decline with the depth at all sites. In general, the greatest amounts of soil organic carbon are located within the first 30 cm. Site I and Floresta are the only two soil profiles that show an increase in organic carbon with depth in the first 100 cm. The highest value measured was about 28 kg/m<sup>2</sup> at SI. Overall, the measured values vary between 4.8 and 18.2 kg/m<sup>2</sup> for the top soil (0 to 30 cm) and 1.2 and 26.7 kg/m<sup>2</sup> for the sub soil (30-100 cm). On average, the measured value for the top soil was 10.2 kg/m<sup>2</sup>, while the measured value for the sub soil was 8.3 kg/m<sup>2</sup>. Below a one-metre depth, all samples tend to become zero. Furthermore, *fig. 25* shows the total measured SOC stocks for the entire investigated soil profiles in relation to their calculated age. A local trend among the data is visible for the sites Sila, Sila-DH, SII and SIII. The results seem to indicate that the higher the stocks, the older the soils. The highest value was reached at SI with an amount of 102 kg/m<sup>2</sup>, while the lowest value was measured at Floresta with 19 kg/m<sup>2</sup>.

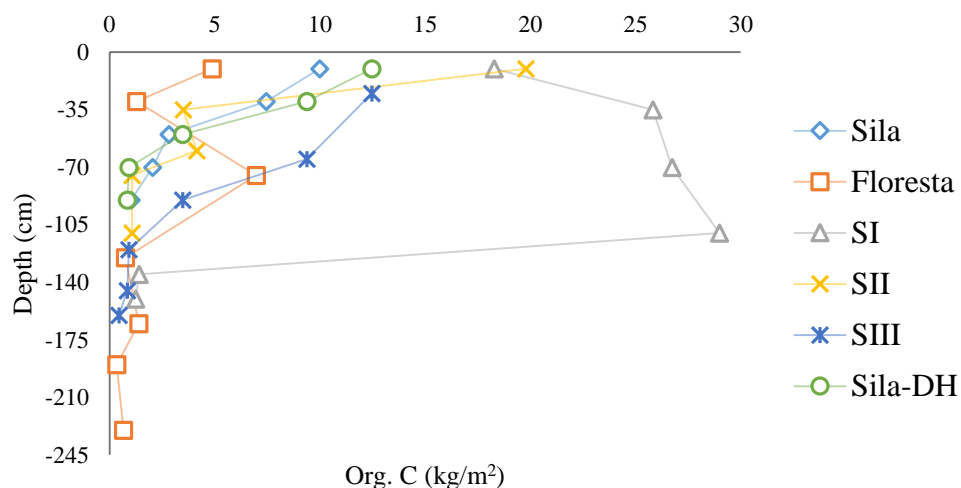


Fig. 24 Soil organic carbon content as depth function.

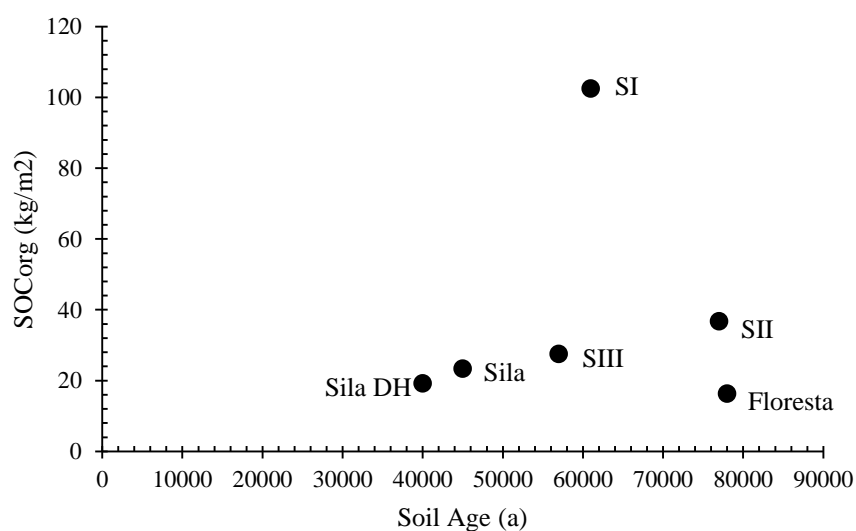


Fig. 25 SOC stocks as an age function.

## XRD Analysis

Tab. 9 Minerals found within Sila and Floresta via XRD.

Mineral	Sample	Sila (Ca)			Floresta		
	Depth	0-20	40-60	80-100	0-20	35-110	>200
Quartz		xxx	xx	xxx	xxx	?	xxx
Orthoclase		x	x	x	x	x	x
Albite		x	x	xx	x	xx	x
Mica		x	x	x	x	x	xx
Pyroxene		x	x	x	x	?	x
Amphibole					x		?
Smectite		x	x	xx	x	xx	xx
Vermiculite		x	x	x	x	x	x
Goethite		x	x	xx	x	x	x
Hematite		x	x	x	x	?	x
Calkite		-					
Chlorite							

? = Traces, questionable. X = Low measured amounts. XX = present. XXX = High amounts.

Mica = Biotite, muscovite and illite.

As aforementioned, some soil minerals found via DRIFT were further confirmed by means of R-statistics. Fig. 26 shows an example of how the mineral kaolinite was confirmed in one soil horizon of the site SII.

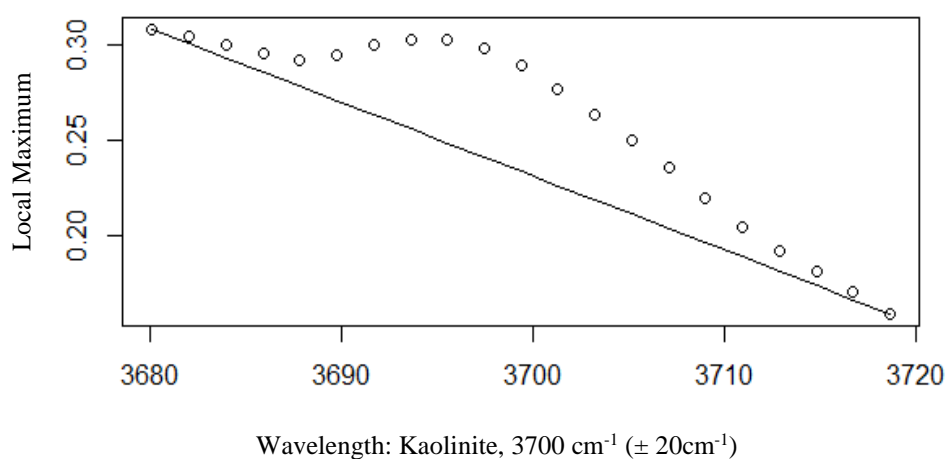


Fig. 26 DRIFT peak detection using R-statistics.

## DRIFT Analysis

Site	Horizon	Sample	Kaolinite	Gibbsite	Chlorite	Imogolite	Illite (Mica)	Quartz	Smectite	Okt. Mg/Fe	AlMgOH	Enstatite	Forsterite	Amphibole
Sila	A1	0-20	x	x	(x)	x	x	(x)		x	(x)			
	A2	20-40	x	x		x	(x)	(x)	(x)					(x)
	Bw	40-60	x	x		(x)	(x)	(x)	(x)					x
	B	60-80	x	x	?	?								x
	C	80-100	x	x		(x)	(x)							x
Floresta	A1	0-20	x	?		?	x	x						x
	A2	20-35	x	?				x						x
	Btm	35-115	x			(x)	(x)			(x)				
	2C	115-135	?	x	?	?			x					x
	3Co	135-180	x	(x)		(x)	(x)	(x)						
	4Cb	180-200	x	?		(x)		x						
5C	>200	(x)			(x)		x							
SI	A	0-20	x	x	?	(x)	x	x	(x)					x
	A	20-50	x	x	(X)	(x)	x	x	(x)					
	A	50-90	x	(x)			(x)	x	(x)					
	A	90-130	x	?		(x)	x	x	(x)					
	AB	130-140	x	(X)			x	x	(x)					
	B	140-160	x	?				x						
SII	A1	0-15	x	(X)			x		(X)		(x)			
	A2	15-50	x	x	(x)			x	(X)	(x)				
	IIBA	50-65	?	x				x						
	IIBw	65-90	(x)	x	(x)	(x)	(x)	(x)	(X)		(x)		x	
	IIIBc	90-130	?	?		(x)		x	(X)			x		
	IV Bc	130-170	?	?		(x)	(x)	(x)	(X)					
SIII	A1	0-50	(x)	x		(x)	x	(x)	(X)		x	(x)		
	A2	50-75	x	x	?		x	x	x		(x)	(x)		
	IIBw	75-110	x	x	X		x	x	(x)			(x)		
	IIIBCg	110-135	x	x	?	(X)	x	(x)			X			
	IIIBC	135-155	x	x	?	(X)	x	x	x		X			
	IV Bc	155-170	x	x		(X)	x	(x)	(X)	x	X	x		

? = Traces questionable. X = Low measured amounts. (X) = Assumed.

Tab. 10 Minerals found within the analysed soil profiles via DRIFT.

## Origin Determination

### Total Alkali-Silica (TAS)

According to the total-alkali-silica analysis, the investigated soil materials of the Nebrodi region belong to the sub-alkali series (*fig. 27*). Sub-alkali series encompass those rocks that are rich in silica ( $\text{SiO}_2$ ) compared to alkali metals ( $\text{Na}_2\text{O} + \text{K}_2\text{O}$ ) (Imperial College a\*, 2012). The igneous volcanic rocks found at the sites Floresta, SI, SII and SIII were classified as basalt, basaltic andesite, andesite, dacite and rhyolite (*tab. 11*). In the TAS-diagram, the samples coming from Nebrodi are located at an interval ranging from 49 to 80 % silica ( $\text{SiO}_2$ ) and 1.7 to 6.2 % alkali metals ( $\text{Na}_2\text{O} + \text{K}_2\text{O}$ ) (*fig. 28*). However, on average, the main volcanic rocks found in the Nebrodi area were dacite and rhyolite (*fig. 31*). These samples were located at a much smaller interval ranging from 64 to 75 % silica ( $\text{SiO}_2$ ) and 3.7 to 5.6 % alkali metals ( $\text{Na}_2\text{O} + \text{K}_2\text{O}$ ) (*fig. 29*). Dacite is an igneous volcanic rock of intermediate composition (meaning, a rock that has approximately 60 to 70 %  $\text{SiO}_2$ ) located between andesite and rhyolite (Fisher & Schmincke, 1984). Dacites are felsic extrusive rocks formed in subductions zones and like andesite, dacite encompasses plagioclase and feldspar as well as biotite, pyroxene and amphibole (Pffiffner et al., 2012). Geologically speaking, dacites are commonly formed as intrusive rocks. However, because of its moderate silica content the melt created by dacite is quite viscous and thus prompt to explosive eruptions (Fisher & Schmincke, 1984). Rhyolite is also an igneous volcanic rock with a high content of silica (ca. > 75% according to the TAS-diagram). The main mineral assembles of rhyolite are quartz and alkali feldspar (Imperial College b\*, 2013). Similar to dacite, rhyolite forms a highly viscous melt due to its high silica content and therefore many eruptions of rhyolite are highly explosive. The main deposits left by a rhyolite eruption largely consist of fallout ash (*ibid.*).

Based on the data provided by Egli et al. (2008), it was possible to investigate the chemical soil characteristics of Mount Etna's soils. The results suggest an alkali series (*fig. 28*). Consequently, volcanic soils stemming from Mount Etna are rich in alkali metals but poor in silica. The conducted analysis yields the following volcanic rocks: basalt, trachybasalt, basaltic trachyandesite and trachydacite (*tab. 11*). However, the majority of the analysed samples suggested that the main volcanic rocks coming from Mount Etna are trachybasalt and basaltic trachyandesite (*fig. 28*). These results are in agreement with the results of Egli et al. (2008). Further chemical analyses revealed that these volcanic rocks correspond to the alkali rocks known as basalt hawaiiite and mugearite due to their high sodic content ( $\text{NaCl}$ ) and low potassic content (*fig. 30*). As the name suggests, alkali rocks are rich in alkali metals ( $\text{Na}_2\text{O} + \text{K}_2\text{O}$ ) over silica ( $\text{SiO}_2$ ). Alkaline rocks are actually rare in nature but mineralogically speaking, they are more diverse and because of this, alkaline rocks comprise a large

number of rock types (Imperial College c\*, 2012). As stated before, in our analysis the majority of the volcanic rocks corresponding to Etna were hawaiite and mugearite. Hawaiite is a volcanic rock mainly made of andesine, anorthoclase, olivine, augite and biotite, while mugearite is mainly made of oligoclase, orthoclase, olivine, augite and biotite (Pfiffner et al., 2012). In accordance with our results, the samples stemming from Mount Etna are located at an interval ranging from 46 to 58 % silica ( $\text{SiO}_2$ ) and 4.3 to 6.5 % alkali metals ( $\text{Na}_2\text{O} + \text{K}_2\text{O}$ ) (*fig. 29*).

According to the data supplied by Mirabella et al. (2005), the investigated soils from the region of Lipari are located in the sub-alkali series of our TAS-diagram (*fig. 27*) Based on our results, the two sites Osservatorio, which are located in the southern part of the island, and the northern-located site Quattropani show a similar rock composition as the sites of Nebrodi. The sites Osservatorio and Quattropani encompass the rocks dacite and rhyolite (*fig. 28*). It is worth noticing that both sites on Lipari may share the same volcanic rock composition as other investigated sites. However, there seems to be a great physical and chemical difference between Osservatorio and Quattropani, which was also noted by Mirabella et al. (2005). According to the authors, Quattropani is made up of older material of basaltic-andesite composition, while Osservatorio consists of younger material chiefly made of rhyolite. Our results are in agreement with this as, according to the TAS-analysis, we found that the site Osservatorio is composed of rhyolite with a high content in silica (ca. 80 %) as well as alkali metals (ca. 7 %), while Quattropani consists of dacite with a low silica content compared to Quattropani (ca. 68 %) and an even lower alkali metal content (ca. 2 %) (*fig. 28*). The samples for the island of Lipari investigated by Mirabella et al. (2005) are located in our TAS-diagram at an interval that spans from 68 to 84 % silica ( $\text{SiO}_2$ ) and 1.9 to 8.5 % alkali metals ( $\text{Na}_2\text{O} + \text{K}_2\text{O}$ ) (*fig. 28*).

The investigated soils for the region of Catania (CT) known as Sila were classified according to our results as being of a sub-alkali series (*fig 27*). Meaning, samples coming from Sila are located at the lowest part of the TAS-diagram where volcanic material has a low concentration of alkali metals compared to the silica content. The samples originated from Sila are located at the following interval in our TAS-diagram: 57 to 67 % silica and 5 to 6 % alkali metals (*fig. 29*). The chemical analysis yielded the following rock types: basaltic andesite, andesite, dacite and basaltic trachyandesite (*tab. 11*). Yet, the main rock types found in the Sila region were classified as andesite and dacite even though some of the samples were close to the border of trachyandesite (*fig. 29*). According to the definition, andesite is the second most abundant volcanic rock besides basalt and the most common type of lava currently erupted by subaerial volcanoes (Fisher & Schmincke, 1984). Chemically speaking, andesites are rich in silica, alumina and calcium but poor in magnesia compared to basalts (Fisher & Schmincke, 1984). In general, andesite is rich in plagioclase, feldspar minerals and it may also include biotite, pyroxene or amphibole (Pfiffner et al., 2012). Dacite, as explained before, is a felsic extrusive rock

formed in subductions zones and encompasses plagioclase and feldspar with biotite, pyroxene and amphibole (Pfiffner et al., 2012). The analysed sites and their volcanic rocks found via the TAS-classification are presented in *tab. 11*.

Region	Site	Series	Rock classification according to the TAS-Analysis
Nebrodi	SI	Sub-Alkali	Dacite, Rhyolite
	SII	Sub-Alkali	Basalt, Basaltic Andesite, Dacite, Rhyolite
	SII	Sub-Alkali	Andesite, Dacite, Rhyolite
	Floresta	Sub-Alkali	Basalt, Basaltic Andesite, , Dacite, Rhyolite
Etna	1	Alkali-Series	Trachybasalt (Hawaiiite) Basaltic trachyandesite (Mugearite), Trachydacite
	2	Alkali-Series	Basalt, Trachybasalt (Hawaiiite), Basaltic Trachyandesite (Mugearite)
	3	Alkali-Series	Trachybasalt (Hawaiiite), Basaltic Trachyandesite (Mugearite)
	4	Alkali-Series	Trachybasalt (Hawaiiite), Basaltic Trachyandesite (Mugearite)
	5	Alkali-Series	Trachybasalt (Hawaiiite), Basaltic Trachyandesite (Mugearite), Trachyandesite
	7	Alkali-Series	Basalt, Trachybasalt (Hawaiiite)
Stromboli	P2	Sub-Alkali	Rhyolite
	G10	Sub-Alkali	Rhyolite
	F10	Sub-Alkali	Rhyolite
	CE	Sub-Alkali	Rhyolite
Sila	Sila	Sub-Alkali	Andesite, Dacite
	Sila_DH	Sub-Alkali	Trachyandesite, Andesite
Lipari	Osservatorio	Sub-Alkali	Rhyolite
	Quattropani	Sub-Alkali	Dacite, Rhyolite

*Tab. 11* Volcanic rock classification according to the TAS-analysis.

TAS-Diagram: Magma Series

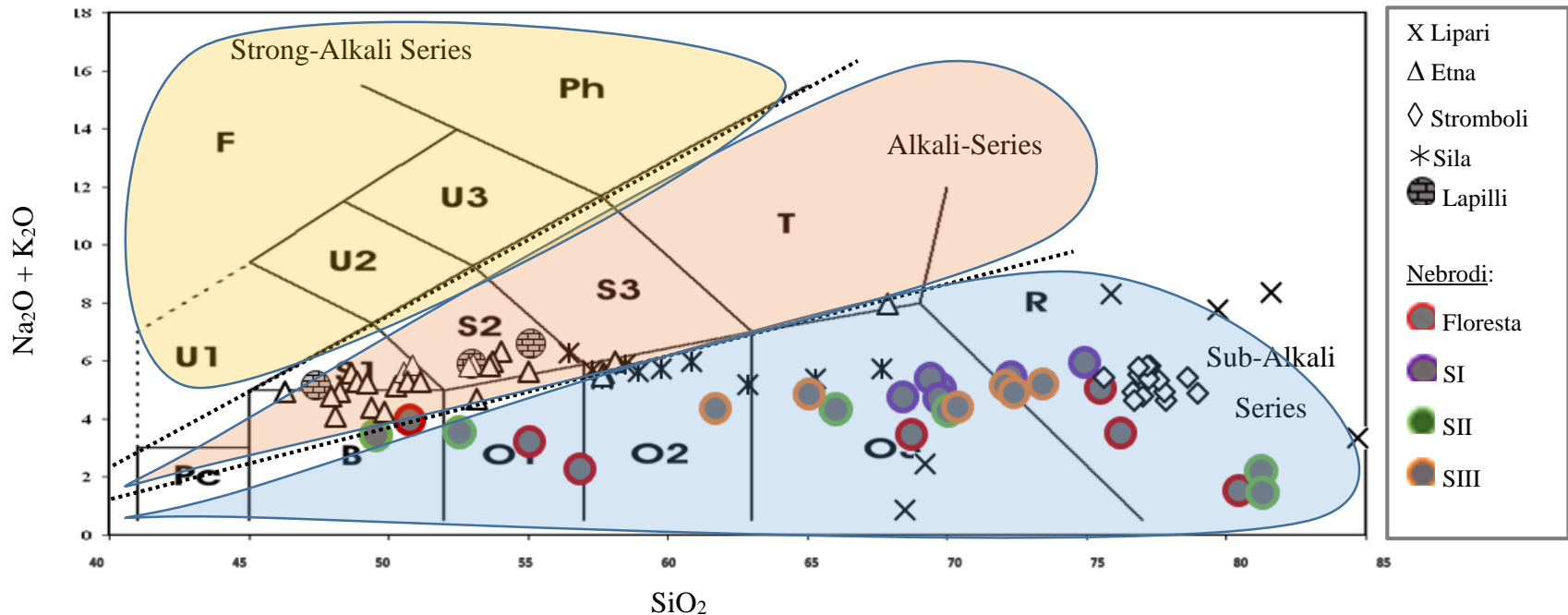


Fig. 27 TAS-Diagram magma series.

TAS-Diagram according to Le Bas et al. (1986). Nomenclature according to Le Maitre et al. (2002): B (Basalt), O1 (Basaltic andesite), O2 (Andesite), O3 (Dacite), R (Rhyolite), T (Trachyte or Trachydacite), Ph (Phonolite), S1 (Trachybasalt) \*Sodic and potassic variants are Hawaiite and potassic Trachybasalt, S2 (Basaltic trachyandesite) Sodic are Mugearite and potassic Shoshonite. S3 Trachyandesite \*Sodic and potassic variants are Benmoreite and Latite, Pc (Picrobasalt), U1 (Basanite or Tephrite), U2 (Phonotephrite), U3 (Tephriphonolite), F (Foidite). Orange area: Strong Alkali-Series. Red area: Alkali-Series. Blue area: Sub-Alkali-Series. The chemical analysis was recalculated to 100% excluding all water, carbon dioxide and organic matter. Represented data: Mirabella et al. (2005), Scarciglia et al. (2008) and Egli et al. (2008).

## TAS-Diagram: Investigated Sites and Their Clusters

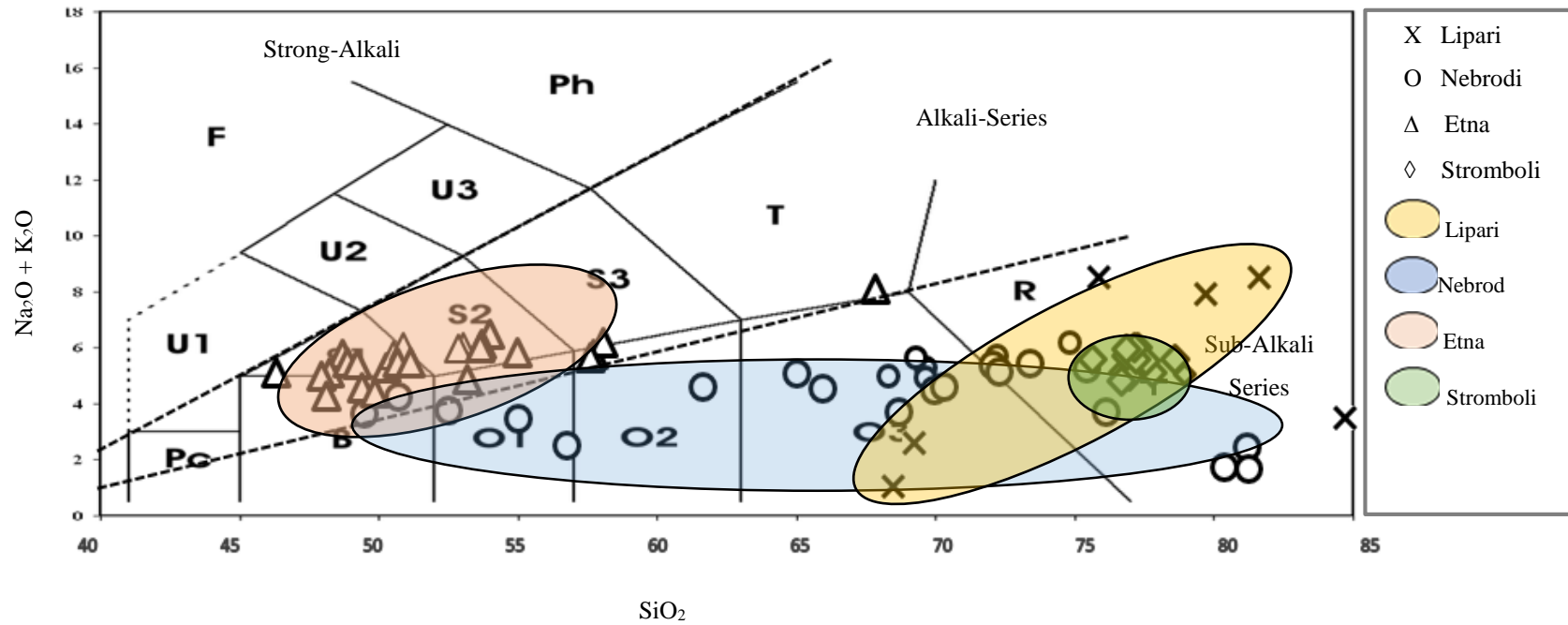


Fig. 28 TAS Diagram. Clusters.

TAS-Diagram according to Le Bas et al. (1986). Nomenclature according to Le Maitre et al. (2002): B (Basalt), O1 (Basaltic andesite), O2 (Andesite), O3 (Dacite), R (Rhyolite), T (Trachyte or Trachydacite), Ph (Phonolite), S1 (Trachybasalt) \*Sodic and potassic variants are Hawaiiite and potassic Trachybasalt, S2 (Basaltic trachyandesite) Sodic are Mugearite and potassic Shoshonite. S3 Trachyandesite \*Sodic and potassic variants are Benmoreite and Latite, Pc (Picobasalt), U1 (Basanite or Tephrite), U2 (Phonotephrite), U3 (Tephriphonolite), F (Foidite). Data from: Mirabella et al. (2005), Scarciglia et al. (2008) and Egli et al. (2008). The chemical analysis was recalculated to 100% excluding all water, carbon dioxide and organic matter.

## TAS-Diagram: Chemical Comparison of Lapilli Among Soil Samples

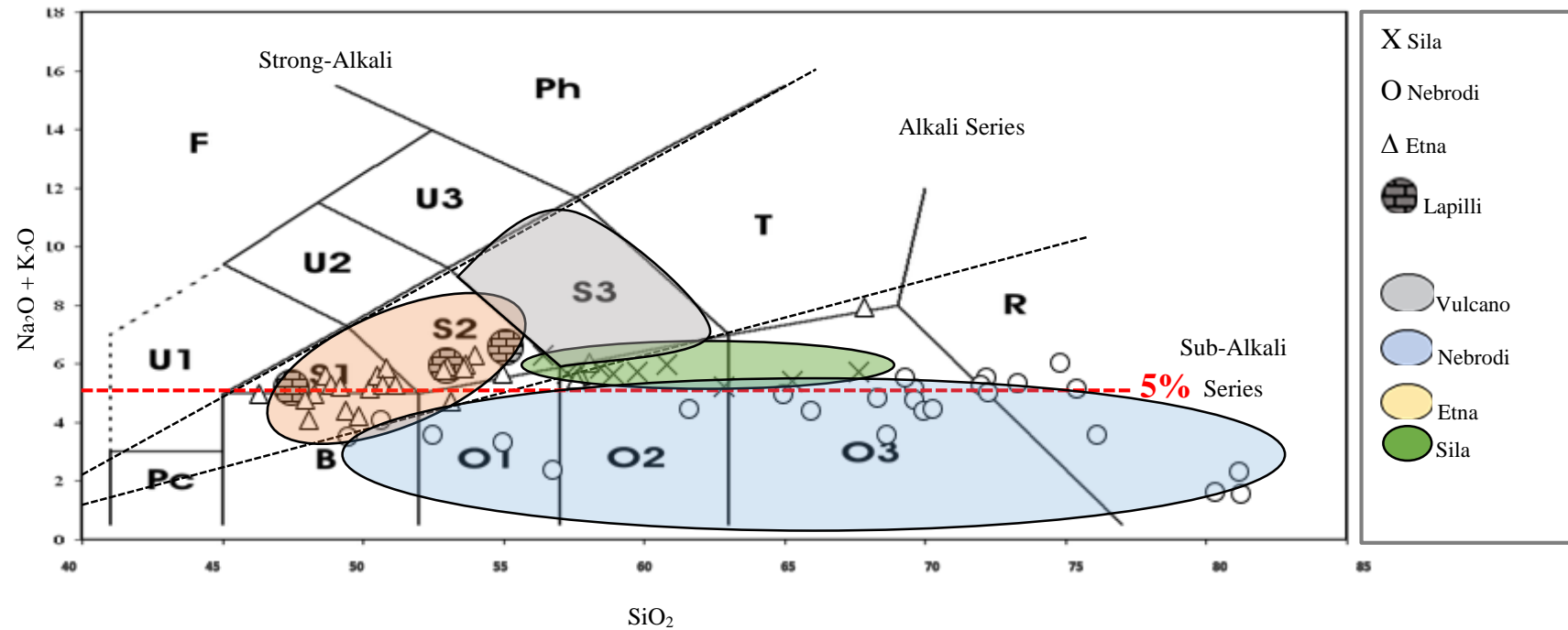


Fig. 29 TAS Diagram. Lapilli comparison among soil samples (Etna, Nebrodi and Sila and Vulcano).

TAS-Diagram according to Le Bas et al. (1986). Nomenclature according to Le Maitre et al. (2002): B (Basalt), O1 (Basaltic andesite), O2 (Andesite), O3 (Dacite), R (Rhyolite), T (Trachyte or Trachydacite), Ph (Phonolite), S1 (Trachybasalt) \*Sodic and potassic variants are Hawaiite and potassic Trachybasalt, S2 (Basaltic trachyandesite) Sodic are Mugearite and potassic Shoshonite, S3 Trachyandesite \*Sodic and potassic variants are Benmoreite and Latite, Pc (Picrobasalt), U1 (Basanite or Tephrite), U2 (Phonotephrite), U3 (Tephriphonolite), F (Foidite). Data from: Mirabella et al. (2005), Scarciglia et al. (2008) and Egli et al. (2008). Red line = 5% alkali metals. Gray cluster = hypothetical position of Shoshonites a typical rock of Vulcano according to Pichler (1981).

## K<sub>2</sub>O/SiO<sub>2</sub> Diagram: Volcanic Material and Their Clusters

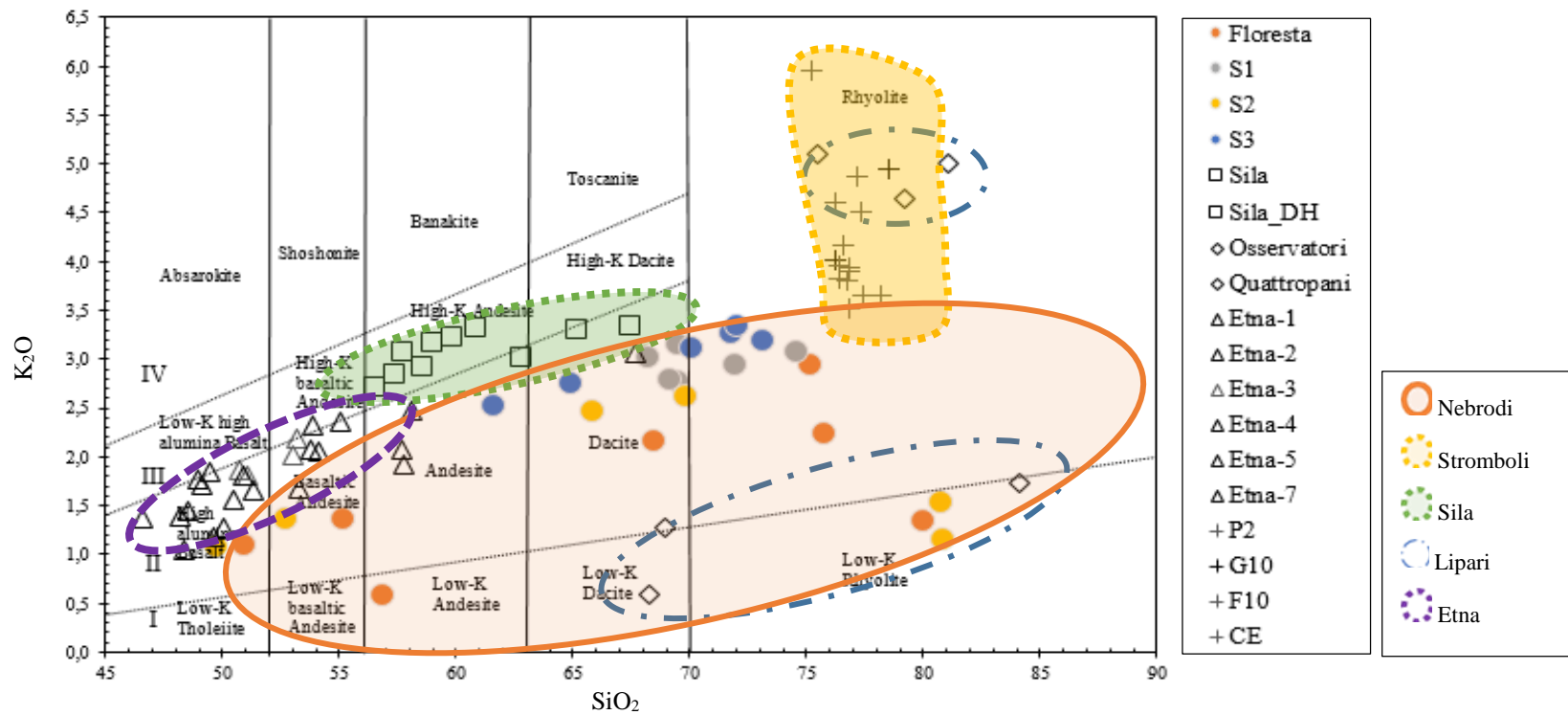


Fig. 30 K<sub>2</sub>O/SiO<sub>2</sub> Diagram: Clusters of the investigated volcanic

Classification of the volcanic material using the ratio of potassium oxide to silicon dioxide ( $K_2O / SiO_2$ ) according to Peccerillo and Taylor (1976). Modification of the four series according to Pichler (1981). I = Potassium poor calc alkaline “Andesite” series (Island-arc “Andesite”; arc tholeiite series). II = Normal calc alkaline “Andesite” series (Continental margin “Andesite”; calc alkaline series). III = Potassium rich calc alkaline “Andesite” series. (High potassium calc alkaline series). IV = Shoshonite series. Represented data from Mirabella et al. (2005), Scarciglia et al. (2008) and Egli et al. (2008).

K<sub>2</sub>O/SiO<sub>2</sub> Diagram: Nebrodi Soils Compared to Other Volcanic Materials

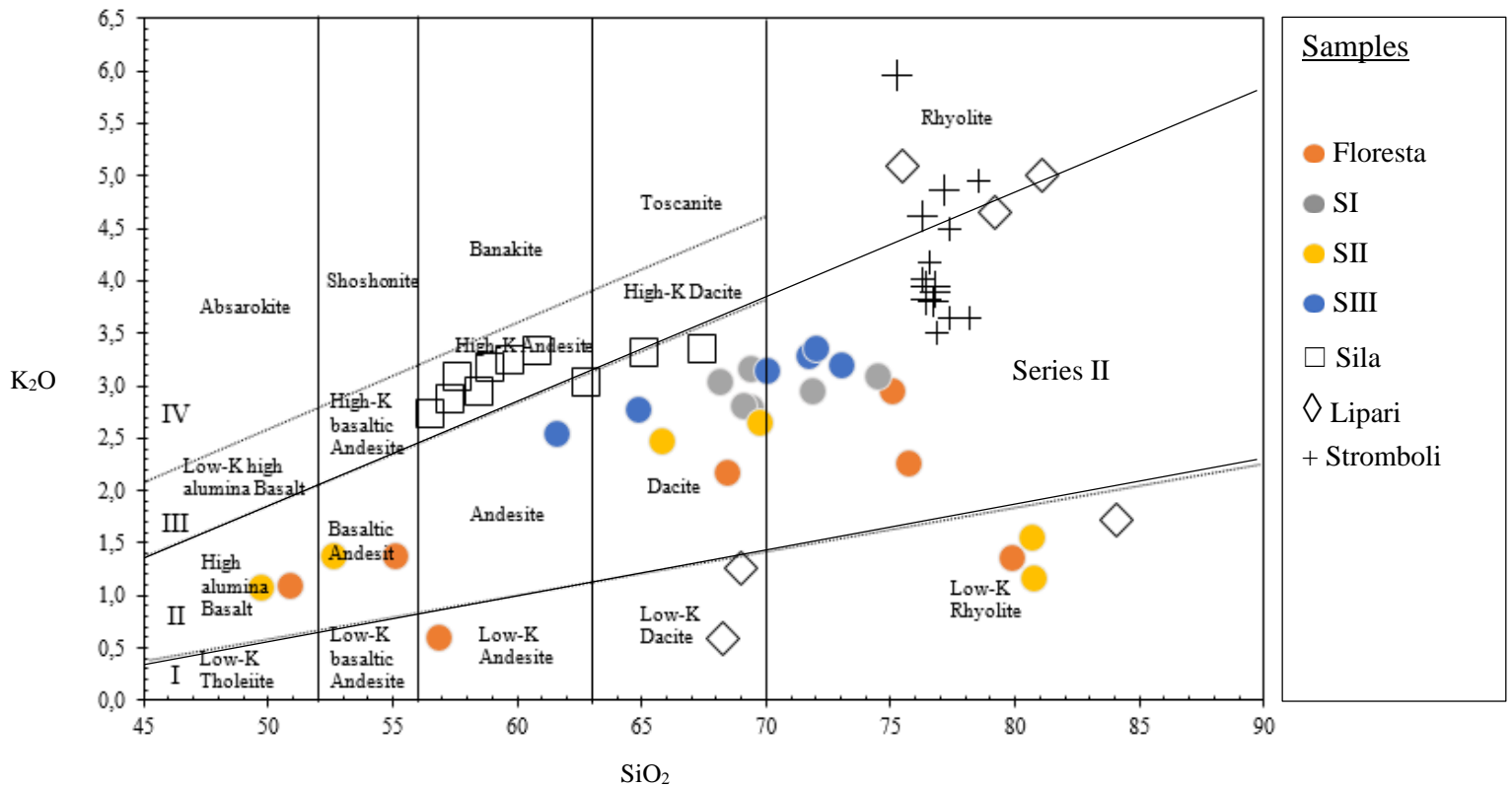


Fig. 31 K<sub>2</sub>O/SiO<sub>2</sub> diagram for Nebrodi.

Classification of the volcanic material using the ratio between potassium oxide and silicon dioxide (K<sub>2</sub>O / SiO<sub>2</sub>) according to Peccerillo and Taylor (1976). Modification of the four series according to Pichler (1981). I = Potassium poor calc alkaline “Andesite” series (Island-arc “Andesite”; arc tholeiite series). II = Normal calc alkaline “Andesite” series (Continental margin “Andesite”; calc alkaline series). III = Potassium rich calc alkaline “Andesite” series. (High potassium calc alkaline series). IV = Shoshonite series. Represented data from Mirabella et al. (2005), Scarciglia et al. (2008) and Egli et al. (2008).

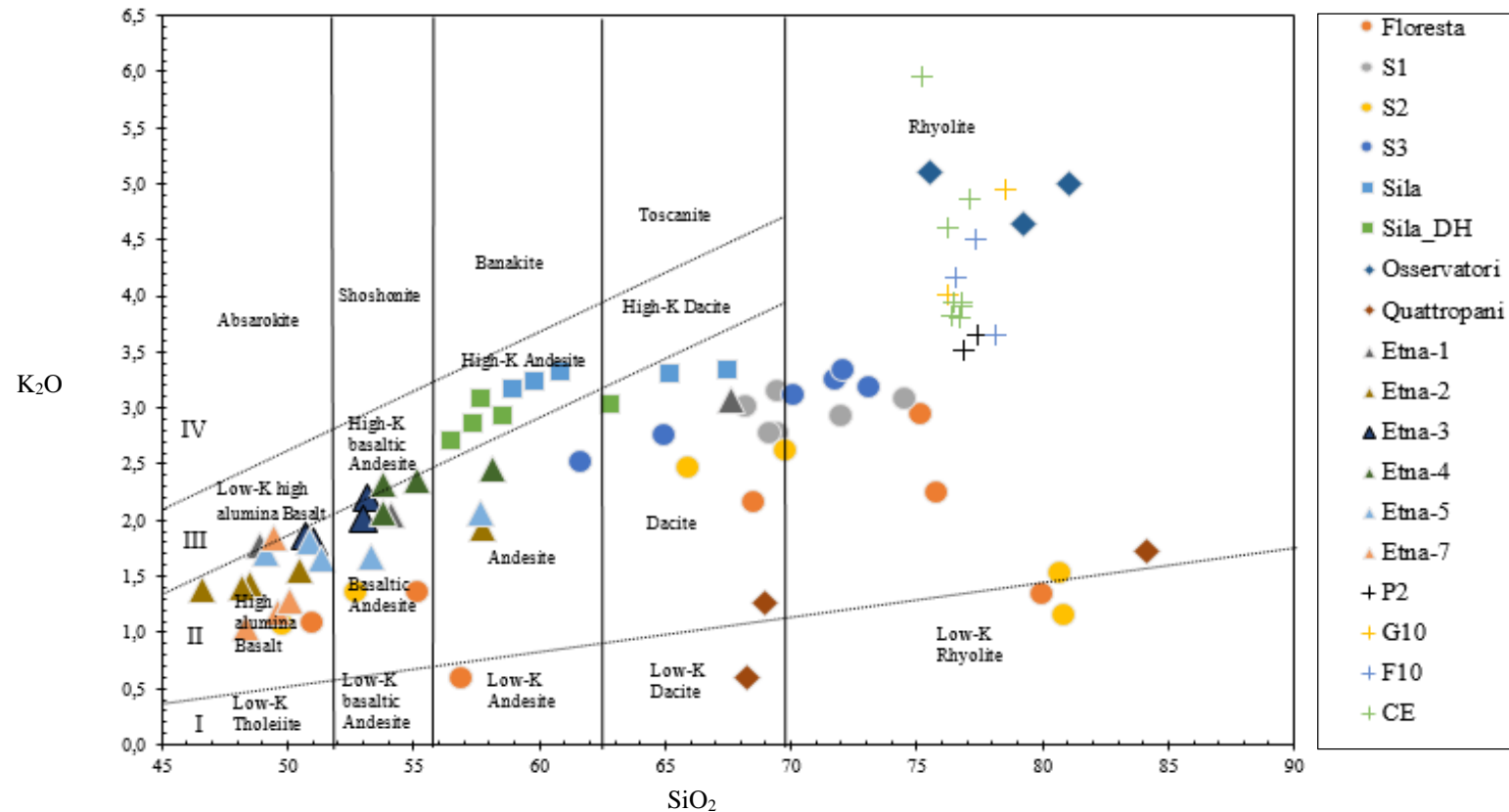
K<sub>2</sub>O/SiO<sub>2</sub> Diagram: Volcanic Material at All Sites

Fig. 32 K<sub>2</sub>O/SiO<sub>2</sub> Diagram: Aeolian Islands, Etna and Sila.

Classification of the volcanic material using the ratio between potassium oxide and silicon dioxide (K<sub>2</sub>O / SiO<sub>2</sub>) according to Peccerillo and Taylor (1976). Modification of the four series according to Pichler (1981). I = Potassium poor calc alkaline “Andesite” series (Island-arc “Andesite”; arc tholeiite series). II = Normal calc alkaline “Andesite” series (Continental margin “Andesite”; calc alkaline series). III = Potassium rich calc alkaline “Andesite” series. (High potassium calc alkaline series). IV = Shoshonite series. Represented data from Mirabella et al. (2005), Scarciglia et al. (2008) and Egli et al. (2008).

K<sub>2</sub>O/SiO<sub>2</sub> Diagram: Average Parent Magmas and Their Development

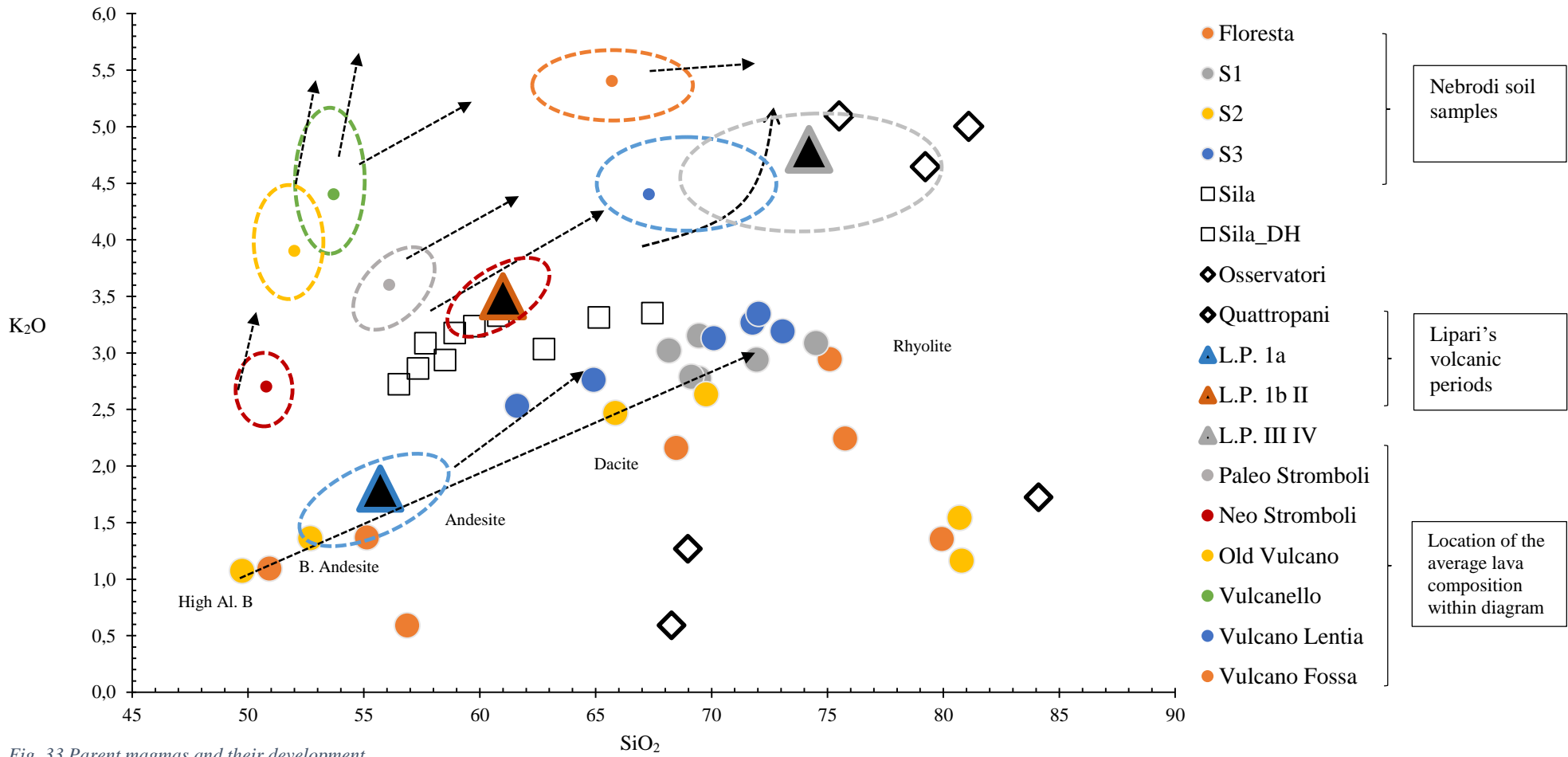


Fig. 33 Parent magmas and their development.

Average chemical composition of the lava. Modified from Pichler (1981). L.P. 1a = Lipari period I, calc alkaline. L.P. 1b II = Lipari period II, potassium rich calc alkaline. L.P. III and IV = Lipari period III and IV. Dark arrows = Fractional differentiation /Parent magma and its development. For comparison consult Pichler (1981, S.40,41, 42, 43). Diagram according to Peccerillo and Taylor (1976). Represented data from Pichler (1981) and Mirabella et al. (2005).

## Elemental Content of the Lava: Comparison Between Aeolian Islands and the Investigated Soil Samples

	P. 1a Lipari	P. 1b II Lipari	P. III and IV Lipari	*Lipari	Salina	Panera	Paleo Stromboli	Neo Stromboli	*Stromboli	Filicudi
Na <sub>2</sub> O	2.3	2.4	4.0	2.9	2.9	3.0	3.4	3.1	3.3	2.9
MgO	5.2	2.3	0.4	2.6	4.0	3.1	2.9	6.0	4.5	4.6
Al <sub>2</sub> O <sub>3</sub>	16.6	17.6	13.2	15.8	17.6	15.7	18.0	16.5	17.3	17.3
SiO <sub>2</sub>	55.7	61.0	74.2	63.6	57.2	63.2	56.1	50.8	53.5	55.7.
P <sub>2</sub> O <sub>5</sub>	0.2	0.2	0.1	0.2	0.2	0.2	0.5	0.9	0.7	0.2
K <sub>2</sub> O	1.8	3.5	4.8	3.4	1.7	2.7	3.6	2.7	3.2	1.9
CaO	9.3	5.9	1.0	5.4	8.3	5.8	7.7	10.9	9.3	9.2
TiO <sub>2</sub>	0.7	0.7	0.1	0.5	0.6	0.6	1.0	1.0	1.0	0.8
MnO <sub>2</sub>	0.0	0.0	0.0	0.0	0.0	0.0	0.0	0.0	0.0	0.0
Fe <sub>2</sub> O <sub>3</sub>	8.2	6.4	2.2	5.6	7.5	5.7	6.8	8.1	7.5	7.8
Total	100.0	100.0	100.0	100.0	100.0	100.0	100.0	100.0	100.0	100.0

	Floresta	SI	SII	SIII	Sila	Sila DH	+Nebrodi	+Sila
Na <sub>2</sub> O	1.9	2.2	1.7	2.0	2.5	2.9	2.0	2.7
MgO	0.5	0.8	0.6	0.8	0.5	0.5	0.7	0.5
Al <sub>2</sub> O <sub>3</sub>	19.9	21.2	21.3	20.1	24.4	26.9	20.6	25.6
SiO <sub>2</sub>	64.8	63.1	63.4	67.5	59.6	56.4	64.7	58.0
P <sub>2</sub> O <sub>5</sub>	0.3	0.6	0.6	0.2	0.3	0.3	0.4	0.3
K <sub>2</sub> O	1.6	2.7	1.6	3.0	3.1	2.8	2.2	3.0
CaO	1.8	1.8	1.6	1.0	3.2	3.7	1.6	3.4
TiO <sub>2</sub>	1.3	1.1	1.3	0.8	0.8	0.8	1.1	0.8
MnO <sub>2</sub>	0.2	0.2	0.2	0.1	0.1	0.1	0.2	0.1
Fe <sub>2</sub> O <sub>3</sub>	7.7	6.3	7.7	4.5	5.5	5.7	6.6	5.6
Total	100.0	100.0	100.0	100.0	100.0	100.0	100.0	100.0

Tab. 12 Average elemental content of lava.

\* Historical data provided by Pichler (1981).

+ Regional average of elemental concentration. Data retrieved via XRF analysis.

# Age Determination

## Weathering Indices

### Index B

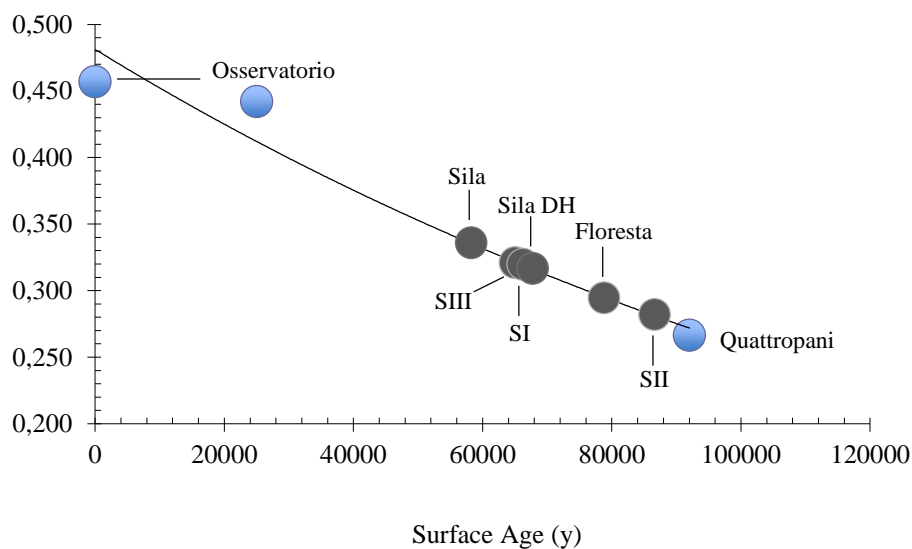


Fig. 34 Index B, upper soils of the Nebrodi sites compared to Lipari. Graphic modified from Mirabella et al. (2005).

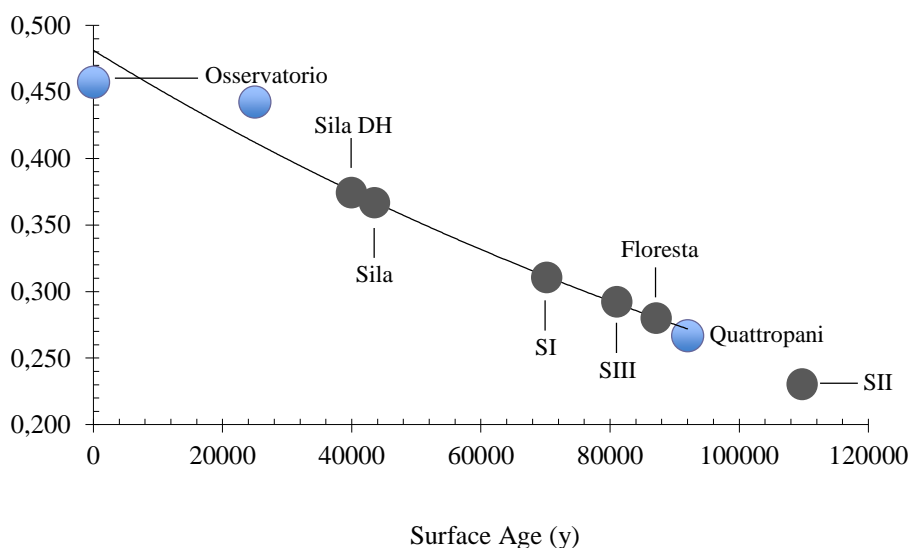


Fig. 35 Index B, sub soils of the Nebrodi sites compared to Lipari. Graphic modified from Mirabella et al. (2005).

Index B.	Top-Soil	Sub-Soil	Approx. Age		Age Span per Region
Site			T. Soil (y)	S. Soil (y)	
Floresta	0.30	0.28	76,000	86,000	
S1	0.32	0.31	64,000	70,000	
S2	0.28	0.24	88,000	110,000	
S3	0.30	0.29	64,000	82,000	
Nebrodi Messina					
AVG.	0.3075	0.2825	73,000	87,000	64,000 – 110,000
Sila-DH*	0.31	0.38	66,000	39,000	
Sila*	0.33	0.37	59,000	42,000	
Sila Calabria*					
AVG.	0.32	0.375	62,500	40,500	39,000 – 66,000
Observatorio	0.44	0.46	25,000	0*	
Quattropani	0.27	n.a.	92,000	n.a.	
Lipari					
AVG.	0.355	0.46	58,500		0 - 92,000

Tab. 13 Index-B results age determination.

\* Data regarding *Observatorio* and *Quattropani* was taken from *Mirabella et al. (2005)*. The value “zero” represents the C horizon, which marks the starting point of soil formation. B-index calculations for the sub-soil of *Quattropani* was not available.

### Index B Results: Description

Based on this index, a clear “enrichment of Al over Ca, K and Na occurs over time” (Egli et al., 2008). According to the results, the soil samples from the area of *Nebrodi* have on average a maximum estimated age of < 90,000 years BP. The estimated average age for the soils samples stemming from *Sila* was about < 70,000, while the age of the soils of *Lipari* was estimated to be less than 100,000 years. Ranked according to their estimated age, the oldest soil profile was SII, followed by *Floresta*, SIII and SI being the youngest one. As was expected in the case of *Nebrodi*, the Index B always yielded lower values for the sub soil than for the top soil, indicating the existence of older material beneath the top soil. Further, according to the Index B, the estimated age for *Sila* and *Sila-DH* was about 40,000 and 60,000 years respectively. Interestingly however, both sites exhibit a strange behaviour in having – according to the results – an older top soil compared to the sub soil (*tab. 13*).

*Weathering Index of Parker (WIP)*

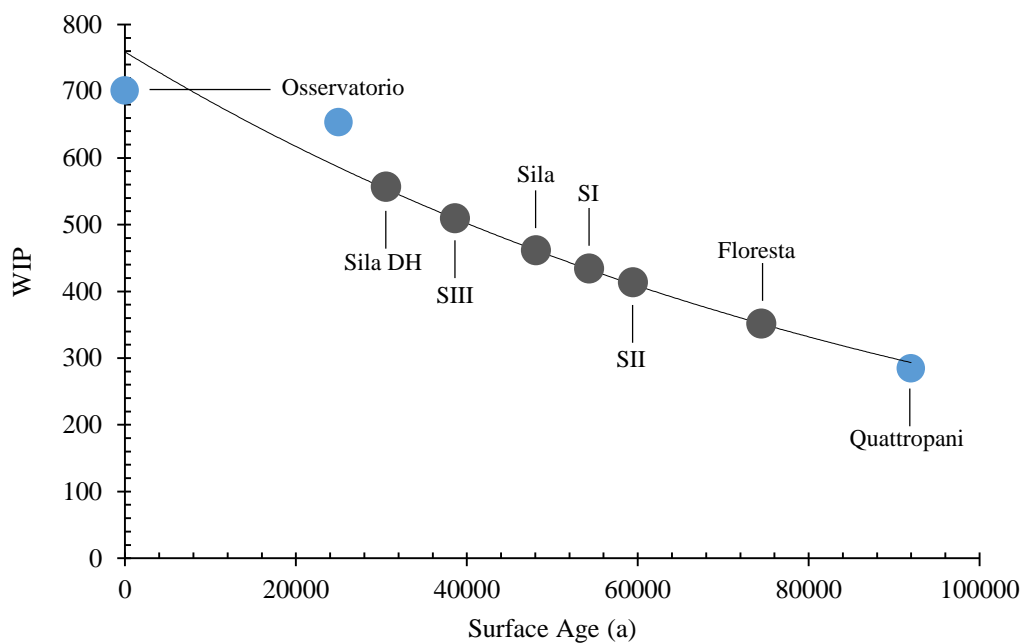


Fig. 36 WIP upper soils of the Nebrodi sites compared to Lipari. Graphic modified from Mirabella et al. (2005).

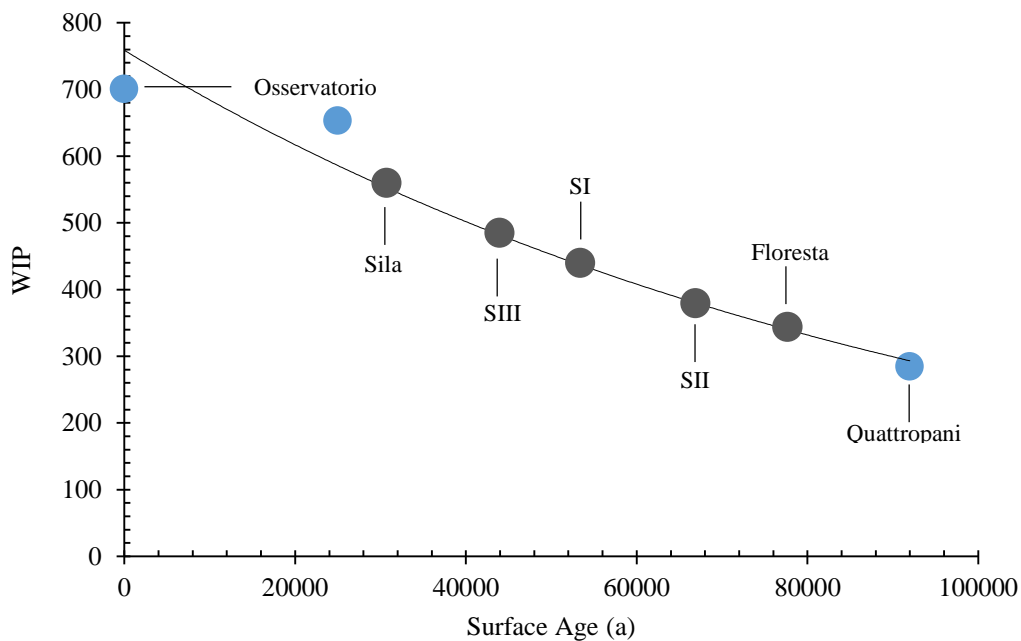


Fig. 37 WIP sub soils of the Nebrodi sites compared to Lipari. Graphic modified from Mirabella et al., (2005).

WIP.	Top-Soil	Sub-Soil	Approx. Age		Age Span per Region
Site			T. Soil (y)	S. Soil (y)	
Floresta	365.81	346.09	74,000	78,000	
SI	448.68	444.22	54,000	54,000	
S2	426.29	383.46	66,000	67,000	
S3	512.85	486.22	43,000	44,000	
Nebrodi Messina					
AVG. WIP	438.41	415.00	59,250	60,750	43,000 – 78,000
Sila-DH*	567.11	770.93	30,000	A.r.*	
Sila*	470.20	565.93	48,000	30,000	
Sila Calabria*					
AVG. WIP	518.65	668.43	39,000	30,000	30000 - 48000
Obsservatorio	653.41	701.07	25,000	0*	
Quattropani	284.62	n.a.	92,000	n.a.	
Lipari					
AVG. WIP	469.02	701.07	58,500		0 - 92,000

\* Value out of range

Tab. 14 WIP age determination.

### *Weathering Index of Parker Results: Description*

According to the results, the soil samples from the area of Nebrodi have a maximum estimated age of < 80,000 years BP. The estimated age for the soils of Sila was about < 50,000, while the age of the soils of Lipari was estimated to be less than 100,000 years. Ranked according to their estimated age, the oldest soil profile was Floresta, followed by SII, SI and lastly SIII. In the case of Nebrodi, the WIP always yielded lower values for the sub soil than for the top soil indicating the existence of older material below the top soil. Further, according to the WIP, Sila and Sila-DH have an estimated age of about 40,000 to 60,000 years. Interesting is that similar to the results of the B-index, both sites seem to have an older top soil compared to the sub soil since the lower values were achieved for the top soil and not for the sub soil, as was expected (*tab. 14*).

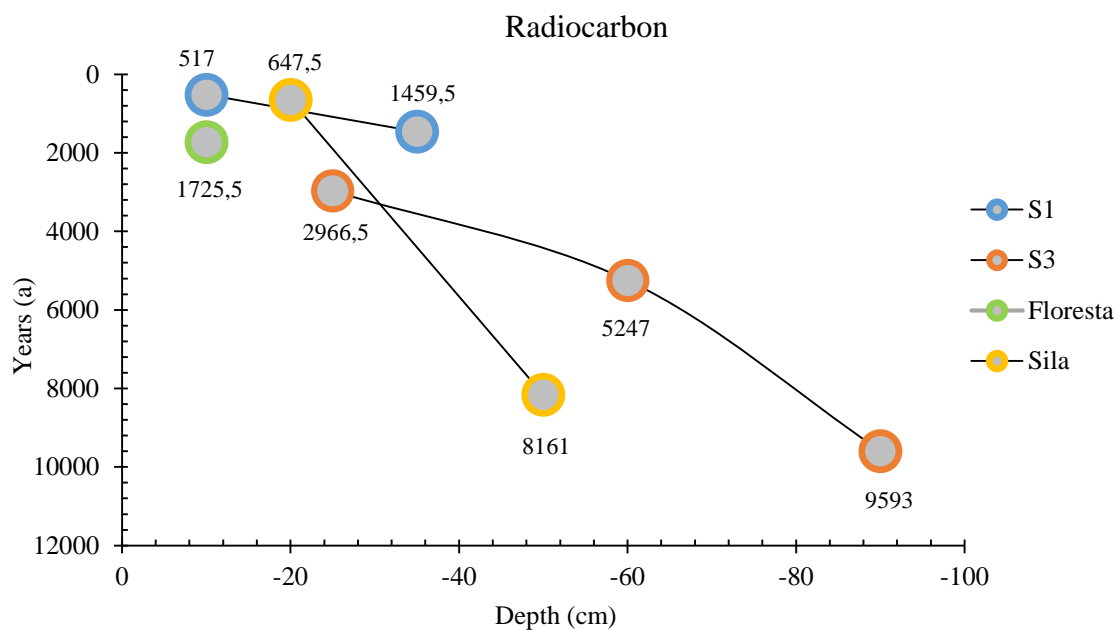
Radiocarbon  $^{14}\text{C}$ 

Fig. 38 Radiocarbon dating.

Origin	Site	Depth (cm)	Corrected Age (y BP)	F14C	d13C (‰)	Calibrated Ages (cal. BP) <sup>3</sup>	
						1σ (68.2%)	2σ (95%)
Nebrodi	S1	0-20	470 ± 30	0,943 ± 0,004	-14,0 ± 1,0	525 - 505	541 - 493
Nebrodi	S1	20-50	1565 ± 35	0,823 ± 0,004	-7,7 ± 1,0	1,521 - 1411	1,538 - 1,381
Nebrodi	S3	0-50	2850 ± 35	0,701 ± 0,003	-12,7 ± 1,0	3,004 - 2884	3,066 - 2,867
Nebrodi	S3	50-75	4562 ± 29	0,5667 ± 0,002	-15,9 ± 1,0	5,315 - 5085	5,437 - 5,057
Nebrodi	S3	75-110	8607 ± 35	0,3425 ± 0,002	-21,2 ± 1,0	9,595 - 9531	9,662 - 9,524
Nebrodi	Floresta	0-10	1810 ± 30	0,798 ± 0,003	-17,4 ± 1,0	1,810 - 1709	1,823 - 1,628
Calabria	Sila-DH	0-20	380 ± 30	0,954 ± 0,004	-19,0 ± 1,0	500 - 333	505 - 319
Calabria	Sila	0-20	725 ± 30	0,914 ± 0,003	-19,8 ± 1,0	686 - 663	725 - 570
Calabria	Sila	40-60	7345 ± 33	0,4008 ± 0,002	-28 ± 1,0	8,195 - 8051	8,292 - 8,030

Tab. 15 Radiocarbon results.

<sup>3</sup> Current Date: Year 1950.

## IV. Discussion

### General Soil Analyses

The investigated region of Nebrodi is considered to be a very suitable area for distal tephra sedimentation due to its proximity to the Aeolian arc and Mount Etna. Our preliminary low-intensity ash survey of the surroundings not only confirmed this claim, but also implied that andosol-like soils are well represented in the region. The physical, chemical and mineralogical results show that the investigated soils (Nebrodi and Sila) might have different properties. However, as stated by Mirabella et al. (2005), these differences can be due to the different age of the soils or simply because of the inherent characteristics of the volcanic material since the vegetation and climate are quite similar at all sites. In general, the investigated soils had an upper organic-mineral (A) horizon with umbric and sometimes ochric characteristics. The soil profiles show typical features of volcanic soils with andic properties. The displayed colours in the (A) horizons – according to the Munsell table – ranged from black to dark brown in wet conditions. When dry, the soils displayed light colours. The texture of the material was variable but mostly powdery, friable and sometimes smeary. The materials behaved non-plastic. The density was low due to the high porosity. The successive deeper horizons were characterized by being more brownish-yellow to yellowish-brown cambic (Bw) and transition horizons (Bc) probably “dominated by iron oxyhydroxides such as goethite and ferrihydrite” (Scarciglia et al. 2008). The soil profile Floresta presented one massive argillic horizon (Bt) with clay and a reddish-colour. However, the profile was polygenetic. Meaning, its lithology changed five times with depth overshadowing any trend. Like Scarciglia et al. (2008) (Sila) and Egli et al. (2008) (Etna), all soil profiles presented a dominance of the sand fraction. All studied soils had a sandy loam to clay loam texture (*fig. 17*), similar to the texture reported by Mirabella et al. (2005) in Lipari. Grain sizes generally increased from the top soil to the bottom of the soil profiles, where the lower silt and clay values were measured. According to Egli et al. (2008), this effect is a “concomitant effect of weathering”. As stated before, all soils can be classified as “very strong acidic” or “strong acidic”. Consequently, our soils’ milieu is more acidic than those measured on Etna (Egli et al., 2008), Sila (Scarciglia et al. 2008; Vingiani et al., 2014) or Lipari (Mirabella et al., 2005). Although the C/N-ratio reached extremely high values in some horizons (in some cases the equipment was not able to measure the ratio) the average value varied between 10 and 20 among all soils, a value that is similar to Mount Etna’s C/N-ratio (Egli et al., 2008). Bulk density was low with an average of 1.14 g/cm<sup>3</sup> for all soil profiles. The mean percentage of organic matter was about 5 % with a minimum close to zero and a maximum around 18

%. Similar to other studies conducted on volcanic soils (Pichler, 1981; Pichler, 1984; Mirabella et al., 2005; Scarciglia et al., 2008; Egli et al., 2008; Vingiani et al., 2014), the total chemical composition of major and trace elements shows a dominance of  $\text{SiO}_2$  and  $\text{Al}_2\text{O}_3$  (*tab. 5*). According to Egli et al. (2008) and Scarciglia et al. (2008), high availability of aluminium and silica in the soil profiles might be explained through weathering processes affecting glass fragments. On average, the soils of Nebrodi have a slightly higher  $\text{SiO}_2$  value (64.7 %), followed by those of Sila (58.0 %) (*tab. 12*). This assumption is in agreement with the values for the region of Sila provided by Scarciglia et al. (2008) and Vingiani et al. (2014).

## DRIFT and XRD

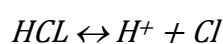
The XRD and the XRF analyses showed high concentrations of quartz. This was expected, due to its dominance in the sand fraction as reported in previous works (Scarciglia et al., 2008; Mirabella et al., 2005). Quartz was detected through the double peaks at 780 and 800  $\text{cm}^{-1}$  and the single peak at 692  $\text{cm}^{-1}$ . Furthermore, based on the achieved results (*tab. 9 and 10*) it is possible to state that in the clay fraction kaolinite was the dominant mineral for all investigated soils. The peaks at 3620  $\text{cm}^{-1}$  and 3694  $\text{cm}^{-1}$  confirmed the presence of this mineral. Kaolinite is a clay product that has been extracted since ancient times in places such as Lipari (Mirabella et al., 2005). Kaolinite is typically found in volcanic soils under heavy rainfall and strong drainage where it forms as a result to chemical weathering of aluminium silicates (Sumner, 1999). Presumably, it was created through the weathering sequence: glass > halloysite > kaolinite (Mirabella et al., 2005; Egli et al., 2008). Another mineral present in all soil profiles was gibbsite which, similar to kaolinite, is a mineral produced by the chemical weathering of aluminium-rich rocks. In addition to this, the analysis exposed traces of hematite and goethite. The mineral smectite was also found, however in smaller amounts than kaolinite. As Mirabella et al. (2005) stated, we assume smectite not to be of pedogenic origin but rather inherited from the parent material. According to Sumner (1999), Mirabella et al. (2005) and Egli et al. (2008), smectite is a mineral often found within volcanic soils possibly created through hydrothermal processes. This assumption seems to be confirmed by the fact that small traces of vermiculite were also found in the soil samples. Vermiculite is a well-known mineral created through hydrothermal alteration of primary micas (Sumner 1999). Interestingly, the amounts of vermiculite seem to be related to the presence of mica and illite. According to Sumner (1999), “increasing intensity of weathering towards the surface in a soil profile generally leads to loss of mica/illite at expenses of breakdown products such as vermiculite”. This may explain why the positive amount of vermiculite seems to reflect the unclear presence of illite at sites such as Floresta. Similar findings were noticed by Waroszewsky et al. (2015).

Furthermore, the DRIFT analysis also revealed the presence of imogolite, a typical mineral found in volcanic soils formed from ashes/tephra (Sumner, 1999), confirming once again the volcanic origin of the samples. Additionally, it is also worth noting that the mineral amphibole was not always easily detectable. According to our DRIFT analysis, the mineral was only found in the profiles stemming from Sila, while the Nebrodi results were always negative (*tab. 11*). This is partially confirmed by Scarciglia et al. (2008), who, in a previous study, claimed that amphibole can be present in the soils of Sila. In contrast to this, the XRD analyses suggested the mineral only to be found at the sites of Nebrodi (*tab. 9*). In spite of these results, we assume amphibole to be present in all soil profiles due to the fact that dacite – an amphibole-rich rock – was found at all sites (*tab. 11*).

## Soil Reaction pH

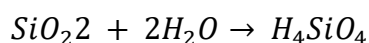
As aforementioned, the pH generally decreases with depth, leading to a soil acidification of the profiles. Soil acidification or the increase of hydrogen ions ( $H^+$ ) is a natural process of a soil profile over time that leads to a decrease of the pH. There are many drivers that can cause this effect in a vertical soil column, ranging from acid rain to overuse of fertilizers. Therefore, there is no single reason but rather numerous factors that simultaneously contribute to the overall process of soil acidification. The following list presents some possible causes that may have led our soils to turn into acidic milieus:

First and foremost, by definition the pH of a soil is the measured amount of hydrogen ions in a solution. Because the hydrogen ion is an acid cation, the greater the concentration the lower the pH (Stahr et al., 2012). Thus, the question is how the concentration of hydrogen ions ( $H^+$ ) increases along the analysed soil profiles. It is known that after a volcanic eruption, an increase in (volcanic) gases in the atmosphere is measurable (Blong, 1984). Some of these gases, such as hydrogen chloride (HCl) and hydrogen fluoride (HF), are known for being extremely acidic (USGS, 2010). Hydrogen chloride, short HCL, is a highly soluble gas. Consequently, HCL is completely dissociated into its ionic components in water, which subsequently increases the amounts of  $H^+$  (USGS, 2010).



Like HCL, hydrogen fluoride (HF) is a highly soluble gas that promotes acid rain by having the ability to attach itself to ash particles that are later brought into the soil through rain (Symonds et la., 1994). Another possibility is the so-called desorption of basic cations (Stahr et al., 2012). Due to (acid) rain, basic cations such as Ca, Mg, K and Na are leached out of the colloidal system leaving a higher concentration of hydrogen and aluminium ions behind, which lower the pH (Hue and Ikawa, 2007;

Stahr et al, 2012). These assumptions are supported by the XRF results as they show a low content of base cations compared to other more stable elements like aluminium. The concentration of these basic cations decreases from top to bottom of the investigated soil profiles. Another possible driver is the so-called “silicic acid”, which forms when water (H<sub>2</sub>O) – presumably rain – infiltrates the soil and subsequently reacts with free quartz (SiO<sub>2</sub>) stemming from the parent material, as for example igneous rocks. Silicic acid, as the name suggests, is an acid that increases H<sup>+</sup> and hence shifts the soil solution towards a lower pH (Sumner, 1999).



Regardless of the driver, it is inarguable that the soil profiles have been highly weathered. The presence of imogolite detected by the DRIFT analysis and the large concentrations of Fe and Al oxides found via the oxalate extraction method (*fig. 18 and 19*) confirm this assumption. It is important to mention that soil acidification can only happen once the soil buffering capacity is exhausted. Therefore, it is safe to say that the low pH-values do not only reflect the soils' conditions, but also the exposure to time and thus the age of the soils.

## Soil Carbon

As mentioned before, the results show a negative trend with depth for all soil profiles. Overall, the carbon content has its maximum within the topsoil layers. This was actually expected since organic carbon typically finds its way into the soil from the surface to deeper layers. Thus, it is common to measure larger quantities of organic carbon in the initial centimetres of the soil. Besides, physical and chemical characteristics in the deeper soil layers, such as the increasing density and acidification of the profiles, hinder vegetation growth and hence the reallocation of organic carbon. Furthermore, the differences in carbon content among the analysed soil profiles can be explained as the result of many external factors, such as the kind of vegetation, climate, type of land use and elevation (Jenny, 1941). Carbon enrichment at half depth between top and sub soil like in the case of Floresta or SII (*fig. 24*) can be seen as natural carbon translocation due to soil dynamics (Waroszewski et al., 2015), such as leaching processes or the existence of an old buried soil horizon.

## Origin Determination

Given the geographical location of the area of interest, several volcanoes were considered as the potential source of the sampled material; more precisely, the four volcanoes known as Mount Etna, Vulcano, Lipari and Stromboli. Regarding their activity, the volcanoes are classified as follows: Mount Etna and Stromboli are active volcanoes, while Lipari and Vulcano are considered to be dormant volcanoes.

Overall, the main challenge in determining the origin of our material consisted in finding a method to differentiate the volcanoes from one another. Thus, in a first step we focused on the analysis of chemical components since it has been shown in the past (e.g Pichler, 1967; Scarciglia et al., 2008; Vingiani et al., 2014) that the analysis of the chemical composition can be used for source differentiation among volcanic material. According to Scarciglia et al. (2008), the volcano Mount Etna can easily be differentiated from the rest of the Aeolian Islands volcanoes by means of comparing the amount of silica with the alkali metals given that products high in silica have characterised the activity of the Aeolian Islands for the last quaternary period (Keller et al., 1978; Pichler, 1981; Paterne et al., 1988; Narcisi and Vezzoli, 1999). Therefore, the first question to tackle was to investigate if it was possible to arrange our samples according to one of these two groups. Initially, it was assumed that the complex and active stratovolcano known as Mount Etna was the source of our analysed material because of its close proximity to the researched area as well as the enormous effusion rates for the past four centuries (Condomines and Tanguy, 1995). As a result, the first volcano to be analysed and compared was Mount Etna.

According to several authors, such as Pichler (1981, 1984), Condomines and Tanguy (1995) and Scarciglia et al. (2008), Mount Etna's principal rocks belong to a series known as alkaline-series even though it is well known that, in the past, Mount Etna also produced sub-alkali rocks. However, rocks from sub-alkali series such as tholeiitic basalt and their differentiations make up less than 20 percent of the produced material originated from this volcano (Pichler, 1984). What is more, these rocks are confined to the first two eruptive stadiums of the volcano and are thus hardly represented at all (Pichler, 1984; Coltelli et al., 2000). Consequently, the main volcanic product, which makes up around 80 percent or more, is made of alkali-basaltic lava that has been the uniform product created by Mount Etna for the last 200,000 years according to Condomines and Tanguy (1995).

In his work about Mount Etna, Pichler (1984) states that the main rock types produced by this volcano are tholeiitic-basalt, alkali-hawaiite, alkali-mugearite, nepheline-phonolite, tephrite and basanite. True basalts are absent in historical eruptions (Le Bas et al., 1986). The majority of the basaltic lava was produced after 1970 A.D. and was classified as potassic-trachy-basalt for its

irregularly high  $K_2O/Na_2O$  ratio (Condomines and Tanguy, 1995). Consequently, it is correct to assume that the average volcanic rocks for the past 200,000 years stemming from Mount Etna are tholeiitic basalt and tholeiitic hawaiite from the aci-castello and simeto stadium (Pichler, 1984). Hence, the material deriving from Mount Etna mostly presents a high concentration of alkali elements compared to silica. The archived results via TAS-classification confirmed these claims (*fig. 27*). Using the data of Egli et al. (2008), it was possible to reconstruct the specific volcanic rocks found on Mount Etna. As stated in the results (*tab. 11*) and in accordance with the statements of Egli et al. (2008), the main volcanic rocks found at the seven sites were classified as: trachybasalt (hawaiite) and some basaltic trachyandesite (mugearite), all of which are consistent with the above-mentioned arguments (*fig. 28*). In sum, Mount Etna's principal rocks are part of an alkali series and thus chemically speaking under-saturated with silica ( $SiO_2$ ) compared to the alkali metals ( $Na_2O + K_2O$ ) (*fig. 27*). The chemical composition of the analysed volcanic soil of Nebrodi and Sila clearly differs from that of Etna suggesting an origin from the Aeolian arc. However, the analysed volcanic material classified as Lapilli – which was only found within some layers at site II – chemically pointed towards Etna as the source because of the high concentration of alkali elements (*fig. 29*). This result was expected due to the fact that Lapilli – despite their small size – are physically speaking unable to travel large distances compared to ash (Fisher & Schmincke, 1984), making Etna the most likely candidate. Nonetheless, the amounts of Lapilli found within the soil pit only make up a small part of the overall soil profile. Subsequently, it is concluded that the volcanic material from Etna is not consistent with the achieved results for the sites of Nebrodi and Sila and it is for this reason that Mount Etna was dismissed as the source of our material.

Since Etna was no longer considered to be the source of the samples, the analysis was further concentrated on the islands of the volcanic arc. According to Pichler (1967), the volcanic archipelago formed by the seven Aeolian Islands has always been separated into two groups regarding their chemical composition. The first one (A), consist of the islands Lipari, Salina, Filicudi, Alicudi and Panarea-Basiluzzo, while the other (B) encompasses the islands of Vulcano and Stromboli. The first group (A), is characterised by being of a normal-calk-alkaline magma whereas the second group (B) is characterised by being a potassium-rich calk-alkaline magma. Consequently, a second step in identifying the origin of our soils was to arrange our soil samples into one of these two groups. Stromboli and Vulcano being the smallest group (B) and, according to Pichler (1981), the easiest two to differentiate, it was decided to start with this group. According to several studies (e.g. Joplin, 1968; Munno et al., 1980; Pichler, 1981; Bertagnini et al., 2008), Stromboli and Vulcano clearly differentiate themselves from the rest of the Aeolian volcanoes due to their high amount of potassic-magmatism ( $K_2O$ ), which creates the so-called shoshonite association (Joplin, 1968; Bertagnini et al., 2008). The

shoshonite association is a type of magmatism which is not found in any of the other Aeolian volcanoes. Shoshonites are basaltic rocks rich in potassium and classified as trachyandesite (Joplin 1968; Munno et al., 1980; Pichler 1981) that, together with the calc-alkali-series, typically form in island arcs and subduction zones (Joplin, 1968; Morrison, 1980; Pichler, 1981). According to the definition given by Morrison (1980), some of the criteria that characterise shoshonite rocks are the following: The amount of alkaline metals ( $\text{Na}_2\text{O} + \text{K}_2\text{O}$ ) must be higher than five percent (*fig. 29*) and the silica fraction must be almost saturated. Moreover, the ratio between  $\text{K}_2\text{O}/\text{Na}_2\text{O}$  should be high and the percentage of  $\text{TiO}_2$  must be low. Lastly, according to Pichler (1981), the average chemical curve for shoshonites created by Vulcano – when comparing  $\text{K}_2\text{O}$  to  $\text{SiO}_2$  – must be steeply ascending with low  $\text{SiO}_2$  contents (48-52 %) and then positive but flatter with higher  $\text{SiO}_2$  percentages (50-60 %). Yet, when compared to our results, it is clear that neither the soils of Nebrodi nor Sila match the definition for shoshonites given by Morrison (1980) and Pichler (1981). First of all, none of the Nebrodi samples have an overall alkali concentration higher than five percent. In general, the samples exhibited a very low content of alkali metals compared to silica (*fig. 29*). Further, none of the samples chemically behave as described by Pichler (1981). On the contrary, the site of Floresta shows a negative tendency through an increase of the silica concentration, while, in general, all samples keep rising gradually as the  $\text{SiO}_2$  concentrations increase (*fig. 30*). Besides, none of the analysed sites (Sila, Sila-DH, SI, SII, SIII and Floresta) tested positive for shoshonites according to our TAS classification. Moreover, by using the classification diagram  $\text{K}_2\text{O} / \text{SiO}_2$  of Peccerillo and Taylor (1976), it was noticed that the majority of the soils for the area of Nebrodi and Sila are found within the so-called series “II” and “III” respectively as displayed in *fig. 30*. According to Morrison (1980) and Pichler (1981), series “II” encompasses the so-called normal calc-alkaline “andesite” series (continental edge – “andesite”; calc-alkaline series), while series III encompasses the potassium-rich calc-alkaline series. Neither series “II” nor “III” are clearly of Stromboli or Vulcano origin since, according to Pichler (1981), Stromboli’s and Vulcano’s material is encompassed within the series III and IV of the  $\text{K}_2\text{O} / \text{SiO}_2$  classification diagram of Peccerillo and Taylor (1976) due to their potassium-rich magmatism. Consequently, it becomes evident that our soils must have their origin elsewhere.

As aforementioned, in the past, the five remaining Aeolian Islands (Lipari, Salina, Filicudi, Alicudi and Panarea-Basiluzzo) have comprised a group characterized by having a sub-alkaline magmatism. The rock types found on these five volcanic islands ranges from basaltic andesite to rhyolite, which makes them all suitable candidates for being the source of our investigated soils. However, according to Giaccio (2008), these volcanoes might share similar chemical characteristics but not identical (Pichler 1981). Local and small differences due to fractional differentiation make it possible to distinguish between them. A closer look at their elemental composition exposes patterns

and signatures which can be used to differentiate them from each other. Consequently, by comparing our data to Pichler's study (1981) it becomes evident that the island of Lipari (Italy) is the most likely origin of our investigated soils (*tab. 12*). In an attempt to corroborate this statement, the average elemental content of Lipari's volcanic history (Period I, II, III and IV) was plotted and superimposed onto ours (*fig. 33*).

The results for the area of Nebrodi not only matched those belonging to Lipari's first period (PI), but also followed the trajectory of their development towards rhyolite (*fig.33*). According to Pichler (1981), the initial concentrations of SiO<sub>2</sub> and K<sub>2</sub>O for products belonging to Lipari's first period are located between 50 and 60 % and 1.0 and 1.5 % respectively. This initial concentration of the PI is classified as normal calc-alkaline and extends from andesite to rhyolite in the K<sub>2</sub>O / SiO<sub>2</sub>. Lastly, samples belonging to PI should experience a positive increase of both SiO<sub>2</sub> and K<sub>2</sub>O through their development from andesite to rhyolite due to fractional crystallisation processes (Pichler, 1981). All arguments are supported by our chemical analyses as visible in *fig. 33*. What is more, based on the findings it is safe to say that the external soils provided for this master thesis stemming from the area of Sila in the region of Catania (RC) are not identical to those of Nebrodi. A closer look at the results displayed on *fig. 29, 30, 31* as well as *tab. 11* and *12*, makes evident that these soils' chemical components present differences from those of Nebrodi: Firstly, in contrast to those of Nebrodi the soils of Sila generally have a higher amount of alkali metals reaching values above 5 % (*fig. 29*). Additionally, all of the Sila soils showed rather high values of potassium compared to the other soils (*fig. 30, 32*). Lastly, the TAS-Diagram (*fig. 31*) loosely classifies the Sila samples as trachyandesite with a high amount of potassium. According to Rosi et al. (2000), Petrone et al. (2006) and Bertagnini et al. (2008), potassium-rich trachyandesite – also called shoshonite – is known for being a volcanic rock product of Stromboli's eruptive behaviour during the previous centuries. In other words, chemically speaking the samples Sila and Sila-DH could point towards Stromboli as their origin, not only due to the achieved result, but also due to the proximity to the volcano. Nonetheless, this does not seem to be the case. In fact, the Sila samples' potassium values are not sufficiently high in order to be classified as shoshonites nor any type of potassium-rich material stemming from Stromboli (Pichler, 1981). Other results further emphasise this assumption. According to *fig. 33*, the material stemming from Sila and Nebrodi is indeed Lipari's volcanic material. However, they stem from different temporal periods which explains their chemical differences (Mirabella et al., 2005). The Sila samples matched the average values of Lipari's second period (PII). According to Pichler (1981), Lipari's second period is characterised by a potassium-rich calc andesite with a typical average concentration of K<sub>2</sub>O between 2.2 and 3.8 % and 54.0 to 62.0 % for Silica. This is in agreement with the achieved results (*fig. 31, 33*). The existence of Lipari's potassium-rich calc andesite has also been corroborated by Vingiani et al.

(2014) who have analysed distal soils in Sila belonging to Lipari. Hence, we conclude that the analysed soil material known as Sila and Sila-DH also have their origin in the distant volcano of Lipari. Based on the achieved data the following conclusions can be made:

- a. The volcano of Lipari must be the source of the investigated soils of Nebrodi and Sila.
- b. The analysed material stemming from Nebrodi suggests Lipari's first period, while the samples from Sila imply Lipari's second period as their origin.
- c. Lipari's most recent periods III and IV do not seem to be present in our samples as none of the result could be placed close to the average position of these magmas according to our  $K_2O / SiO_2$  index.

## Age Determination

The second aim of this master thesis consisted in dating the analysed material. Hence, in order to determine the age of the collected samples, we focused firstly on the analysis of time-dependent soil processes such as weathering and the rates at which these processes happen. As stated before, soil weathering is a natural process that occurs during the development of any soil and therefore by studying the rates at which these processes happen one may achieve an insight into the influence of time on the soil formation (Dahms et al., 2012). In the context of this master thesis, we used the Index B of Kronberg and Nesbitt (1981) and the weathering index of Parker (1970). Both indices are based on the same principle: Over time, mobile minerals are being washed out of the colloidal system leaving more weathering resistant and therefore less mobile elements. Consequently, the ratio between mobile and immobile elements should reveal its time-dependent nature and allow us to quantify it. Similar to this, we have also attempted to correlate the carbon stocks with the calculated age of the soil profiles under the assumption that carbon stocks are built over a long period of time as the soils develop (Mavris et al., 2010). Additionally, as recommended by Böhler et al. (2011), we have also opted to add the numerical method  $^{14}C$  in order to quantify the age of our samples. Finally, we have tried to correlate the chemical analyses of the soil to a specific lava type and thus to a specific eruptive period in time.

## Radio Carbon Analysis $^{14}C$

As stated before, only some selected samples could be analysed by using this method since not all samples encompassed organic material on which the study could be conducted. Consequently, deeper

layers or parent material (C-horizons) having a small or no amount of organic material were not investigated. Thus, only some horizons of the sites SI, SIII, Floresta and Sila were analysed. Overall, there is a visible trend between the depth and the age of the sample. In other words, deeper samples are older samples. As shown in *fig. 38* and *tab. 15*, the age span of the organic material encompassed within the samples ranges from  $470 \pm 30$  years to  $8607 \pm 35$  years BP. Thus, all samples belong to the geological epoch known as Holocene, which includes the last 11,700 years. According to the analysis, the top soil of SI is  $470 \pm 30$  years old, while the sub soil is  $1565 \pm 35$  years old. The top soil material located at SIII is  $2850 \pm 35$  years old and the sub soil  $8603 \pm 35$  years. Floresta's top soil is  $1810 \pm 30$  years old, while its subsoil could not be dated as this soil profile is polygenetic. As visible in *fig. 15*, the lithology of the profile Floresta changes five times with the depth. As a consequence, trends are completely overshadowed and cannot be recognised. Further, Sila's top soil is  $725 \pm 35$  years and its sub soil  $7345 \pm 33$  years old according to the analyses. As expected, the results are much younger than those calculated for the inorganic material. It is also worth noting that the  $^{14}\text{C}$  results achieved for our samples stemming from the region of Sila are quite different from those achieved by Scarsiglia et al. (2008) for the same area. Therefore, the validity of the results must be reconsidered. The confidence in the archived results remains low.

## Weathering Indices

It is worth noting that information concerning mid to long term weathering rates is rare and quite uncertain (Egli et al., 2008). Nonetheless, knowledge concerning weathering rates is fundamental (Mavris et al., 2010) as it may provide us with important information about the influence of time. In accordance with the chemical analysis, the soil samples from the area of Nebrodi have show clear similarities to the material stemming from the Aeolian Arc domains, especially to those of Lipari. It is due to this reason that we have attempted to quantify the age of the soils of Nebrodi by setting our model and its parameters based on the study of Mirabella et al. (2005) for the volcanic material extracted from the island of Lipari. For this task, we used the Index B of Kronberg and Nesbitt (1981), the weathering index of Parker (1970) and the  $(\text{K}+\text{Ca}) / \text{Ti}$  index presented in the study of Dahms et al. (2012). Accordingly, weathering ratios for the top soils and sub soils were represented separately in the same way as Mirabella et al. (2005). This decision was made not only because of the need for reproducibility, but also because of the magnitude of the soil profiles, for which different trends and ages were expected. The results achieved via Index B can be consulted in *fig. 34* and *35* as well as *tab. 13*. The results obtained with the WIP are presented in *fig. 36* and *37* as well as *tab. 14*. Furthermore, the  $(\text{K}+\text{Ca}) / \text{Ti}$  index could not be displayed as an age function since the achieved values were out of

the range of our model. However, the achieved data provides important information regarding the movements of base cations as well as the enrichment of immobile elements. This information can be consulted in *fig. 21*. As expected, the weathering indices showed a difference between shallow and deeper soil horizons, the latter being older than the former. The only exception was found at the sites of Sila where, according to the results, the sub soils were slightly younger than the top soils. This effect can be the result of erosion or accumulation processes. However, since the weathering indices only make rough estimates and because the age differences are too small, this irregularity is insignificant and can be disregarded. The indices also reflect the strong chemical weathering that the soils have undergone. This raises some concerns regarding the reliability of the results since it is assumed that the higher the weathering the older the soils. However, as stated by Mavris et al. (2010) and Dahms et al. (2012), weathering rates of a mineral or a rock decrease with time, which may in turn disguise the real age of the soils. Thus, to ensure reliability, more analyses would have to be conducted. Regarding the measured age of the soil profiles, it is of interest that overall the analysed samples matched those plotted by Mirabella et al. (2005), lying within the time span provided by their investigation, i.e. less than 100,000 years BP. A closer look at the indices revealed the following ages: According to the Index B, the investigated top soil of Nebrodi has on average an estimated age of 73,000 years, while the sub soil is 87,000 years old (*tab. 13*). Yet, according to the WIP, on average the top soil of Nebrodi is 44,000 and the sub soil is 78,000 years old. Compared to one another, the Index B yielded smaller quantities and thus older values than the WIP. This age difference may lie within the nature of the indices. According to Price and Velbel (2003), the WIP has proved to be a more resistant index and hence suitable for locations with heterogenic underground such as ours. This is probably the reason why the results achieved by the WIP seem to vary less than those of the Index B. In short, both indices appear to work well with our samples. Both have yielded similar results which, given the major uncertainties concerning weathering processes, can only be seen as a success. Based on the results, the investigated area of Nebrodi has an age of less than  $90,000 \pm 10,000$  years. Presumably, they must stem from a series of volcanic events that occurred between 92,000 and 45,000 years ago (Mirabella et al., 2005). If we consider the soils to be the product of Lipari's volcanic history, then it can be stated that these achieved results appear to be reasonable. The results are in full agreement with the investigation of Mirabella et al. (2005) and with Crisci et al. (1983). According to Crisci et al. (1983), the estimated age for the soils of Lipari must lie around 100,000 years. Therefore, it is concluded that the use of weathering indices in order to achieve approximated ages can be seen as a good tool for dating analyses even though it is known that with time, weathering indices tend to yield asymptotic values (Egli et al., 2008). The confidence in the archived results via weathering indices remains high.

## Carbon Stocks

According to Egli et al. (2008), information regarding accumulation rates of SOC in volcanic regions in a Mediterranean climate is almost non-existent. Nevertheless, as mentioned before, we have attempted to create an average age using the results of both weathering indices in order to correlate them with the measured soil organic carbon stocks (SOC) to see whether a trend could be detected. The achieved results looked promising as described in the results section (*fig. 25*), where a trend seemed to become visible between the increasing amounts of C-stocks and the age of the soil profiles. However, further analyses revealed that due to the low number of data this effect could also be a spurious relationship with no correlation. According to Egli et al. (2008), carbon stocks are indeed built in the course of time as the soil develops. However, soil carbon stocks are part of the soil system which is managed through inputs and outputs and as the soil reaches maturity a certain stability is achieved. Hence, the values tend to remain constant over time. Within their study, Egli et al. (2008) noticed that after about 15,000 years the accumulations rates of SOC tend to become zero and after 20,000 years the soil organic carbon reaches an asymptotic value. Therefore, it is clear that in soils as old as ours (according to our results) an asymptotic value must have been reached a long time ago. For this reason, the SOC-stocks are not considered to be a suitable indicator for measuring the long-time evolution of soils.

## Chemical Composition of the Volcanic Material

Based on the achieved results, it is assumed that the collected and analysed soils of Nebrodi are the result of years of offshore volcanism. More precisely, volcanic ash from Lipari carried by the wind and deposited on the island of Sicily at a distance of approximately 30 km. As mentioned before, the chemical analysis of the investigated materials yields two different periods of volcanic eruption or rather production. As shown in *fig. 33*, the investigated soils of Nebrodi exhibit similar chemical characteristics as the volcanic material stemming from the first eruptive period. The analysed materials of Sila, on the other hand, showed chemical characteristics from what appears to be the second eruptive period. According to Pichler's study (1981), the denominated period "I" (PI) is encompassed within the middle Pleistocene epoch. This period – often referred to as the Ionian stages – comprises the volcanic material produced at about 120,000 years BP. The second period (PII) refers to a younger volcanic activity. PII belongs to a time span of about 30,000 to 60,000 (?) years BP (Pichler 1981). More importantly, both results seem to agree with the results achieved via weathering indices, which not only raises the confidence in the employment of the weathering indices, but also in the achieved

results. Additionally, it is worth noting that the approximated age or rather period of time does not differ greatly from the results obtained by Mirabella et al. (2005). For this reason, the analysis of the chemical composition and its relation to the eruptive periods is considered to be a suitable method to date volcanic material. For these results the confidence remains high. Based on the achieved results the following conclusions can be made:

- a. The age of the volcanic material according to the weathering indices lies around  $< 90,000 \pm 10,000$  years.
- b. The analysed soil profiles of Sila are on average younger than those of Nebrodi.
- c. According to the chemical composition of the volcanic material, the soil profiles belonging to Nebrodi were formed during the Pleistocene. Presumably around 60 ka (?) to 12 ka BP.
- d. Similar to this, the chemical composition of the volcanic material stemming from Sila suggests Lipari's second period as the time of formation, i.e. 30 ka to 60 (?) Ka BP. Hence, during a much younger Pleistocene.

## V. Conclusion

Overall, it can be said that this master thesis has provided answers to the questions raised at the beginning of the investigations. As a result, the following conclusions can be drawn:

- a) **Origin determination:** This master thesis has shown that it is possible to identify the source of volcanic material comprising the investigated soils even when primary eruptive products were not visible. For this task, we primarily focused on the analysis of chemical components. The application of the TAS diagram and the ratio between  $K_2O$  and  $SiO_2$  have proved to be very useful for the distinction between the different volcanoes surrounding the area of investigation.
- b) **Element losses:** Notwithstanding the fact that the soils were presumably influenced by ash inputs over time, element losses were measurable through the use of the weathering indices. According to the indices, base cations have been leached out of the colloidal system leading to an enrichment of more stable and thus immobile elements such as Ti. Particularly the upper layers indicated a lower content of base cations compared to the deeper soil layers.
- c) **Age determination:** For this task, relative and absolute dating methods were employed. In the context of geological time spans, the results suggest the pyroclastic inputs to be of more or less the same age. Therefore, a late Pleistocene to Holocene age can be assumed for the investigated sites. Despite uncertainties, weathering indices performed well and nicely fitted the model of Mirabella et al. (2005). Contrary to this, the organic material dated with the help of the numerical method  $^{14}C$  yielded a time span only encompassed within the Holocene and thus younger than the surrounding inorganic soil material. In addition, it has been attempted to correlate the SOC with the age of soil profiles in order to detect soil development trends. The achieved results and the aforementioned trends remain of speculative character due to the low amount of samples.
- d) **Site analysis:** This master thesis has revealed the site of Nebrodi to be a distal archive of sub-alkaline volcanic material having a strong relation to the Aeolian Islands and in particular to the volcanic island of Lipari. Consequently, it is assumed that the collected and analysed soils are the result of thousands of years of offshore volcanism carried and deposited by the wind in the near region of Nebrodi, Messina. Recent studies such as the one of Scarciglia et al. (2008) have

shown that distal tephra deposition in the central Mediterranean peri-volcanic is indeed possible and thus distance does not represent a problem for material transport.

- e) Soil genesis: The presence of some minerals such as illite, imogolite as well as kaolinite indicate a soil genesis related to volcanic ash. The latter is considered to be the end result of the following weathering sequence: glass > halloysite > kaolinite (Mirabella et al., 2005; Egli et al., 2008). Besides, the presence of some of these minerals reflects the age of the investigated soil material as they are only created after long periods of intense chemical weathering.
- f) Chemical weathering: The soil profiles show signals of high chemical weathering. For instance, the archived values via weathering indices were quite low, which can only mean that the mobile elements were being leached from the soil through weathering processes. Other results further emphasise this assumption: First of all, the strong acidic condition measured at all sites as well as the passive enrichment on alumina (Egli et al., 2008) are clearly related to chemical weathering (Mavris et al., 2010). Secondly, the XRF measured lower amounts of basic cations such as calcium, magnesium, potassium and sodium compared to those considered as immobile elements like Ti or Al. Thirdly, similar to the XRF, results for the  $(K+Ca) / Ti$  ratio of the first 100 cm have shown that the basic cations have been washed out of the upper soil layers leading to an enrichment in immobile elements.

To summarise, this master thesis represents a valuable contribution within the framework of quaternary analysis. More precisely, it can provide a better understanding of the history of the Nebrodi region, a peri-volcanic area within the Mediterranean basin where distal deposition of volcanic eruptions has not only constructed, but also shaped the landscape.

## **VI. Acknowledgements**

First and foremost, I would like to thank Prof. Dr. Markus Egli for his target-oriented support at any point of time during the process of this master thesis. Furthermore, I also thank Sandra Röthlisberger, Ivan Woodhatch and Michael Hilf, who enabled me to conduct all laboratory analyses. Then, I would like to give special thanks to my family, Lydia Diaz Henry Maciel and Nils Halpern Diazhenry, for their continuing support. Lastly, I owe the success of this master thesis as well as my entire studies to Sandra Gut, who has always stood at my side, encouraging me at all times.

## **VII. Personal Declaration**

I hereby declare that the submitted thesis is the result of my own, independent work. All external sources are explicitly acknowledged in the thesis.

Zurich, January 2016

Dieter Halpern

## VIII. References

- Beckhoff, B., Kanngießer, B., Langhoff, N., Wedell, R., & Wolff, H. (2006). Handbook of practical X-ray fluorescence analysis. Springer Science & Business Media.
- Bertagnini, A., Métrich, N., Francalanci, L., Landi, P., Tommasini, S., & Conticelli, S. (2008). Volcanology and magma geochemistry of the present-day activity: Constraints on the feeding system. The Stromboli volcano. An integrated study of the 2002-2003 eruption, 19-37.
- Blong, R. J. (1984). Volcanic hazards: A sourcebook on the effects of eruptions. Academic Press, Australia, 424.
- Bodenkunde, A. G. (1994). Bodenkundliche Kartieranleitung (BKA), Bundesanstalt für Geowissenschaften und Rohstoffe und Geologische Landesämter, Hannover, 4. Aufl. 392.
- Böhlert, R., Egli, M., Maisch, M., Brandová, D., Ivy-Ochs, S., Kubik, P. W., & Haeberli, W. (2011). Application of a combination of dating techniques to reconstruct the late glacial and early Holocene landscape history of the Albula region (eastern Switzerland). *Geomorphology* 127, 1–13.
- Bohn, H. L., McNeal, B. L., O'Connor, G., (1985). Soil Chemistry. Wiley-Interscience, John Wiley & Sons, New York.
- Bradley, R. S. (2015). Paleoclimatology: reconstructing climates of the Quaternary. Chapter: dating methods I pp: 55-101 Academic Press.
- Climate Temps (2015). Messina, Sicily climate and temperature. Available at: <<<http://www.sicily.climatemp.com/>>> (accessed on 25 November 2015).
- Colman, S. M., Pierce, K. L., & Birkeland, P. W. (1987). Suggested terminology for Quaternary dating methods. *Quaternary research*, 28(2), 314-319.
- Coltelli, M., Del Carlo, P., Vezzoli, L. (2000). Stratigraphic constraints for explosive activity in the past 100 ka at Etna Volcano, Italy. *International journal of earth sciences*, 89, 665–677.
- Condomines, M., & Tanguy, J. C. (1995). Magma dynamics at Mt Etna: constraints from U-Th-Ra-Pb radioactive disequilibria and Sr isotopes in historical lavas. *Earth and planetary science letters*, 132(1), 25-41.
- Crisci, G. M., Delibrias, G., De Rosa, R., Mazzuoli, R. & Sheridan, M. F. (1983). Age and petrology of the Late-Pleistocene brown tuffs on Lipari, Italy. *Bulletin of Volcanology*, 46, 381-391.
- Dahms, D., Favilli, F., Krebs, R. & Egli, M. (2012). Soil weathering and accumulation rates of oxalate-extractable phases derived from alpine chronosequences of up to 1 Ma in age. *Geomorphology*, 151, 99-113.
- Di Vito, M. A., Sulpizio, R., Zanchetta, G., & D'Orazio, M. (2008). The late Pleistocene pyroclastic deposits of the Campanian Plain: New insights into the explosive activity of Neapolitan volcanoes. *Journal of Volcanology and Geothermal Research*, 177(1), 19-48.

- Drouza, S., Georgoulas, F. A., & Moustakas, N. K. (2007). Investigation of soils developed on volcanic materials in Nisyros Island, Greece. *Catena*, 70(3), 340-349.
- Eash, N., Green, C. J., Razvi, A., & Bennett, W. F. (2008). *Soil science simplified*. (Fifth ed.) Blackwell, Iowa, USA.
- Egli, M., & Fitze, P. (2000). Formulation of pedologic mass balance based on immobile elements: A revision. *Soil Science*, 165, 437–443.
- Egli, M., Brandová, D., Cherubini, P., Ivy-Ochs, S. (2012). *Geochronology I (GEO 351.2): Mosaiksteine der Geochronologie Methoden und Anwendungen*.
- Egli, M., Fitze, P., Mirabella, A., (2001). Weathering and evolution of soils formed on granitic, glacial deposits: Results from chronosequences of Swiss alpine environments. *Catena* 45, 19–47.
- Egli, M., Nater, M., Mirabella, A., Raimondi, S., Plötze, M., & Alioth, L. (2008). Clay minerals, oxyhydroxide formation, element leaching and humus development in volcanic soils. *Geoderma*, 143(1), 101-114.
- FAO (2013). Holdridge life zones: Map. Available at: <<<http://data.fao.org/map?entryId=c6f35470-88fd-11da-a88f-000d939bc5d8>>> (accessed on 25 September 2015).
- FAO (2015) Soil survey: Guidelines. Available at <<[ftp://ftp.fao.org/FI/CDrom/FAO\\_Training/FAO\\_Training/General/x6706e/Index.htm](ftp://ftp.fao.org/FI/CDrom/FAO_Training/FAO_Training/General/x6706e/Index.htm)>> (accessed on 13 September 2015).
- Fisher, R. V., & Schmincke, H. U. (1984). *Pyroclastic rocks*, 472 pp. Springer, Berlin, doi, 10, 978-3.
- Fitton, G. (1997). X-ray fluorescence spectrometry. *Modern analytical geochemistry: An introduction to quantitative chemical analysis techniques for earth, environmental and materials scientists*, 87-115.
- Giaccio, B., Isaia, R., Sulpizio, R., & Zanchetta, G. (2008). Explosive volcanism in the central Mediterranean area during the late Quaternary-linking sources and distal archives. *Journal of Volcanology and Geothermal Research*, 177(1), v-vii.
- Harrington, C. D. & Whitney, J. W. (1987.) Scanning electron microscope method of rock-varnish dating. *Geology*, 15, pp. 976–970.
- Hitz, C., Egli, M., Fitze, P. (2002). Determination of the sampling volume for representative analysis of alpine soils. *Zeitschrift für Pflanzenernährung und Bodenkunde* 165, 326–331.
- Hue, N. V., & Ikawa, H. (2007). Department of Agronomy and Soil Science, College of Tropical Agriculture and Human Resources. *Acid soils in Hawaii: Problems and management*. University of Hawaii at Manoa. Available at <<[http://www.ctahr.hawaii.edu/huen/hue\\_soilacidity.htm](http://www.ctahr.hawaii.edu/huen/hue_soilacidity.htm)>> (accessed on 25 November 2015).
- Imperial Collage London a\* (2012). Imperial College rock library: Sub-alkaline rocks. Available at <<<https://www.imperial.ac.uk/earthscienceandengineering/rocklibrary/viewglossrecord.php?gID=0000000019>>> (accessed on 6 November 2015).
- Imperial Collage London b\* (2013). Imperial College rock library: Rhyolite. Available at <<<https://www.imperial.ac.uk/earthscienceandengineering/rocklibrary/viewglossrecord.php?gID=00000000075>>> (accessed on 25 November 2015).

- Imperial Collage London c\* (2012). Imperial College rock library: Alkaline rocks. Available at<<<https://www.imperial.ac.uk/earthscienceandengineering/rocklibrary/viewglossrecordphp?Term=alkaline%20rock>>> (accessed on 6 November 2015).
- Jenny, H. (1941). *Factors of soil formation*. McGraw-Hill, New York.
- Joplin, G. A. (1968). The shoshonite association: A review. *Journal of the Geological Society of Australia*, 15(2), 275-294.
- Keller, J., Ryan, W. B. .F., Ninkovich, D., Altherr, R. (1978). Explosive volcanic activity in the Mediterranean over the past 200,000 yr as recorded in deep-sea sediments. *Geological Society of America Bulletin* 89, 591–604.
- Kronberg, G. I., Nesbitt, H. W. (1981). Quantification of weathering of soil chemistry and soil fertility. *Journal of Soil Science* 32, 453–459.
- La Tour, T. E. (1989). Analysis of rocks using X-ray fluorescence spectrometry. *The Rigaku Journal*, 6 (1), 3-9.
- Le Bas, M. J., Le Maitre, R. W., Streckeisen, A., & Zanettin, B. (1986). A chemical classification of volcanic rocks based on the total alkali-silica diagram. *Journal of petrology*, 27 (3), 745-750.
- Le Maitre, R. W. (1984). A proposal by the IUGS Subcommittee on the systematics of igneous rocks for a chemical classification of volcanic rocks based on the total alkali silica (TAS). *Australian Journal of Earth Sciences*, 31 (2), 243-255.
- Le Maitre, R. W. (2005). *Igneous rocks: A classification and glossary of terms: Recommendations of the International Union of Geological Sciences. Subcommittee on the systematics of igneous rocks*, 2nd Edition. Cambridge University Press.
- Le Maitre, R. W., Streckeisen, A., Zanettin, B., Le Bas, M. J., Bonin, B., & Bateman, P. (2002). *Igneous rocks: A classification and glossary of terms: Recommendations of the International Union of Geological Sciences. Subcommittee on the systematics of igneous rocks*. Cambridge University Press.
- Mavris, C., Egli, M., Plötze, M., Blum, J. D., Mirabella, A., Giaccai, D., & Haerberli, W. (2010). Initial stages of weathering and soil formation in the Morteratsch proglacial area (Upper Engadine, Switzerland). *Geoderma*, 155 (3), 359-371.
- McKeague, J. A., Brydon, J. E., Miles, N. M., (1971). Differentiation of forms of extractable iron and aluminium in soils. *Soil Science Society of America Proceedings* 35, 33–38.
- Mirabella, A., Egli, M., Raimondi, S., & Giaccai, D. (2005). Origin of clay minerals in soils on pyroclastic deposits in the island of Lipari (Italy). *Clays and clay minerals*, 53 (4), 410-422.
- Morrison, G. W. (1980). Characteristics and tectonic setting of the shoshonite rock association. *Lithos*, 13 (1), 97-108.
- Munno, R., Rossi, G., & Tadini, C. (1980). Crystal chemistry of kimzeyite from Stromboli, Aeolian Islands, Italy. *American Mineralogist*, 65 (1-2), 188-191.
- Munroe, J. S., Farrugia, G. & Ryan, P. C. (2007). Parent material and chemical weathering in alpine soils on Mt. Mansfield, Vermont, USA. *Catena*, 70, pp. 39–48.

- Narcisi, B., Vezzoli, L. (1999). Quaternary stratigraphy of distal tephra layers in the Mediterranean an overview. *Global and Planetary Change*, 21, 31–50.
- Nesbitt, H. W., Young, G. M. (1989). Formation and diagenesis of weathering profiles. *Journal of Geology* 97, 129–147.
- Parker, A. (1970). An index for weathering for silicate rocks. *Geological Magazine*, 107, pp. 129 – 147
- Paterne, M., Guichard, F., Labeyrie, J. (1988). Explosive activity of the South Italian volcanoes during the past 80,000 years as determined by marine tephrochronology. *Journal of Volcanology and Geothermal Research*, 34, 153–172.
- Peccerillo, A., & Taylor, S. R. (1976). Geochemistry of Eocene calc-alkaline volcanic rocks from the Kastamonu area, northern Turkey. *Contributions to mineralogy and petrology*, 58 (1), 63-81.
- Pendleton, R. L., & Nickerson, D. (1951). Soil colours and special Munsell soil charts. *Soil Science*, 71(1), 35-44.
- Petrone, C. M., Olmi, F., Braschi, E., & Francalanci L. (2006). Mineral chemistry profile: A valuable approach to unravel magma mixing processes in the recent volcanic activity of Stromboli, Italy, *per. Min.*, 75(2–3), 277–292.
- Pfiffner, A. O., Engi, M., Schlunegger, F., Mezger, K., & Diamond, L. (2012). *Erdwissenschaften*. UTM.
- Pichler, H. (1967). Neue Erkenntnisse über Art und Genese des Vulkanismus der Äolischen Inseln (Sizilien). *Geol. Rdsch.*, 57, 102 – 126, Stuttgart.
- Pichler, H. (1981). *Sammlung Geologischer Führer* 69, Lipari, Vulcano, Stromboli, Tyrrhenisches Meer Italianische Vulkan-Gebiete III. Gebrüder Bornträger Berlin-Stuttgart.
- Pichler, H. (1984). *Sammlung Geologischer Führer* Ätna, Sizilien. Italianische Vulkan-Gebiete IV. Gebrüder Bornträger Berlin-Stuttgart.
- Price, J., R. and Velbel, M., A. (2003). Chemical weathering indices applied to weathering profiles developed on heterogeneous felsic metamorphic parent rocks. *Chemical Geology*, 202, pp. 397–416.
- Rosi, M., A. Bertagnini, and Landi P. (2000). Onset of the persistent activity at Stromboli volcano (Italy), *Bull. Volcanol.*, 62, 294–300.
- Scarciglia, F., De Rosa, R., Vecchio, G., Apollaro, C., Robustelli, G., & Terrasi, F. (2008). Volcanic soil formation in Calabria (southern Italy): the Cecita Lake geosol in the late Quaternary geomorphological evolution of the Sila uplands. *Journal of Volcanology and Geothermal Research*, 177(1), 101-117.
- Schmid, R. (1981). Descriptive nomenclature and classification of pyroclastic deposits and fragments: Recommendations of the UIGS submission on the systematic of igneous Rocks. *Geology*, 9, 41-43.
- Schwertmann, U. (1964). Differenzierung der Eisenoxide des Bodens durch Extraktion mit Ammoniumoxalat Lösung. *Zeitschrift Pflanzenernährung Düng Bodenkunde*, 105, 195-202.

- Siddig, A. A., Ellison, A. M., Ochs, A., Villar-Leeman, C., & Lau, M. K. (2015). How do ecologists select and use indicator species to monitor ecological change? Insights from 14 years of publication in ecological indicators. *Ecological Indicators*, 60, 223-230.
- Soil Survey Division Staff USDA. (1993). Soil survey manual. Soil Conservation Service. U.S. Department of Agriculture Handbook 18.
- Stahr, K., Kandeler, E., Herrmann, L., & Streck, T. (2012). *Bodenkunde und Standortlehre* (Vol. 2967). Ulmer Verlag UTB Stuttgart Germany.
- Stiles, C. A., Mora, C. I., Driesse, S. G. (2003). Pedogenetic processes and domain boundaries in avertisol climosequence: evidence from titanium and zirconium distribution and morphology. *Geoderma*, 116, 279–299.
- Streckeisen, A. (1978). Classification and nomenclature of volcanic rocks, lamprophyres, carbonatites and melilitic rocks. *N. Jb. Miner. Abh*, 134, 1-14.
- Sumner, M. E. (Ed.). (1999). *Handbook of soil science*. CRC press.
- Symonds, R. B., Rose, W. I., Bluth, G., and Gerlach, T. M. (1994). Volcanic gas studies: methods, results, and applications, in Carroll, M. R., and Holloway, J.R., eds., *Volatiles in Magmas: Mineralogical Society of America Reviews in Mineralogy*, v. 30, p. 1-66.
- Thorarinsson, S. (1954). The eruption of Hekla 1947- 48, part 2, ch. 3: The tephra falls from Hekla on March 29, 1947. *Soc. Sci. Isandica, Reykjavik*, 1-68.
- Troia, A., Raimondo, F. M., & Mazzola, P. (2012). Mediterranean island biogeography: Analysis of fern species distribution in the system of islets around Sicily. *Plant Biosystems-An International Journal Dealing with all Aspects of Plant Biology*, 146(3), 576-585.
- United States Department of Agriculture USDA (2014). Soil texture calculator. Available at <<[http://www.nrcs.usda.gov/wps/portal/nrcs/detail/soils/survey/?cid=nrcs142p2\\_054167](http://www.nrcs.usda.gov/wps/portal/nrcs/detail/soils/survey/?cid=nrcs142p2_054167)>> (accessed on 25 November 2015).
- United States Geological Survey USGS (2009). Volcanic hazards. Available at <<<http://volcanoes.usgs.gov/hazards/tephra/>>> (accessed on 14 November 2015).
- United States Geological Survey USGS (2010). Volcanic gases and their effects. Available at <<<http://volcanoes.usgs.gov/hazards/gas/>>> (accessed on 5 December 2015).
- Vingiani, S., Scarciglia, F., Mileti, F. A., Donato, P., & Terribile, F. (2014). Occurrence and origin of soils with andic properties in Calabria (southern Italy). *Geoderma*, 232, 500-516.
- Wagner, A. (1995). *Alterbestimmung von jungen Gesteinen und Artefakten. Physikalische und chemische Uhren in Quartärgeologie und Archäologie*. Ferdinand Enke Verlag Stuttgart Germany.
- Walworth, J. L. (2006). *Soil Sampling and Analysis*. Tucson, Arizona: College of Agriculture and Life Sciences, Arizona Cooperative Extension.
- Waroszewski, J., Egli, M., Kabala, C., Kierczak, J., & Brandova, D. (2015). Mass fluxes and clay mineral formation in soils developed on slope deposits of the Kowarski Grzbiet (Karkonosze Mountains, Czech Republic/Poland). *Geoderma*.

- Zimmerer, M. J., Lafferty, J., & Coble, M. A. (2016). The eruptive and magmatic history of the youngest pulse of volcanism at the Valles caldera: Implications for successfully dating late Quaternary eruptions. *Journal of Volcanology and Geothermal Research*, 310, 50-57.

## IX. APPENDIX

### *XRF Analyses (Total Content)<sup>4</sup>*

Site Floresta	Depth cm	0-20	20-35	35-115	115-135	135-180	180-200	>200
Element								
Na	%	1.19	0.95	1.23	1.83	1.26	0.99	0.34
Mg	%	0.89	1.05	1.19	1.25	0.74	0.93	0.88
Al	%	6.55	8.86	11.90	12.21	12.80	6.48	4.85
Si	%	25.26	27.34	21.21	19.71	24.20	32.26	35.53
P	%	0.08	0.05	0.20	0.30	0.22	0.00	0.00
K	%	1.76	1.53	0.93	0.75	0.45	1.70	1.07
Ca	%	0.78	0.70	1.44	2.52	1.56	0.57	0.32
Ti	%	0.38	0.58	0.94	0.94	1.02	0.39	0.32
Mn	%	0.08	0.10	0.11	0.16	0.24	0.15	0.01
Fe	%	2.87	4.27	5.84	5.80	5.81	3.17	5.09
Element								
Na	g/kg	11.9	9.5	12.3	18.3	12.6	9.9	3.4
Mg	g/kg	8.9	10.5	11.9	12.5	7.4	9.3	8.8
Al	g/kg	65.5	88.6	119.0	122.1	128.0	64.8	48.5
Si	g/kg	253	273	212	197	242	323	355
P	g/kg	0.805	0.505	1.983	3.031	2.244	0.039	0.044
K	g/kg	17.6	15.3	9.3	7.5	4.5	17.0	10.7
Ca	g/kg	7.8	7.0	14.4	25.2	15.6	5.7	3.2
Ti	g/kg	3.85	5.81	9.42	9.36	10.23	3.85	3.18
Mn	g/kg	0.803	0.991	1.054	1.568	2.395	1.469	0.062
Fe	g/kg	28.7	42.7	58.4	58.0	58.1	31.7	50.9

Site: Sila	Depth cm	0-20	20-40	40-60	60-80	80-100
Element						
Na	%	1.32	1.26	1.66	1.68	1.86
Mg	%	0.98	0.99	0.79	0.77	0.74
Al	%	10.08	10.47	12.33	12.21	11.71
Si	%	23.01	23.85	24.62	24.52	26.62
P	%	0.11	0.10	0.10	0.11	0.09
K	%	2.03	2.15	2.37	2.35	2.59
Ca	%	1.50	1.60	2.17	2.32	2.60
Ti	%	0.439	0.437	0.376	0.398	0.350
Mn	%	0.068	0.063	0.031	0.026	0.025
Fe	%	3.53	3.59	3.25	3.46	3.12
Element						
Na	g/kg	13.2	12.6	16.6	16.8	0.0
Mg	g/kg	9.8	9.9	7.9	7.7	7.4
Al	g/kg	100.8	104.7	123.3	122.1	117.1
Si	g/kg	230	239	246	245	266
P	g/kg	1.102	1.022	0.983	1.117	0.873
K	g/kg	20.3	21.5	23.7	23.5	25.9
Ca	g/kg	15.0	16.0	21.7	23.2	26.0
Ti	g/kg	4.39	4.37	3.76	3.98	3.50
Mn	g/kg	0.682	0.635	0.314	0.258	0.250
Fe	g/kg	35.3	35.9	32.5	34.6	31.2

<sup>4</sup> XRF analyses do not include any corrected factor the elements Si, Al, Mn.

Site Sila DH	Depth cm	0-20	20-40	40-60	60-80	80-100
Element						
Na	%	1.59	1.642	2.348	3.002	1.949
Mg	%	1.386	0.932	0.946	1.042	0.773
Al	%	14.23	14.67	15.37	16.53	13.09
Si	%	28.02	24.91	29.24	30.37	24.65
P	%	0.1137	0.1589	0.1497	0.1633	0.1376
K	%	2.403	2.367	2.606	2.597	2.185
Ca	%	1.784	2.356	3.257	3.45	2.864
Ti	%	0.6104	0.5243	0.4579	0.4495	0.3804
Mn	%	0.09711	0.04049	0.03241	0.03274	0.02754
Fe	%	4.835	4.546	3.991	3.963	3.196
Element						
Na	g/kg	15.9	16.42	23.48	30.02	19.49
Mg	g/kg	13.86	9.32	9.46	10.42	7.73
Al	g/kg	142.3	146.7	153.7	165.3	130.9
Si	g/kg	280.2	249.1	292.4	303.7	246.5
P	g/kg	1.137	1.589	1.497	1.633	1.376
K	g/kg	24.03	23.67	26.06	25.97	21.85
Ca	g/kg	17.84	23.56	32.57	34.5	28.64
Ti	g/kg	6.104	5.243	4.579	4.495	3.804
Mn	g/kg	0.9711	0.4049	0.3241	0.3274	0.2754
Fe	g/kg	48.35	45.46	39.91	39.63	31.96

Site: SI	Depth	0-20	20-50	50-90	90-130	130-140	140-160
Element							
Na	%	1.415	1.439	1.384	1.441	1.326	1.242
Mg	%	1.218	1.258	1.269	1.231	1.727	1.893
Al	%	9.109	10.25	10.34	9.829	10.63	9.878
Si	%	22.68	25.06	25.48	23.18	30.45	31.92
P	%	0.3038	0.3038	0.307	0.2953	0.0953	0.0306
K	%	1.669	1.819	1.807	1.661	2.397	2.572
Ca	%	1.297	1.156	1.176	1.172	0.9557	1.01
Ti	%	0.6369	0.7003	0.7009	0.6616	0.4221	0.4093
Mn	%	0.1395	0.1529	0.1535	0.1402	0.07031	0.04361
Fe	%	4.247	4.576	4.548	4.22	2.769	2.803
Element							
Na	g/kg	14.15	14.39	13.84	14.41	13.26	12.42
Mg	g/kg	12.18	12.58	12.69	12.31	17.27	18.93
Al	g/kg	91.09	102.5	103.4	98.29	106.3	98.78
Si	g/kg	226.8	250.6	254.8	231.8	304.5	319.2
P	g/kg	3.038	3.038	3.07	2.953	0.953	0.306
K	g/kg	16.69	18.19	18.07	16.61	23.97	25.72
Ca	g/kg	12.97	11.56	11.76	11.72	9.557	10.1
Ti	g/kg	6.369	7.003	7.009	6.616	4.221	4.093
Mn	g/kg	1.395	1.529	1.535	1.402	0.7031	0.4361
Fe	g/kg	42.47	45.76	45.48	42.2	27.69	28.03

Site: SII	Depth cm	0-15	15-50	50-65	65-90	90-130	130-170
Element							
Na	%	1.166	1.143	1.539	1.591	0.78	0.502
Mg	%	1.526	1.211	1.371	1.2	1.126	1.35
Al	%	9.749	10.7	15.14	16.44	6.584	6.592
Si	%	28.25	23.69	22.32	20.25	43.37	43.73
P	%	0.1795	0.2773	0.4277	0.5227	0.02636	0.00717
K	%	1.893	1.578	1.025	0.7759	1.471	1.119
Ca	%	1.624	1.437	1.185	1.342	0.4271	0.4518
Ti	%	0.6119	0.7038	1.158	1.153	0.355	0.4085
Mn	%	0.1584	0.1686	0.1425	0.2077	0.1488	0.00483
Fe	%	4.463	5.072	7.037	6.784	3.762	4.35
Element							
Na	g/kg	11.66	11.43	15.39	15.91	7.8	5.02
Mg	g/kg	15.26	12.11	13.71	12	11.26	13.5
Al	g/kg	97.49	107	151.4	164.4	65.84	65.92
Si	g/kg	282.5	236.9	223.2	202.5	433.7	437.3
P	g/kg	1.795	2.773	4.277	5.227	0.2636	0.0717
K	g/kg	18.93	15.78	10.25	7.759	14.71	11.19
Ca	g/kg	16.24	14.37	11.85	13.42	4.271	4.518
Ti	g/kg	6.119	7.038	11.58	11.53	3.55	4.085
Mn	g/kg	1.584	1.686	1.425	2.077	1.488	0.0483
Fe	g/kg	44.63	50.72	70.37	67.84	37.62	43.5

Site: SIII.	Depth cm	0-50	50-75	75-110	110-135	135-155	155-170
Element							
Na	%	1.625	1.418	1.463	1.62	1.344	1.102
Mg	%	1.621	1.391	1.553	1.549	1.706	1.906
Al	%	9.811	11.86	13.59	9.968	9.807	10.03
Si	%	34.72	26.16	28.66	35.98	35.25	33.61
P	%	0.07289	0.2352	0.2294	0.02515	0.02412	0.02046
K	%	2.693	1.976	2.091	2.909	2.908	2.664
Ca	%	0.769	0.7426	0.8867	0.5763	0.6103	0.6181
Ti	%	0.3802	0.6625	0.6674	0.351	0.3194	0.4337
Mn	%	0.06172	0.1043	0.07883	0.05722	0.04956	0.05575
Fe	%	2.548	4.24	3.992	2.621	2.412	3.311
Element							
Na	g/kg	16.25	14.18	14.63	16.2	13.44	11.02
Mg	g/kg	16.21	13.91	15.53	15.49	17.06	19.06
Al	g/kg	98.11	118.6	135.9	99.68	98.07	100.3
Si	g/kg	347.2	261.6	286.6	359.8	352.5	336.1
P	g/kg	0.7289	2.352	2.294	0.2515	0.2412	0.2046
K	g/kg	26.93	19.76	20.91	29.09	29.08	26.64
Ca	g/kg	7.69	7.426	8.867	5.763	6.103	6.181
Ti	g/kg	3.802	6.625	6.674	3.51	3.194	4.337
Mn	g/kg	0.6172	1.043	0.7883	0.5722	0.4956	0.5575
Fe	g/kg	25.48	42.4	39.92	26.21	24.12	33.11

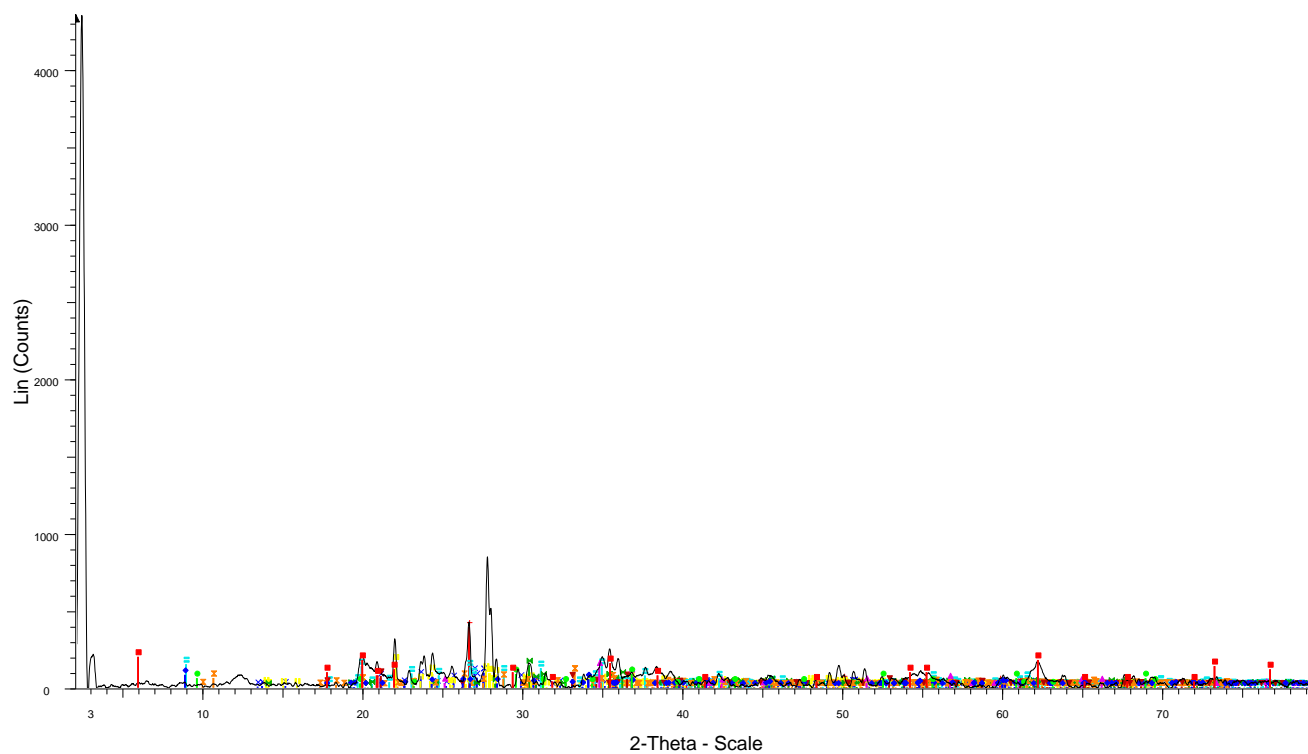
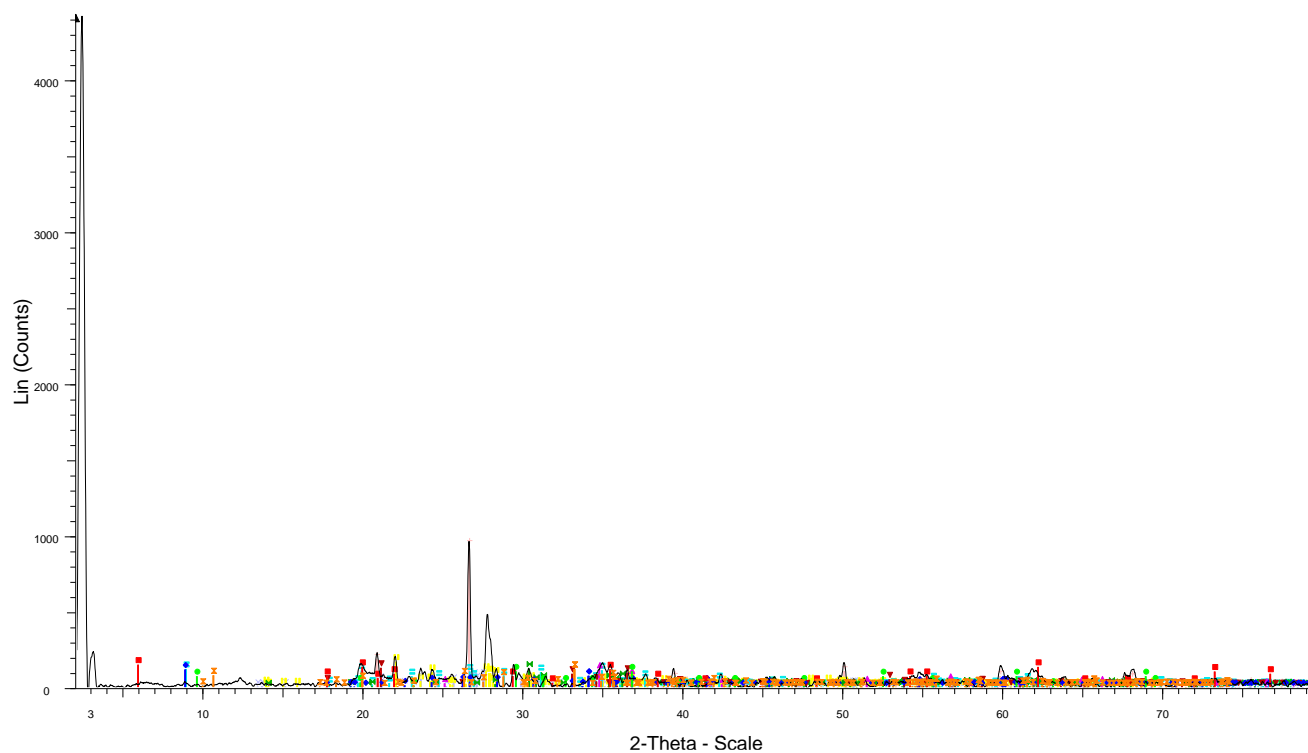
*R-Code for DRIFT Analysis*

```

# Char 1
N1<- "10"
str(DR1 <- read.csv("/Users//dieter/Desktop/Drifft/Drift-Etna/dpt/s1_0-
20.dpt",header = TRUE))
colnames(DR1)<-c("Wavelength",N1)
# Integration
# Kaolinite
lw<-3644
hw<-3744
Intw<-subset(DR1, Wavelength>lw & Wavelength<hw)
y1<-Intw[which.min(Intw$Wavelength),N1]
y2<-Intw[which.max(Intw$Wavelength),N1]
a<-(y2-y1)/(max(Intw$Wavelength)-min(Intw$Wavelength))
b<-y2-a*max(Intw$Wavelength)
Intw<-within(Intw,{bsl<-a*Intw$Wavelength+b})
colnames(Intw)<-c("Wavelength","char","bsl")
plot(Intw$Wavelength,Intw$char)
lines(Intw$Wavelength,Intw$bsl)
Intw
Mv<-max(Intw$char)
Mb<-mean(Intw$bsl)
MKaolinite <-Mv-Mb
MKaolinite
# cellulose
lw<-1180
hw<-1220
Intw<-subset(DR1, Wavelength>lw & Wavelength<hw)
y1<-Intw[which.min(Intw$Wavelength),N1]
y2<-Intw[which.max(Intw$Wavelength),N1]
a<-(y2-y1)/(max(Intw$Wavelength)-min(Intw$Wavelength))
b<-y2-a*max(Intw$Wavelength)
Intw<-within(Intw,{bsl<-a*Intw$Wavelength+b})
colnames(Intw)<-c("Wavelength","char","bsl")
plot(Intw$Wavelength,Intw$char)
lines(Intw$Wavelength,Intw$bsl)
Intw
Mv<-max(Intw$char)
Mb<-mean(Intw$bsl)
Mcel<-Mv-Mb
Mcel

```

## XRD Diffractograms



3 - File: Gruppe\_A3.raw - Type: 2Th/Th locked - Start: 2.000 ° - End: 79.592 ° - Step: 0.013 ° - Step time: 45.1 s  
 Operations: X Offset 0.039 | Smooth 0.147 | Background 0.145,1.000 | Import

<ul style="list-style-type: none"> <li><span style="color: red;">+</span> 01-085-0457 (I) - Quartz, low, syn - SiO<sub>2</sub> - Y: 9.01 % - d x by: 1. - WL: 1.5406 - Hexagonal - a 4.92100 - b 4.921</li> <li><span style="color: blue;">x</span> 01-071-0956 (*) - Orthoclase - K<sub>4</sub>Al<sub>4</sub>Si<sub>12</sub>O<sub>32</sub> - Y: 2.23 % - d x by: 1. - WL: 1.5406 - Monoclinic - a 8.55400 - b 1</li> <li><span style="color: yellow;"> </span> 00-019-1184 (I) - Albite, ordered - NaAlSi<sub>3</sub>O<sub>8</sub> - Y: 3.88 % - d x by: 1. - WL: 1.5406 - Triclinic - a 8.13800 - b 12.7</li> <li><span style="color: cyan;"> </span> 01-082-1852 (I) - Muscovite 3T, siliceous - (K<sub>0.93</sub>Na<sub>0.03</sub>)(Al<sub>1.54</sub>Fe<sub>0.25</sub>Mg<sub>0.21</sub>Ti<sub>0.04</sub>)(Si<sub>3.34</sub>Al<sub>0.66</sub>O<sub>10</sub>)(OH)</li> <li><span style="color: green;">x</span> 01-070-2129 (*) - Calcium Aluminum Silicate - CaAl<sub>2</sub>Si<sub>2</sub>O<sub>6</sub> - Y: 3.34 % - d x by: 1. - WL: 1.5406 - Monoclinic - a</li> <li><span style="color: orange;">x</span> 01-089-6412 (*) - Sodium Magnesium Chromium Silicate Fluoride - Na(Na<sub>1.97</sub>Mg<sub>0.03</sub>)Mg<sub>3</sub>(Mg<sub>1.03</sub>Cr<sub>0.97</sub>)Si<sub>8</sub>O</li> </ul>	<ul style="list-style-type: none"> <li><span style="color: red;">v</span> 01-073-6522 (I) - Goethite - FeO(OH) - Y: 1.74 % - d x by: 1. - WL: 1.5406 - Orthorhombic - a 4.64000 - b 10.00</li> <li><span style="color: magenta;">^</span> 01-072-6230 (I) - Iron Oxide - Fe<sub>2</sub>O<sub>3</sub> - Y: 3.02 % - d x by: 1. - WL: 1.5406 - Rhombo.H.axes - a 4.88230 - b 4.88</li> <li><span style="color: blue;">v</span> 01-088-2198 (I) - Biotite 1M, aluminous barian - (K<sub>1.77</sub>Ba<sub>0.23</sub>)(Mg<sub>3.16</sub>Fe<sub>2.01</sub>Al<sub>0.49</sub>Ti<sub>0.34</sub>)(Al<sub>2.83</sub>Si<sub>5.17</sub>O<sub>20</sub>)O</li> <li><span style="color: red;"> </span> 00-002-0014 (D) - Montmorillonite (Clay) - NaMgAlSi<sub>2</sub>O<sub>2</sub>(OH)H<sub>2</sub>O - Y: 4.58 % - d x by: 1. - WL: 1.5406 -</li> <li><span style="color: green;"> </span> 00-002-0628 (D) - Vermiculite - (Mg,Fe+2,Al)<sub>3</sub>(Si,Al)<sub>4</sub>O<sub>10</sub>(OH)<sub>2</sub>·4H<sub>2</sub>O - Y: 2.03 % - d x by: 1. - WL: 1.5406 -</li> </ul>
--	--

Fig. 39 XRD Sila, horizons 0-20 (top) and 40-60 (bottom).

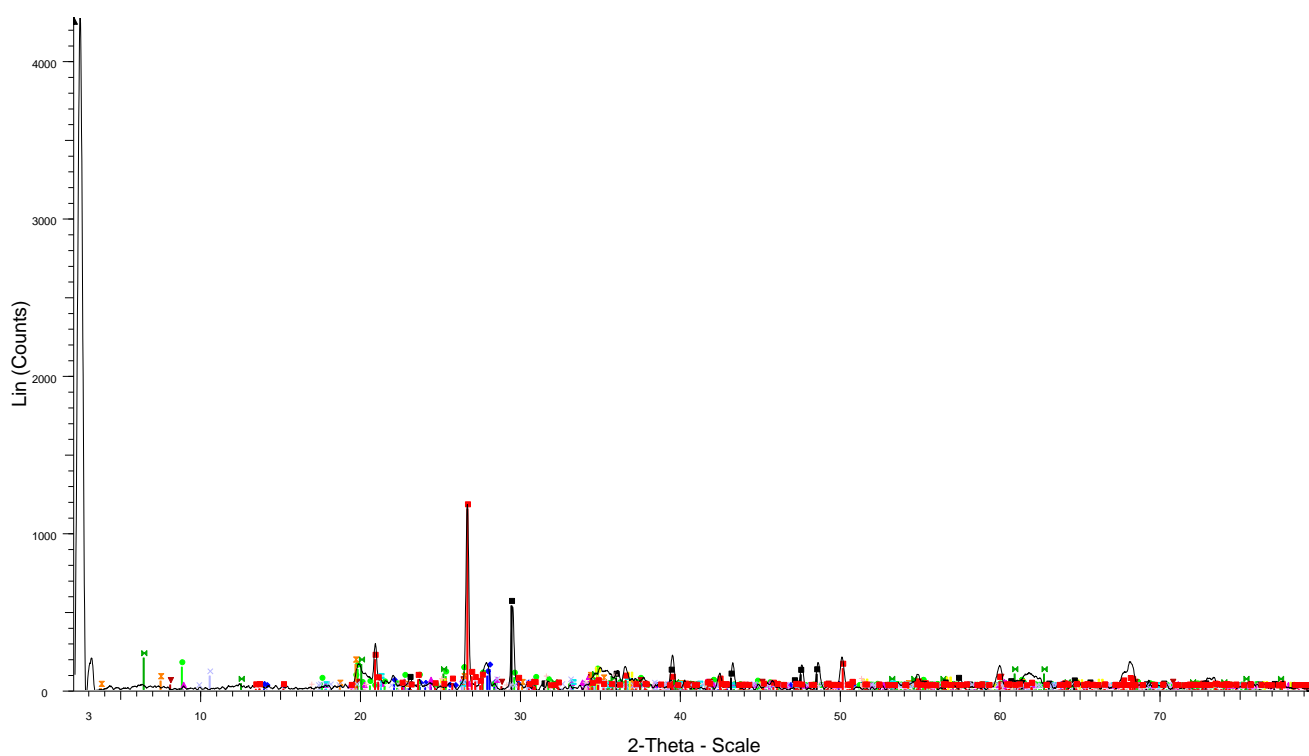
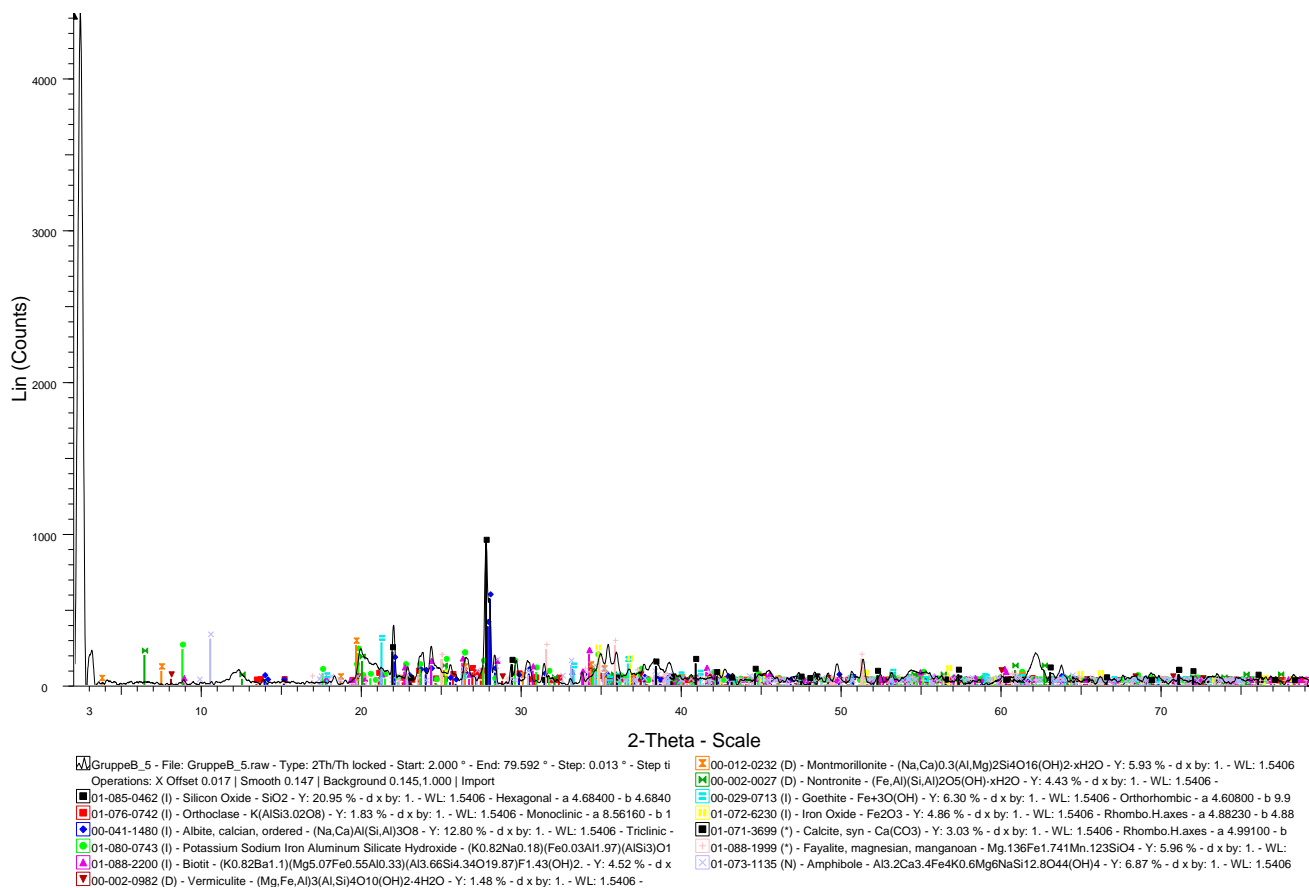


Fig. 40 XRD Sila, horizon 80-100 (top), Floresta, horizon 0-20 (bottom).

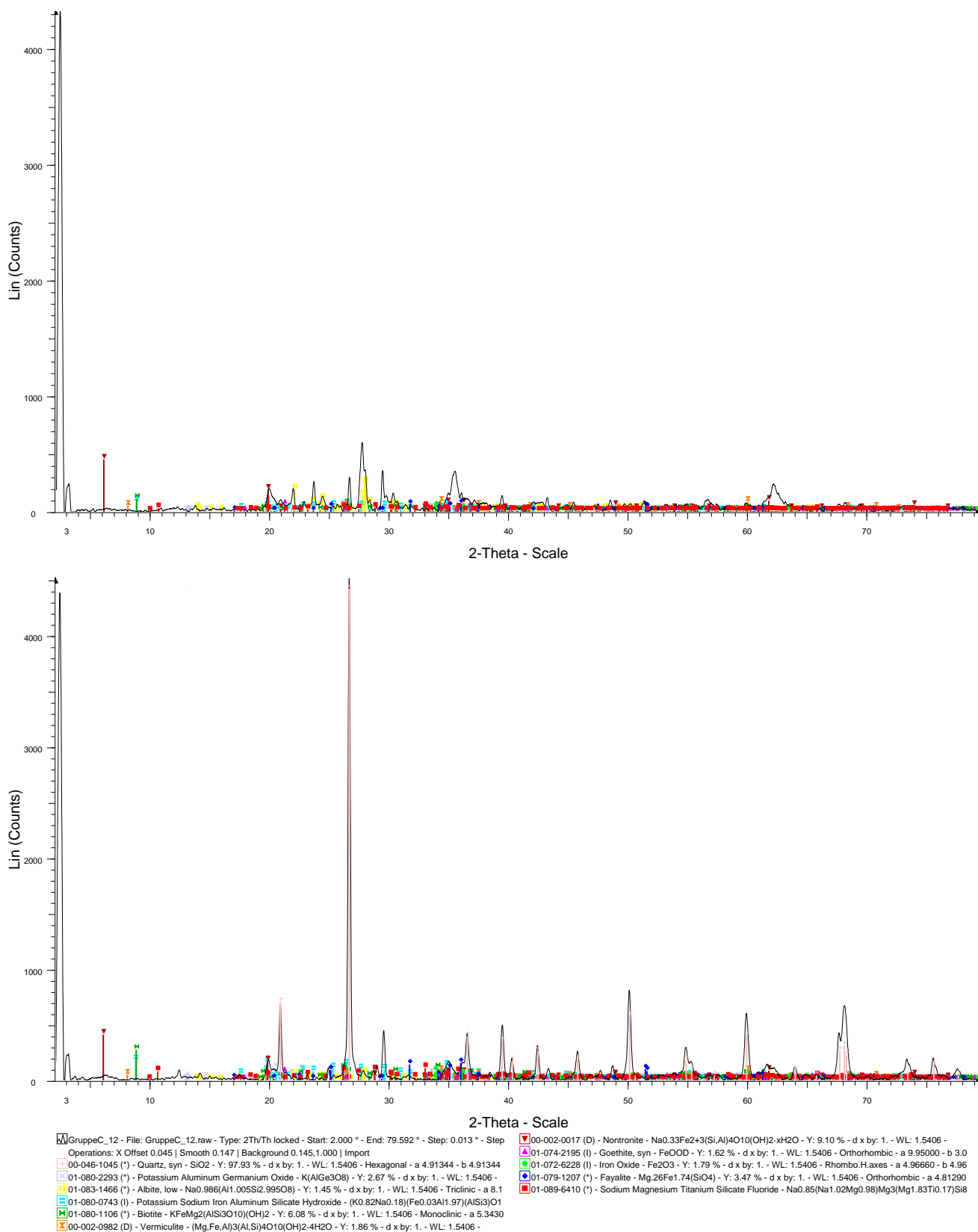


Fig. 41 XRD Floresta, Horizons 35-115 (top) and >200 (bottom).

## Laboratory course 14 - DRIFT-measurements (mineral structures)

Typical peaks/bands and their significance

	Sample											
(cm <sup>-1</sup> )	Sila	Sila	Sila	Sila	Sila	Floresta						
Kaolinite	3694	x	x	x	x	x	x	x	x	x	x	(x)
	3652	(x)	x	(x)	x	x						
	3620	x	x	x	x	x	x	x	x	x		x
	474	x	x	(x)		x	x		(x)		x	
	348	x				x			x			
Gibbsite	3620	x	x	x	x	x	x		x	x	x	
	3526	(x)	x	x	x	x			x			
	3469	(x)			(x)	x						
	1017	(x)	x								(x)	x
	366				x				x			
Chlorite	3676	(x)			x							
	3575	x				(x)						
	3428										x	
	750		x	x	x	(x)		x		x		
Imogolite	375	x	x	x		(x)	x		x	x	x	x
	348	x	(x)		(x)	x		x	x			
Kaolinite, Qz or Illite	474	x	x	(x)			x	x	(x)	(x)		x
Illit, Muskovite	531/474	x		(x)			x					
	831/752	(x)	(x)			(x)			(x)			
oct. Mg/Fe	650	x							(x)			
dioc. Smectite	690		(x)	(x)		(x)				x		
Quartz	692	x	x	x		x	x	x	(x)	x	x	x
Muskovite and Chlorite	750		x	x	x				x	x		
Qz-Doublet	780/800					x	x	(x)		(x)	x	x
AlMgOH	830	(x)										
Kaolinite	915	x	x	x	x	x	x	x		x		x
Enstatite (Pyr)	1064											
	952	(x)										
	645	x										
	513							x	x	x	x	x
Forsterite (Pyr)	885											
	490									(x)		
	315	x										
Amphibole	3674	(x)	(x)	(x)	x							
	3618		x	x		x	x		x			
Calcite	3692											
	3622											
	2980											
	2893											
	2875											
	2513											
	1796											
	1430											
	877											
	848											
	714											

		SI	SI	SI	SI	SI	SII	SII	SII	SII	SII	SII
	(cm <sup>-1</sup> )	20-50	50-90	90-130	130-140	140-160	0-15	15-50	50-65	65-90	90-130	130-170
Kaolinite	3694	x	x	x	x	x	x	x				
	3652											
	3620	x	x	x	x	x	x	(x)	x	x	x	x
	474	x	x	(x)	x		x					
	348	x	x	(x)	(x)		x			(x)		
Gibbsite	3620	x	x	x	x	x	x	(x)	x	x	x	x
	3526							x	x	x		
	3469	(x)							x			(x)
	1017	(x)	x	(x)	(x)	(x)	(x)	x	(x)	x		
	366	x			x		(x)	(x)	x			
Chlorite	3676							(x)		x		
	3575	x	x					(x)	(x)	(x)	(x)	
	3428	(x)				(x)		x		(x)		
	750						(x)					
Imogolite	375										x	x
	348	x		(x)			(x)			x		
Kaolinite, Qz or Illite	474	x	(x)	x	x		x					(x)
	531/ 474	x	x	x	x		x			(x)	(x)	x
Illit, Muskovite	831/ 752						(x)			x		
	650							(x)				
oct. Mg/Fe dioct. Smectite	690	(x)	(x)	(x)	(x)		(x)	(x)		(x)	(x)	(x)
Quartz	692	x	x	x	x		(x)	x			(x)	(x)
Muskovite and Chlorite	750						(x)					
Qz- Doublet	780/ 800	x	x	x	x		x	x			x	x
AlMgOH Kaolinite	830						(x)			x		
	915			(x)	x		x	x			x	(x)
Enstatite (Pyr)	1064											
	952									x		
	645						(x)				x	
	513	x							x		x	x
Forsterite (Pyr)	885									(x)		
	490		(x)							x		
	315									(x)		
Amphibole	3674											
	3618											
Calcite	3692											
	3622											
	2980											
	2893											
	2875											
	2513											
	1796											
	1430											
	877											
	848											
	714											

		SIII	SIII	SIII	SIII	SIII	SIII
	(cm <sup>-1</sup> )	0-50	50-75	75-110	110-135	135-155	155-170
Kaolinite	3694		x	(x)	x	x	x
	3652						
	3620	x	x	x	x	x	x
	474	x	x	x	x	x	x
	348			x		x	x
Gibbsite	3620	x	x	x	x	x	x
	3526	x	(x)	(x)	x	x	
	3469		x	(x)	x		
	1017	x	x	x	x	x	x
	366		x				
Chlorite	3676			x			
	3575						
	3428	x	(x)	(x)	x	x	
	750		x	x	(x)	(x)	(x)
Imogolite	375	x	(x)	x	(x)		
	348			x	x	x	x
Kaolinite, Qz or Illite	474	x	x	x	x	x	x
Illit, Muskovite	531/474	x	x	x	x	x	x
	831/752	x	(x)	(x)	x	x	x
oct. Mg/Fe	650						x
dioc. Smectite	690	(x)	x	(x)		x	(x)
Quartz	692	(x)	x	x	(x)	x	(x)
Muskovite and Chlorite	750	(x)	x	x		(x)	
Qz-Doublet	780/800	x	x	x	x	x	x
AlMgOH	830	x	(x)		x	x	x
Kaolinite	915	x	x	x	x	x	x
Enstatite (Pyr)	1064						
	952			(x)			
	645	(x)	x	x	x	x	x
	513	(x)	(x)				x
Forsterite (Pyr)	885						
	490						x
	315		x			x	
Amphibole	3674						
	3618		(X)		(x)	(x)	(x)
Calcite	3692						
	3622						
	2980						
	2893						
	2875						
	2513						
	1796						
	1430						
	877						
	848						
	714						